Quinoxolinol based Ligand for Molecular Recognition and Selective Extraction

by

Michael Alan DeVore II

A dissertation submitted to the Graduate Faculty of
Auburn University
in partial fulfillment of the
requirements for the Degree of
Doctor of Philosophy in Chemistry

Auburn, Alabama
May 4, 2014

Keywords: Sensing, Actinides, Nuclear Chemistry, Extractions

Approved by

Anne Gorden, Chair, Associate Professor, Department of Chemistry and Biochemistry
Rik Blumenthal, Associate Professor, Department of Chemistry and Biochemistry
Christopher Easley, Knowles Associate Professor, Department of Chemistry and Biochemistry
Christian Goldsmith, Associate Professor, Department of Chemistry and Biochemistry

Abstract

As the current age of nuclear reactors gets older, more waste and a greater possibility of leaks can occur. There is a need for an on-site real time ability to be able to detect actinides in the environment to prevent a greater problem, or to help remedy clean up. Due to competing metals such as copper or iron, designing a ligand to selectively detect actinides is often very difficult. 2-quinoxolinol backbone was synthesized and two 3,5-di-*t*-butylsalicylaldehydes were attached as imines to provide a 2N-2O donor system as a binding pocket. This ligand by itself gave a signal in the UV-Vis at ~389 nm. When bound to uranyl, the peak shifted to higher energies to ~367 nm with a shoulder at 450 nm. When bound to copper, the peak was lower energy shifted to 450 nm. The detection limits were ~25 ppm for uranyl and ~1 ppm for copper. This became the starting point for designing a better sensor using computational chemistry. What was found was that changing from a salicylaldehyde to a 2-aminobenzaldehyde should give greater selectivity in the UV-Vis spectrum. Much needs to be investigated to increase the signal to noise and lower the detection limit. Finally, extractions were performed to determine the ligands ability to separate actinides from lanthanides. Typical of mixed N,O-donor ligands, the Salqu ligand decomposed at >1 M HNO_3 and would only have efficient extractions between $1x10^{-1}$ – $1x10^{-3}$ M HNO_3 with distribution for uranyl ~3 and separation factors ~5.

Acknowledgments

The author would like to foremost thank my parents, Mike and Avalyn DeVore, and family for their support and any help I needed. I would like to thank my committee members, Dr. Rik Blumenthal, Dr. Christopher Easley, Dr. Christian Goldsmith, and outside reader Dr. Paul Cobine, for letting me get out alive. I would like to thank my boss Dr. Anne Gorden for the years of helpful advice, discussion, and learning that took place under your tutelage. I would like to thank my best friend and former roommate Dr. Kennon Deal for being there for me and getting me out of the house enough times not to go crazy, I miss you buddy. I would like to thank my lab mates, Dr. Kushan Weerasiri, Dr. Branson Maynard, Dr. Mohan Bharrara, Dr. Yuanchen Li, Charmaine Tutson, and Nick Klann, for all the help with any questions about reactions, synthesis, and techniques. Good luck to new graduate students Chasity Ward, Maya West, and Emily Hardy. I have to thank Dr. Cobine again for use of his ICP-OES for much of this research on extractions. I would like to thank Dr. Enrique Batista for allowing me to intern at LANL for the summer and pick up new skills in computational chemistry that will hopefully be worthwhile. Perhaps my second best friend Dr. Leah Godwin. I still talk to you on a weekly basis about BBT and HIMYM. The conversations are hilarious. This is the culmination of a very long 6 years and I am happy that I got to spend it at Auburn University and make a number of new friends both in and out of the department. And finally Auburn University Department of Chemistry and Biochemistry, Thank You!

Table of Contents

List of Tables

List of Figures

List of Schemes

List of Abbreviations

6-31g(d)	basis set
AAS	Atomic absorption spectrometry
AES	Atomic emission spectrometry
B3LYP	hybrid functional
BTBP	6,6'-bis(5,6- dialkyl[1,2,4]triazine-3-yl)[2,2']bipyridines
BTP	bis-1,2,4-triazin-3-yloligopyridines
CHON	Carbone, Hydrogen, Oxygen, Nitrogen principle
CMPO	(N,N'-diisobutylcarbamoylmethyl)-octylphenylphosphine oxide
Cyanex 272	bis-(2,4,4-trimethylpentyl)phosphinic acid
$CyMe_4$-BTP	2,6- bis(5,5,8,8,-tetramethyl-5,6,7,8,-tetrahydrobenzo[1,2,4]triazine-3-yl)pyridine
D2HEPA	di-(2-ethylhexyl)-phosphoric acid
DCM	methylene chloride
D_{Eu}	distribution of europium
DFT	density functional theory
DIAMEX	Diamide Extraction
DIPEA	di-isopropylethylamine
DMDBTDMA	N,N'-dimethyl-N,N'-dibutyltetradecylmalonamide
DMDOHEMA	N,N'-dimethyl-N,N'-dioctylhexylethoxymalonamide

DMF	N,N'-dimethylformamide
DMSO	dimethylsulfoxide
DTPA	diethylenetriamine-N,N,N',N'',N''-pentacetic acid
D_U	Distribution of uranium
EtOH	ethanol
FBR	fast breeder reactors
FES	flame emission spectrometry
FP	fission products
GANEX	Group Actinide Extraction
HDEHP	di(2-ethylhexyl)phosphoric acid
HEPES	(2-4[-(2-hydroxyethyl)piperazine-1-yl]ethanesulfonic acid)
HOMO	Highest occupied molecular orbital
HSAB	Hard-soft-acid base theory
ICP	Inductively couple plasma
ICP-AES	inductively couple plasma-atomic emission spectrometry
ICP-MS	inductively couple plasma-mass spectrometer
ICP-OES	Inductively Couple Plasma-Optical Emission Spectrometer
K_b	binding constant
LUMO	lowest unoccupied molecular orbital
m/z	mass over charge
MeOH	Methanol
MOX	mixed oxide reactors
NTO	natural transition orbitals
P&T	Partitioning and transmutation

PC88A	2-ethylhexylphosphonic acid mono-2-ethylhexyl ester
ppb	parts per billion
ppm	parts per million
PUREX	Plutonium Uranium Recovery by Extraction
Salqu	di-substituted ligand
SANEX	Selective actinide extraction
SERS	surface enhanced raman spectroscopy
SF	Separation Factor
SF	separation factor defined as D_U / D_{Eu}
SNF	spent nuclear fuel
SNF	Spent Nuclear Fuel
TALSPEAK	Trivalent actinide-lanthanide separation by phosphorous reagent Extraction from Aqueous Komplexes
TBP	tri-n-butyl phosphate
TDDFT	time-dependent density functional theory
TFA	trifluoroacetic acid
THF	tetrahydrofuran
TRUEX	Transuranium Extraction
UV-Vis	Ultra-violet visible
v/v	volume/volume
XAS	X-ray absorption spectroscopy
XRF	X-ray fluorescence
ε	Extinction coefficient ($M^{-1} \bullet cm^{-1}$)

Chapter 1

Introduction

About 13-14% of the world's electricity is produced from nuclear sources, and nuclear power is the dominant source of electrical power for most of Europe. Nuclear power should become a dominant source of electricity in the world because of the dependence on oil in manufacturing and petroleum products are highly sought after as chemical feedstocks.[1] Experts are predicting that the maximum allowable oil production using current methods will occur in the next 5-25 years, and the needs of nuclear power and other alternative fuel sources is growing.[2] A shift away from oil as an energy source is critical for ensuring that energy remains available and reasonably priced.[2-4]

As of the end of 2010, only 8.4% of the electrical supply of the United States civilian energy production was from nuclear power, 8% was from renewable sources such as wind and solar, with the remaining 83% from fossil fuels.[1] Along with wind and solar, nuclear energy is an attractive source because it can generate a significant amount of energy with minimal atmospheric emissions;[5] however, the use of actinides in both military and nuclear fuel applications has resulted in a plethora of waste and contamination issues.[6-9] Critical issues currently being addressed include stockpile

stewardship, long- term nuclear waste storage, recycling of spent fuel, and remediation and detection of actinides in the environment.[1,4,10]

New technologies will be required to support the next generation of nuclear power production;[2,3,8,9] however, reprocessing of nuclear fuel wastes is made much more difficult because of the gaps remaining in our fundamental understanding of *f*-element chemistry. A resurgence of interest in the chemistry of the actinides (in particular uranium, neptunium, and plutonium) has been inspired by the needs to address these environmental concerns, to develop new separation technologies, and to continue to develop our fundamental understanding of the chemical behavior of actinides.[11-28] Some fundamental misunderstandings involve coordination of *f*-elements, radionuclide movement through the environment, and separation of nuclear waste streams for reprocessing.

1.1 Coordination Chemistry of the Actinides and Lanthanides

Of the utmost concern in research for characterizing the 5*f* elements is the potential for radiological hazards and increasing expenses of working with and obtaining materials and equipment that must be dedicated for use with those materials.[11] Other metal ions have been used as less hazardous analogs for characterization such at Th(IV) and U(VI) complexes as models for the more highly active Pu(IV,VI), increasing the analytical tools available.[11] Because of their similar ionic radii, and, for the later actinides, similar oxidation states, lanthanide metals are

seen as potential coordination models for the actinide metals. Both 4*f* and 5*f* elements prefer large coordination numbers (8 or 9), possess flexible ligand coordination geometries, and can act as Lewis Acids in solution.[7] It is incorrect to assume that since lanthanides and actinides are similar in a number of ways, that their chemistry would be similar. While the lanthanides can be useful models, the actinides with their larger 5*f* orbitals, have a more covalent interaction with ligands, particularly soft donors, and therefore can form more stable complexes.[3,7,29] Covalent interaction in bonding of actinides is defined as mixing between two orbitals, in accordance with recently published studies.[30,31] There is an inherent flaw in relying on modeling of lanthanides to determine the small difference between 4*f* and 5*f* elements that could be exploited for actinide selective extractions and sensing.[11] Although the models can be great tools, many systems make critical but erroneous assumptions in the characterization of the *f*-elements; therefore a crucial need of modern techniques for characterizing the chemistry of the actinides and their complexes still exists.[11]

1.2 5*f* Coordination Compounds

For complete understanding of separation processes or the usefulness of ligands in the detection of actinides, it is best to establish bonding parameters across the 5*f* series.[32-34] Generally, a multidentate ligand that contains soft donors such as nitrogen and sulfur would be used for liquid-liquid separations of trivalent lanthanides and actinides of different oxidation states due to the greater binding affinity between actinides and soft base ligands. Because the behavior of the 5*f*

orbitals have been much less studied, it is difficult to determine ligand selectivity and optimum efficiency for separations or sensing, or optimal coordination environment for these 5*f* metal ions in the solid state.[34]

1.3 Sensing of Actinides in the Environment

Prior to the Manhattan Project, the only radioactive actinide elements believed to be on the planet were those that were naturally occurring (^{235,238}U, ^{232}Th), and the manmade isotopes that had been created in scientific research.[35] The Manhattan Project and eventual Cold War of the 1940s-1970s introduced considerable amounts of new radioisotopes, including most significantly, thousands of kilogram quantities of transuranium elements into the environment.[35] After the ban on atmospheric testing of nuclear weapons, the major significant injections of radioactivity into the environment have occurred due to the atomic testing program, and the disasters at Chernobyl in 1986, and Fukushima in 2011.[36] These disasters are not the only fears people have of nuclear materials. Due to the current threat of a dirty bomb attack and the possibility of a nuclear waste spill during transport prove that there is a clear need for a water-borne counter-terrorist technology, one capable of providing a stand-alone alarm sensing solution around a priority asset such as a water treatment plant or government installation.[11]

1.4 Methods for Detecting Actinides

1.41 Alpha Spectrometry

Alpha spectrometry allows the analyst to identify and quantify individual α-emitting radionuclide (isotopes) based on the detection of emitted α-particles and determination of α-particle energies specific to the radionuclide of interest.[37] Among the methods suitable for isotopic determination of α-nuclides (mass spectrum, neutron activation, α-spectroscopy) α-spectroscopy has an advantage of being low-cost and robust, and used in natural and technical samples. Although the range of α-particles through matter is short (they can be stopped with a sheet of paper), analysis based on their detection possess advantages compared to the detection of β-particle and γ-rays due to the extremely low backgrounds achievable.[37] Prior to alpha-radiometric analysis, pre-concentration and separation of the radionuclide from the matrix was required because of the relatively low radionuclide concentration in the samples. In addition, interference of inactive substances with the emitted α-particles will lead to a lower spectral resolution and higher detection limits.[38] The pre-concentration and separation procedures involve co-precipitation, extraction, and/or ion-exchange.[38] There are a number of spectral interference peaks from americium, plutonium, and neptunium when trying to detect thorium, uranium, neptunium, and plutonium isotopes.

Photon Electron Rejecting Liquid Alpha Spectroscopy (PERALS®) is a relatively new method that combines chemical separation by liquid-liquid extraction and the measurement of alpha activity by a water-immiscible scintillator.[39,40] This technique lowers the limit of detection by a factor of 10 in comparison with classical alpha spectroscopy by rejecting up to 99.9% of β-γ background radiation;[39] however the alpha energy resolution of the PERALS spectrometer is rather poor in comparison to that of α spectrometry. This analysis of α nuclides therefore combines chemical separation by liquid-liquid extraction with measurement of α activity by liquid scintillation in the same procedure.[41] Dacheux *et. al* developed a procedure to separate uranium, thorium, plutonium, americium, and curium nuclides from each other before α liquid scintillation counting to improve the results.[41]

1.42 Gamma Spectrometry

Gamma Spectrometry allows an analyst to identify and quantify individual actinide nuclides based on the detection of emitted γ-rays possessing energies that are specific to the nuclear transition in the actinide of interest.[37] Unlike α-particles, γ-rays are highly penetrating and the measurement of individual actinide ions is relatively straightforward because the peaks can be resolved individually by high-resolution detectors.[37] This technique requires little sample preparation, is non-destructive, and multiple radionuclides can be detected simultaneously.[37] Daughter products can also be detected and are sometimes the only route for determining ^{238}U and ^{232}Th, this requires an assumption of radioactive equilibrium.[37] The sensitivity is dependent on

the half-life of the radionuclide and the percent γ-ray intensity.[37] Of the transuranic actinides, ^{237}Np, ^{239}Pu, ^{240}Pu, and ^{241}Am can be detected. The plutonium isotopes have intensity yields < 1 x 10^{-3}, making their direct determination in environmental samples impossible.[37] Broader applications of gamma spectroscopy to most naturally occurring actinides and the environmentally important transuranic actinides are limited by typical long half-lives and/or low intensities for emitted γ-rays.[37]

1.43 Atomic Absorption Techniques

Atomic Absorption techniques are used for quantitative determination of chemical elements based on the absorption and emission of electromagnetic radiation from the atoms and ions. This technique requires a standard, but it works by exciting electrons into higher orbitals by absorbing energy. Each energy is related to a specific electron transition on each individual element.[42] The actinides are able to be measured and determined by atomic absorption spectrometry (AAS), atomic emission spectrometry (AES), flame emission spectrometry (FES), and inductively couple plasma atomic emission spectrometry (ICP-AES).[42]

1.44 Inductively Coupled Plasma

The Inductively Coupled Plasma (ICP) source is an effective and efficient atomization and ionization source that works best with aqueous samples, usually in nitric acid. The high temperature of the ICP source is sufficient enough to ionize the

actinide elements for concentration determination. Progress in mass spectrometry has led to lowering the detection limits, while being fast and requiring less pre-analysis determination of the actinides from each other.[39] It is still necessary to separate the actinides from the matrix, which contains elements that cause isobaric and polyatomic interferences.[39,43] Interferences such as ^{238}U, contributes to *m/z* during ^{237}Np determinations.[37] Isobaric interferences complicate total Pu isotopic analysis: ^{238}U interferes with ^{238}Pu, and ^{241}Am interferes with ^{241}Pu. These interferences can be minimized by utilizing chemical separation procedures such as coprecipitation, liquid-liquid extraction, ion exchange, extraction chromatography, or speciation separations.[37]

1.45 Laser Induced Kinetic Phosphorimetry

Phosphorimetry is a sensitive and selective analytical technique, with low detection limits and a large linear dynamic range for many phosphors.[44] Under excitation by ultraviolet and visible radiation, many uranyl compounds phosphoresce with the emission of a characteristic green light, while uranium in the +3, +4, and +5 oxidation states is non-luminescent due to the absence of –yl oxygens.[44] In solution, uranyl will quench, and therefore it must be protected by complexing it with phosphoric acid to increase the lifetime to a few hundred microseconds.[42]

1.46 Ultra-Violet Visible Spectroscopy

UV-Vis spectroscopy for use in trace metal analysis has been around for a long time. The important characteristics are wide applicability, high sensitivity, moderate to high selectivity, good accuracy, and most importantly for real-time field analysis, ease, and convenience.[45] Chemosensors are non-living molecules that bind selectively and often reversibly with an analyte which causes a change in one or more properties of the system such as color, fluorescence, or redox potential.[46] Recognition and signaling of ionic and neutral species of individual elements is one of the most extensively studied areas of supramolecular chemistry.[46] Among different types of chemosensors, colorimetric sensors are especially attractive, since complexation can trigger a color change that can be seen without any equipment. This type of chemosensor can find direct applications in the development of optodes and disposable dip-stick arrays based on the absorption changes.[46] In these colorimetric chemosensors, a bathochromic or hypsochromic shift of absorption spectra, or visual color change, is caused by the respective increase or decrease in electron densities on the ligand and complex, which is more effectively carried by the association of a charged analyte such as a cation or anion, than a neutral molecule;[46] therefore, most chromogenic sensors are only useful for charged guests.[46]

Expanded porphyrins have been recognized as ligands able to form complexes with cations that are too large to form stable 1:1 complexes with porphyrins.[47] These

systems have been exploited as colorimetric sensors in the detection of high-valent actinides ($U^{VI,}$ Np^{V}, and Pu^{V}).[47] In 2004, Sessler and co-workers reported isoamethyrin, which undergoes a color change from yellow to pink on the exposure of the ions mentioned earlier.[48] In MeOH, color changes with Np and Pu were instantaneous, while the response to U was only fully achieved after 24 hours.[47] Isoamethyrin in MeOH-CH_2Cl_2 95:5 (v/v), the ligand displayed a detection limit for the uranyl cation of ~6 ppm as determined by naked-eye analysis, and 30 ppb as recorded using a standard UV-Vis spectrometer.[47] The kinetics of uranyl complexation (>1 day) make the system impractical as a viable method for the determination of uranyl cation concentration,[49] and copper contamination can deactivate the sensor.

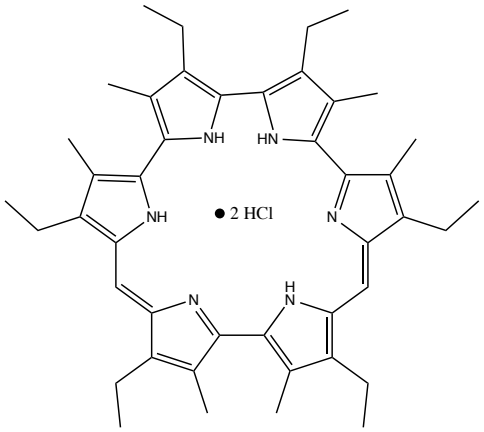

Figure 1.1: Isoamethyrin

In 2008, Melfi, Sessler and co-workers modified isoamethyrin and attached it to a plastic fiber optic for use in the detection of U^{VI} cation in aqueous solution.[50]

Several experiments were used to characterize the structure of the silica-water interface, which demonstrated that cation concentrations may be enhanced at the interface owing to the presence of the native negative charge deriving from the pH dependence of the SiOH groups on the surface.[50] Several chemophotonic molecules were developed as optical sensors for uranyl species; however, like most sensors, they are subject to competitive binding of other metal cations, (such as copper or iron), and therefore false-positive results.[51,52] The ligands in the extraction processes described next are good starting points for sensors and vice-versa because they are often already selective for uranyl or actinides over other metal ions.

1.5 Background for Nuclear Fuel Recycling

The operational life span of a fuel rod in a typical light water reactor is only about 3 years, with only 5% of the energy content contained in the fuel rod being used.[3,8] During the past 60 years, more than 1800 metric tons of plutonium, and substantial quantities of the "minor" actinides, such as neptunium, americium, and curium have been generated in nuclear reactors.[53] There are two strategies concerning the disposition of these heavy elements in nuclear reactors: (1) to "burn" or transmute the actinides using fast breeder reactors or accelerators;[54] and (2) to "sequester" the actinides in chemically durable, radiation resistant materials that are suitable for geological disposal.[55] Reprocessing, while not being performed in the United States currently, is not new, as fuel rods were first processed at the Savannah River Site, with commercial nuclear fuel being reprocessed at the West Valley Reprocessing

plant in New York.[56] Because current reprocessing strategies generate and isolate "weapons-grade" plutonium (^{239}Pu), President Carter suspended reprocessing of spent nuclear fuel (SNF) citing concerns for the potential for proliferation.[56] This has not stopped other nations such as France, the United Kingdom, Russia, Japan, and India from using nuclear power technology and reprocessing their spent fuel.[3] President Reagan lifted the reprocessing ban in 1981, but there was not a substantial enough subsidy to proceed on a private basis, rendering reprocessing commercially impractical.[56] Two reasons cited for considering reprocessing are 1) to increase the available energy from fissile and fertile atoms and (2) to reduce hazards and costs for handling the high-level wastes from the resultant fission products (FPs).[57]

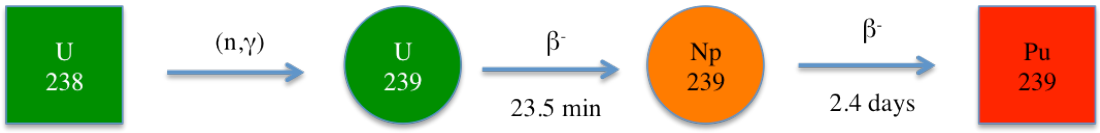

Figure 1.2: Fuel cycle decay to get to Pu-239

There is one additional problem with the reprocessing of spent nuclear fuel and that is the separation of the trivalent actinides from the trivalent lanthanides produced as FPs. This separation is difficult due to the similar oxidation states, chemical properties, and ionic radii. This separation is needed in order to reuse the actinides in either mixed-oxide (MOX) reactors (for uranium and plutonium) or fast-breeder reactors (FBR) (for neptunium, americium, and curium) as part of the partitioning and transmutation (P&T) strategy that is being explored in France and

Japan.[42] The lanthanides possess a large-cross section for neutron capture, thus as lanthanides build up from fission products, the nuclear chain reaction slows down.[58]

1.6 Extraction Processes

1.61 PUREX

The Plutonium Uranium Recovery by Extraction (PUREX) process is the most widely used recycling process for commercial uranium fuel rods.[59,60] The extractant is tri-n-butyl phosphate (TBP) (30%) in either dodecane or kerosene as the solvent.[55,61] TBP has good radiolytic and chemical stability, low aqueous solubility, and its chelating properties made it possible to efficiently eliminate the undesired fission products and minor actinide by-products, while cleanly separating uranium and plutonium.[62] Like the first extraction processes in the 1940s, extraction is repeated several times throughout the cycle even though the first few steps remove over 99% of U(VI) and Pu(IV), 90% of Np(V), and leaving all but 0.1% of the fission products and minor actinides in the aqueous raffinate.[61] After that, Pu and U are separated by reducing Pu(IV) to Pu(III) by a reducing agent such as hydroxylamine or N,N-diethyl-hydroxylamine causing it to precipitate out of solution.[61] The final cycle consists of stripping the uranium using dilute acid, then passing through another cycle of extraction and precipitation for additional decontamination from plutonium and fission products.[62] Currently studied extraction processes, such as the ones below,

hope to improve upon, use in conjunction with, or completely replace the PUREX process.

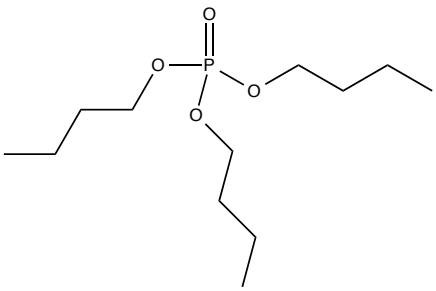

Figure 1.3: tri-n-butlyphosphate (TBP)

1.62 DIAMEX

The Diamide Extraction (DIAMEX) process was developed in France in the late 1980s as a follow-up process to PUREX. The goal of this system was to separate the trivalent actinides from the lanthanides directly from the high activity PUREX raffinate.[63] As the name implies, this process uses a diamide, N,N'-dimethyl-N,N'-dibutyltetradecylmalonamide (DMDBTDMA), a combustible solvating extractant in an aliphatic diluent as the solvent.[64] A new diamide, N,N'-dimethyl-N,N'dioctylhexylethoxymalonamide (DMDOHEMA) has been synthesized. It limits third phase formation due to increased molecular weight. It also enhances the affinity for minor actinides over lanthanide complexation and thereby increasing extraction efficiency.[64] While DMDOHEMA is robust against hydrolysis and radiolysis, there is a narrow range of nitric acid concentrations that allow for good recovery of the

trivalent actinides.[61] The other drawback is increased complexity as compared to TBP.[61]

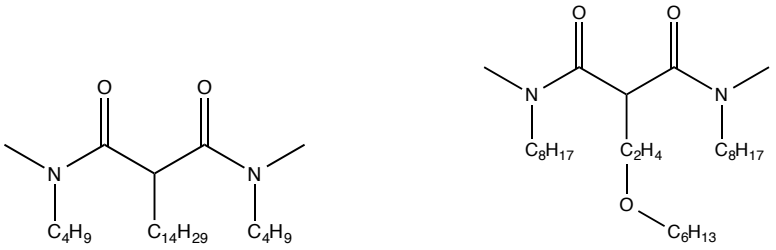

Figure 1.4: DMDBTDMA and DMDOHEMA

1.63 TRUEX

TRUEX stands for Transuranium Extraction, in other words, extraction for the actinides beyond uranium.[65] This process uses (N,N'-diisobutylcarbamoylmethyl)-octylphenylphosphine oxide (CMPO) wherein both the C=O and P=O groups act as bonding donors for extractions.[66] For each metal ion, there are three CMPO molecules.[66] Although the extractions for actinides were very good, the CMPO ligand could not differentiate between the 4*f* and 5*f* elements needed for the transuranium extractions by themselves.[66] The first modification of this extraction process was to combine it with the established PUREX process to create an "all-purpose" actinide extractant from nitric acid waste solutions.[61] While improvements were made immediately, such as the enhanced distribution ratios for Am^{III}, further investigation had problems with stripping and recovery of the metal.[67] There was also the problem

of the lanthanides still being extracted by the CMPO, further complicating reprocessing.[68]

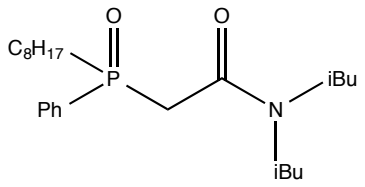

Figure 1.5: CMPO

Much of the focus of research into improving the TRUEX process since 1999 has been to attach CMPO to a fixed structures such as triphenoxy methane[68], or the calixarenes, both the wide and narrow rim.[66,69] The goal was to take advantage of the 3 to 1 binding of the CMPO by preorganizing the supramolecular structure and creating a chelate effect to increase the selectivity for extractions in comparison to mono-CMPO extractants.[68] For the triphenoxy methane platform, it was observed that the ligand would selectively bind thorium over lanthanides, but would have problems binding any higher actinides.[68] The wide and narrow rim calix[4]arenes with CMPO both bound thorium over lanthanides, with the narrow-rim calixarene a considerably better extractant for thorium and maintained the ability to extract it in > 2 M HNO_3.[66] Higher actinide selectivity was unpredictable with some lanthanides having selectivity equal to the actinides.[68]

1.64 Cyanex

Cyanex 301 is the dithio analogue of the carboxylic acid Cyanex 272, which was originally developed for selective extraction of zinc from calcium containing effluent streams.[70] Increasing the sulfur substitution increases the acidity of the extractants making them better suited to extract the softer Lewis acids of the actinides versus the lanthanides.[71-73] While Cyanex 301 can only differentiate between Am^{III} and lanthanides in solutions at a pH lower than 3, the ligand will decompose in these acidic solutions.[74-77] Further studies have been undertaken to investigate different dithiophosphinic acids for minor actinide extractions.[76,77] A modification involving an aromatic dithiophosphinic acid was synthetically challenging but offered a more hydrolytically, radiolytically, and acidically stable system while exhibiting a separation factor (SF) of ~100000 at low pH.[75] This goes against the carbon, hydrogen, oxygen, and nitrogen (CHON) principle. In this principle, it is considered highly desirable to only contain the elements carbon, hydrogen, oxygen or nitrogen (C-H-O-N) because, if the ligand were to be incinerated, it would be a direct cause of acid rain, and thus has been minimally investigated further.

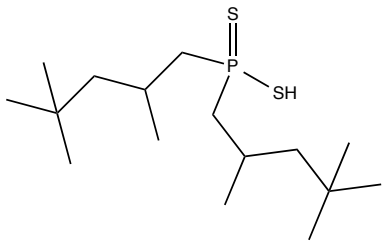

Figure 1.6: Cyanex 301

1.65 TALSPEAK

Trivalent Actinide-Lanthanide Separation by Phosphorous reagent Extraction from Aqueous Komplexes (TALSPEAK) and reverse TALSPEAK are both, in principle, based on the extraction of lanthanides instead of actinides using di(2-ethylhexyl)phosphoric acid (HDEHP) or a similar cation exchanger, from an aqueous phase that uses polyaminopolyacetic acid complexants to retain the actinides.[78] Reverse TALSPEAK selectively strips the actinides from a loaded organic phase, a process that could be used to recover actinides after reprocessing.[78] HDEHP is a cation exchanger and a chelating agent that in the organic phase, will form a tris complex with lanthanides; distribution ratios were for both the actinides and lanthanides were found to be nearly 10^5.[78] Using diethylenetriamine-N,N,N',N",N"-pentacetic acid (DTPA), a complete group separation was achieved using due to the three amine nitrogen atoms in a specific coordination geometry.[78] Recently, the Nash group discovered that a considerable potential for improvement of TALSPEAK-type separations would be achievable by matching the extractant and holdback reagent while reducing the acidity of the extractant.[58] The greater extraction strength of HDEHP may actually be detrimental to the potential of TALSPEAK separations.[58]

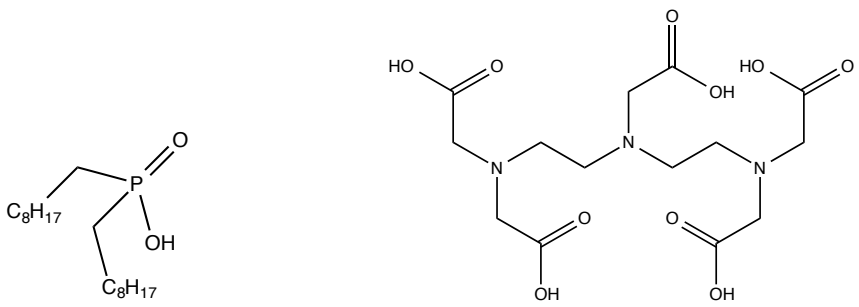

Figure 1.7: HDEHP and DTPA

1.66 SANEX

Another recently developed and promising extraction process is the Selective Actinide Extraction process (SANEX).[79] The first ligand studied was the bis-1,2,4,triazin-3-yloligopyridine (BTP) which was identified as metal extractants specifically with the ability to separate actinides(III) from lanthanides(III) in nitric acid media.[80-82] These early ligands were not able to withstand radiolytic degradation with attacks on the α-benzylic hydrogen atoms by nitrogen oxoacids.[79,83]

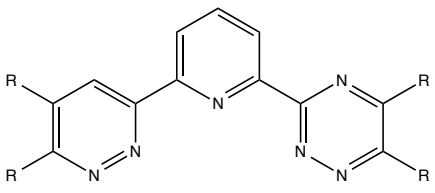

Figure 1.8: BTP

To prevent degradation, the α-benzylic hydrogen atoms were replaced by alkyl groups, and eventually, a cyclohexane ring with four methyl groups to form the 2,6-bis(5,5,8,8,-tetramethyl-5,6,7,8,-tetrahydrobenzo[1,2,4]triazine-3-yl)pyridine ($CyMe_4$-BTP).[79,83] While this ligand was kinetically slower for extractions, the distribution ratio of americium was higher, and the SF between Am^{III} and Eu^{III} was an order of magnitude higher.[79] This was the reference molecule until the 6,6'-bis(5,6-dialkyl[1,2,4]triazine-3-yl)[2,2']bipyridines were developed.[83,84] Much like the BTPs, initially alkyl groups were attached to the annulated rings but the efficiency was lower than that for the BTPs. Putting the same aliphatic ring system from the $CyMe_4$-BTP on the BTBPs, the ligand exhibited affinity toward trivalent actinides and high SFs over the lanthanides while maintaining the stability in nitric acid and radiolytic degradation, allowing recycling of the organic phase in a continuous process.[85,86] This ligand has since become the standard for the SANEX process.[87] More ligands based on the triainzes are currently being developed include the bis-triazines attached to phenanthrolines.[88] This will make the ligand more rigid, which should make complex formation more rapid and thermodynamically favored compared to the bipyridine analogues.[88] The extraction kinetics were much improved as compared to BTBP, and further applications in coordination chemistry are being investigated.[87] Combinations of various processes are being studied to be used as a group actinide extraction process (GANEX), with a combination of PUREX and SANEX leading the way.[89] The other combination is of TALSPEAK and the DIAMEX/SANEX process.[89]

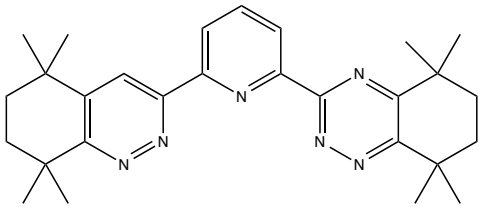

Figure 1.9: $CyMe_4$-BTP

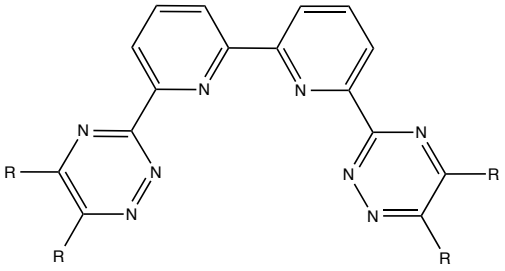

Figure 1.10: BTBP

This research focuses on synthesizing a ligand for molecular recognition of the actinides as a sensor in the environment, and extraction of the actinides as an extractant in nuclear fuel waste.

1.7 References

(1) Administration, U. S. E. I. *Annual Energy Review 2010*, 2011.

(2) Koyama, S.-i.; Suzuki, T.; Mimura, H.; Fujita, R.; Kurosawa, K.; Okada, K.; Ozawa, M. *Prog. Nucl. Energy* **2011**, *53*, 980.

(3) Choppin, G. R. *Sep. Sci. Technol.* **2006**, *41*, 1955.

(4) (NEAC) Nuclear Energy Advisory Committee; Energy, U. S. D. o., Ed. Washington, DC, 2008, p 31 pp.

(5) Agency, I. A. E. *Nuclear Technology Review 2011*, International Atomic Energy Agency, 2011.

(6) Albright, D.; Berkhout, F.; Walker, W. *Plutonium and Highly Enriched Uranium 1996: World Inventories, Capabilities, and Policies*; Stockholm International Peace Research Institute: Oxford University Press: New York, 1997.

(7) Gorden, A. E. V.; Xu, J.; Raymond, K. N.; Durbin, P. W. *Chem. Rev.* **2003**, *103*, 4207

(8) Bruno, J.; Ewing, R. C. *Elements* **2007**, *2*, 343.

(9) Johnson, J. *Chem. Eng. News* **2008**, 15

(10) Committee, M. N. F. C. S. A. *The Future of the Nuclear Fuel Cycle: An Interdisciplinary Study*, Massachussetts Institute of Technology (MIT), 2011.

(11) Gorden, A. E. V.; DeVore, M. A.; Maynard, B. A. *Inorg. Chem.* **2013**, *52*, 3445.

(12) Hayton, T. W.; Boncella, J. M.; Scott, B. L.; Palmer, P. D.; Batista, E. R.; Hay, P. J. *Science* **2005**, *310*, 1941.

(13) Castro-Rodriguez, I.; Nakai, H.; Meyer, K. *Angew. Chem. Int. Ed.* **2006**, *45*, 2389.

(14) Evans, W. J. *Inorg. Chem.* **2007**, *46*, 3435.

(15) Gorden, A. E. V.; Xu, J.; Szigethy, G.; Oliver, A.; Shuh, D. K.; Raymond, K. N. *J. Am. Chem. Soc.* **2007**, *129*, 6674.

(16) Bharara, M. S.; Heflin, K.; Tonks, S.; Strawbridge, K. L.; Gorden, A. E. *Dalton Trans* **2008**, 2966.

(17) Bharara, M. S.; Gorden, A. E. V. *Dalton Trans.* **2010**, *39*, 3557.

(18) Cantat, T. G., Christopher R.; Jantunen, Kimberly C.; Burns, Carol J.; Scott, Brian L.; Schelter, Eric J.; Morris, David E.; Hay, P. Jeffrey; Kiplinger, Jaqueline L. *J. Am. Chem. Soc.* **2008**, *130*, 17537.

(19) Arnold, P. L.; Liddle, S. T. *Chem. Commun.* **2006**, 3959.

(20) Arnold, P. L.; Patel, D.; Wilson, C.; Love, J. B. *Nature* **2008**, *451*, 315.

(21) Wells, D. M.; Ringe, E.; Kaczorowski, D.; Gnida, D.; Andre, G.; Haire, R. G.; Ellis, D. E.; Ibers, J. A. *Inorg. Chem.* **2011**, *50*, 576.

(22) Seaman, L. A.; Fortier, S.; Wu, G. A.; Hayton, T. W. *Inorg. Chem.* **2011**, *50*, 636.

(23) Seaman, L. A.; Hrobarik, P.; Schettini, M. F.; Fortier, S.; Kaupp, M.; Hayton, T. W. *Angew. Chem. Int. Ed. Engl.* **2013**, *52*, 3259.

(24) Ozdemir, N.; Sahin, M.; Bal-Demirci, T.; Ulkuseven, B. *Polyhedron* **2011**, *30*, 515.

(25) Newell, B. S.; Schwaab, T. C.; Shores, M. P. *Inorg. Chem.* **2011**, *50*, 12108.

(26) Marie, C.; Miguirditchian, M.; Guillaumont, D.; Tosseng, A.; Berthon, C.; Guilbaud, P.; Duvail, M.; Bisson, J.; Guillaneux, D.; Pipelier, M.; Dubreuil, D. *Inorg. Chem.* **2011**, *50*, 6557.

(27) Lewis, A. J.; Williams, U. J.; Kikkawa, J. M.; Carroll, P. J.; Schelter, E. J. *Inorg. Chem.* **2012**, *51*, 37.

(28) Benaud, O.; Berthet, J. C.; Thuery, P.; Ephritikhine, M. *Inorg. Chem.* **2011**, *50*, 12204.

(29) Aspinall, H. C. *Chemistry of the f-Block Elements*; Gordon and Breach Publishers: Amsterdam, 2001; Vol. 5.

(30) Minasian, S. G.; Keith, J. M.; Batista, E. R.; Boland, K. S.; Clark, D. L.; Kozimor, S. A.; Martin, R. L.; Shuh, D. K.; Tyliszczak, T. *Chem. Sci.* **2014**.

(31) Neidig, M. L.; Clark, D. L.; Martin, R. L. *Coord. Chem. Rev.* **2013**, *257*, 394.

(32) Clark, D. L.; Keogh, D. W.; Palmer, P. D.; Scott, B. L.; Tait, C. D. *Angew. Chem., Int. Ed. Eng.* **1998**, *37*, 164

(33) Bond, E. M.; Duesler, E. N.; Paine, R. T.; Neu, M. P.; Matonic, J. H.; Scott, B. L. *Inorg. Chem.* **2000**, *39*, 4152.

(34) Schnaars, D. D.; Batista, E. R.; Gaunt, A. J.; Hayton, T. W.; May, I.; Reilly, S. D.; Scott, B. L.; Wu, G. *Chem. Commun.* **2011**, *47*, 7647.

(35) Braley, K. L. N. a. J. C. In *Advanced Separation Techniques for Nuclear Fuel Reprocessing*; Lumetta, K. L. N. a. D. G. J., Ed.; Woodhead Publishing Limited: 80 High Street, Sawston, Cambridge, CB22 3HJ, UK, 2011; Vol. 2, p 3.

(36) Macfarlane, A. M. *Science* **2011**, *333*, 1225.

(37) Wolf, S. In *Chemistry of the Actinide and Transactinide Elements*; 4th ed.; Morss, L. R., Edelstein, N.M., Fuger, J., Ed.; Springer: Dordrecht, The Netherlands, 2010; Vol. 5, p 3273.

(38) Kiliari, T.; Pashalidis, I. *J. Radioanal. Nucl. Chem.* **2010**, *284*, 547.

(39) Ayranov, M.; Krahenbuhl, U.; Sahli, H.; Rollin, S.; Burger, M. *Radiochimica Acta* **2005**, *93*, 249.

(40) Ayranov, M.; Krahenbuhl, U.; Rollin, S.; Burger, M. *J. Radioanal. Nucl. Chem.* **2009**, *279*, 475.

(41) Dacheux, N.; Aupiais, J. *Anal. Chem.* **1997**, *69*, 2275.

(42) *The Chemistry of the Actinide and Transactinide Elements*; 4th ed.; Morss, L. R. E., N.M.; Fuger, J., Ed.; Springs: Dordrecht, The Netherlands, 2010; Vol. 1-6.

(43) Guerin, N.; Calmette, R.; Johnson, T.; Lariviere, D. *Analytical Methods* **2011**, *3*, 1560.

(44) Brina, R.; Miller, A. G. *Anal. Chem.* **1992**, *64*, 1413.

(45) Skoog, D. W., D; Holler F.J.; Crouch, S. *Fundamentals of Analytical Chemistry*; 8th ed.; Thomson Learning Brooks/Cole: Belmont, CA, 2004.

(46) Kaur, N.; Kumar, S. *Tetrahedron* **2011**, *67*, 9233.

(47) Vargas-Zúñiga, G. I.; Sessler, J. L. In *The Rare Earth Elements*; John Wiley and Sons: 2012.

(48) Sessler, J. L.; Melfi, P. J.; Seidel, D.; Gorden, A. E. V.; Ford, D. K.; Palmer, P. D.; Tait, C. D. *Tetrahedron* **2004**, *60*, 11089.

(49) Sessler, J. L.; Melfi, P. J.; Tomat, E.; Lynch, V. M. *Dalton Trans* **2007**, 629.

(50) Melfi, P. J.; Camiolo, S.; Lee, J. T.; Ali, M. F.; McDevitt, J. T.; Lynch, V. M.; Sessler, J. L. *Dalton Trans.* **2008**, 1538.

(51) Park, C.; Huang, H. Z.; Cha, K. W. *Bull. Korean Chem. Soc.* **2001**, *22*, 84.

(52) Teixeira, L. S. G.; Costa, A. C. S.; Ferreira, S. L. C.; Freitas, M. D.; de Carvalho, M. S. *J. Braz. Chem. Soc.* **1999**, *10*, 519.

(53) Ewing, R. C. *Comptes Rendus Geoscience* **2011**, *343*, 219.

(54) Schaffer, M. B. *Energy Policy* **2011**, *39*, 1382.

(55) Agency, I. A. E. *Spent Fuel Reprocessing Options*, 2008.

(56) Andrews, A.; Congress, U. S., Ed.; Library of Congress: Washington, D.C., 2008.

(57) Choppin, G. R.; Liljenzin, J.-O.; Rydberg, J. *Radiochemistry and Nuclear Chemistry*; 3rd ed.; Butterworth-Heinemann: Woburn, Massachussets, 2002.

(58) Braley, J. C.; Grimes, T. S.; Nash, K. L. *Ind. Eng. Chem. Res.* **2012**, *51*, 627.

(59) Joshi, J. M.; Pathak, P. N.; Manchanda, V. K. *Solvent Extr. Ion Exch.* **2005**, *23*, 663.

(60) May, I.; Taylor, R. J.; Wallwork, A. L.; Hastings, J. J.; Fedorov, Y. S.; Zilberman, B. Y.; Mishin, E. N.; Arkhipov, S. A.; Blazheva, I. V.; Poverkova, L. Y.; Livens, F. R.; Charnock, J. M. *Radiochimica Acta* **2000**, *88*, 283.

(61) Paiva, A. P.; Malik, P. *J. Radioanal. Nucl. Chem.* **2004**, *261*, 485.

(62) Mckibben, J. M. *Radiochimica Acta* **1984**, *36*, 3.

(63) Modolo, G.; Vijgen, H.; Serrano-Purroy, D.; Christiansen, B.; Malmbeck, R.; Sorel, C.; Baron, P. *Sep. Sci. Technol.* **2007**, *42*, 439.

(64) Serrano-Purroy, D.; Baron, P.; Christiansen, B.; Malmbeck, R.; Sorel, C.; Glatz, J. P. *Radiochimica Acta* **2005**, *93*, 351.

(65) Horwitz, E. P.; Kalina, D. G.; Diamond, H.; Vandegrift, G. F.; Schulz, W. W. *Solvent Extr. Ion Exch.* **1985**, *3*, 75.

(66) Barboso, S.; Carrera, A. G.; Matthews, S. E.; Arnaud-Neu, F.; Böhmer, V.; Dozol, J.-F.; Rouquette, H.; Schwing-Weill, M.-J. *J. Chem. Soc., Perk. Trans. 2* **1999**, 719.

(67) Chitnis, R. R.; Wattal, P. K.; Ramanujam, A.; Dhami, P. S.; Gopalakrishnan, V.; Bauri, A. K.; Banerji, A. *J. Radioanal. Nucl. Chem.* **1999**, *240*, 721.

(68) Peters, M. W.; Werner, E. J.; Scott, M. J. *Inorg. Chem.* **2002**, *41*, 1707.

(69) Motornaya, A.; Vatsouro, I.; Shokova, E.; Hubscher-Bruder, V.; Alyapyshev, M.; Babain, V.; Karavan, M.; Arnaud-Neu, F.; Böhmer, V.; Kovalev, V. *Tetrahedron* **2007**, *63*, 4748.

(70) Sole, K. C.; Hiskey, J. B. *Hydrometallurgy* **1992**, *30*, 345.

(71) Sole, K. C.; Hiskey, J. B. *Hydrometallurgy* **1995**, *37*, 129.

(72) Hill, C.; Madic, C.; Baron, P.; Ozawa, M.; Tanaka, Y. *J. Alloys Compd.* **1998**, *271*, 159.

(73) Bhattacharyya, A.; Mohapatra, P. K.; Manchanda, V. K. *Sep. Purif. Technol.* **2006**, *50*, 278.

(74) Matloka, K.; Sah, A. K.; Peters, M. W.; Srinivasan, P.; Gelis, A. V.; Regalbuto, M.; Scott, M. J. *Inorg. Chem.* **2007**, *46*, 10549.

(75) Klaehn, J. R.; Peterman, D. R.; Harrup, M. K.; Tillotson, R. D.; Luther, T. A.; Law, J. D.; Daniels, L. M. *Inorg. Chim. Acta* **2008**, *361*, 2522.

(76) Modolo, G.; Odoj, R. *J. Alloys Compd.* **1998**, *271*, 248.

(77) Modolo, G.; Odoj, R. *J. Radioanal. Nucl. Chem.* **1998**, *228*, 83.

(78) Nilsson, M.; Nash, K. L. *Solvent Extr. Ion Exch.* **2007**, *25*, 665.

(79) Hudson, M. J.; Boucher, C. E.; Braekers, D.; Desreux, J. F.; Drew, M. G. B.; Foreman, M. R. S.; Harwood, L. M.; Hill, C.; Madic, C.; Marken, F.; Youngs, T. G. A. *New J. Chem.* **2006**, *30*, 1171.

(80) Chitnis, R. R.; Wattal, P. K.; Ramanujam, A.; Dhami, P. S.; Gopalakrishnan, V.; Bauri, A. K.; Banerji, A. *J. Radioanal. Nucl. Chem.* **1999**, *240*, 727.

(81) Kolarik, Z.; Mullich, U.; Gassner, F. *Solvent Extr. Ion Exch.* **1999**, *17*, 1155.

(82) Kolarik, Z.; Mullich, U.; Gassner, F. *Solvent Extr. Ion Exch.* **1999**, *17*, 23.

(83) Geist, A.; Hill, C.; Modolo, G.; Foreman, M. R. S. J.; Weigl, M.; Gompper, K.; Hudson, M. J. *Solvent Extr. Ion Exch.* **2006**, *24*, 463.

(84) Drew, M. G. B.; Foreman, M. R. S.; Geist, A.; Hudson, M. J.; Marken, F.; Norman, V.; Weigl, M. *Polyhedron* **2006**, *25*, 888.

(85) Magnusson, D.; Christiansen, B.; Glatz, J. P.; Malmbeck, R.; Modolo, G.; Serrano-Purroy, D.; Sorel, C. *Radiochimica Acta* **2009**, *97*, 155.

(86) Magnusson, D.; Christiansen, B.; Malmbeck, R.; Glatz, J. P. *Radiochimica Acta* **2009**, *97*, 497.

(87) Hudson, M. J.; Harwood, L. M.; Laventine, D. M.; Lewis, F. W. *Inorg. Chem.* **2013**, *52*, 3414.

(88) Lewis, F. W.; Harwood, L. M.; Hudson, M. J.; Drew, M. G. B.; Desreux, J. F.; Vidick, G.; Bouslimani, N.; Modolo, G.; Wilden, A.; Sypula, M.; Vu, T. H.; Simonin, J. P. *J. Am. Chem. Soc.* **2011**, *133*, 13093.

(89) Aneheim, E.; Ekberg, C.; Fermvik, A.; Foreman, M. R. S.; Retegan, T.; Skarnemark, G. *Solvent Extr. Ion Exch.* **2010**, *28*, 437.

Chapter 2: Bis-dithiophosphonate ligands for metal extraction

Portions are previously published in DeVore II, M.A., Gorden, A.E.V.; *Polyhedron* **2012,** 42, 271-275

2.1 Introduction

Organophosphorous extractants have played a major role in actinide extractions.[1] Many of these extractants are commercially available, generally inexpensive and stable, and have been widely studied in the last few decades, in particular with respect to transition metal separation from weakly acidic media.[2] Early work by Ritcey, Flett, and co-workers used di-(2-ethylhexyl)-phosphoric acid (D2EHPA) (figure 1), an alkylphosphoric acid.[2] The development of phosphonic and phosphinic acid extractants, such as 2-ethylhexylphosphonic acid mono-2 ethylhexyl ester (PC88A) and bis-(2,4,4-trimethylpentyl)phosphinic acid (Cyanex 272), have led to further improved separations following the order: phosphoric < phosphonic < phosphinic acid.[2-4]

In more recent years, Cyanex 301 and 302 (figure 2.1) have received considerable attention for their ability to differentiate between the trivalent lanthanides and actinides,[5,6] as well as their ability to extract soft transition metals.[2]

What makes Cyanex 301 a good potential extraction agent is that it can clearly differentiate between actinides and lanthanides in solutions of a pH lower than 3.[7]

Whereas several methods of spent nuclear fuel (SNF) separations have focused on extraction agents containing a single dithiophosphinic acid group like Cyanex 301, we report the preparation and simple extractions with bis-dithiophosphinites.[8,9] The purpose of design herein is to incorporate two dithiophosphinic acid groups connected by a linker to take advantage of the chelate effect to increase selectivity for actinides.

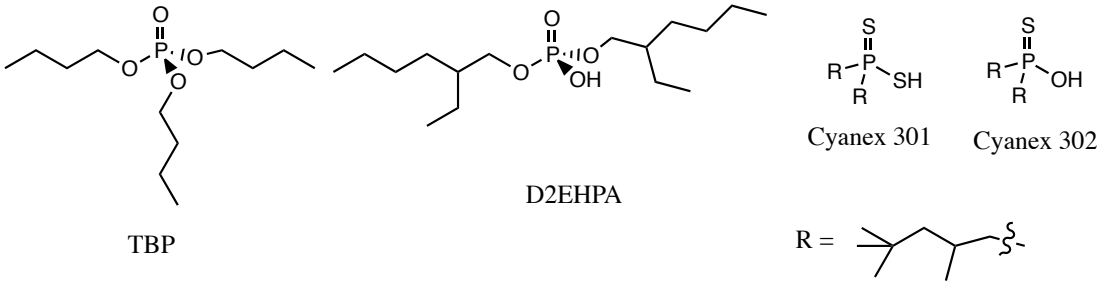

Figure 2.1: Organophosphorous reagents.

2.2 Experimental

Lawesson's reagent, uranyl nitrate, cuprous chloride, gadolinium chloride, 1,3-propanediol, and 1,5-pentanediol, were purchased from Acros and used without any further purification. The pH was recorded on a Fischer Scientific AR15 pH meter. UV-Vis data was collected on a Cary 50 UV-Vis spectrophotometer with a xenon lamp in the range of 200-1100 nm. The ^{1}H, ^{13}C, and ^{31}P NMR data were recorded on a Bruker AV 250 spectrophotometer with CD_3OD, $CDCl_3$ or d_6-DMSO as the solvent using tetramethylsilane as the reference. 100 ppm standards were purchased and diluted to ~2 ppm and used for calibration of the inductively couple plasma-optical emission spectrometer (ICP-OES). Distribution is defined as $[Metal]_{org}$ / $[Metal]_{aq}$. separation factor (SF) is defined as D_{Cu} / D_{Uranyl}.

2.3 Synthesis of the ligands

Ligands were prepared according to literature procedures.[8,9] To a solution of diol (10 mmol) in toluene (30 mL), 4.0 g (10 mmol) of Lawesson's Reagent was added. The mixture was stirred at 70°C until all the solids had dissolved and left to stir overnight. The solvent was removed on a roto-vap until the remaining volume was ~10 mL. Hexane (30 mL) was added to precipitate the product as a green oil

confirmed by ^{1}H NMR (Scheme 2.1). The product could then be precipitated as a salt by bubbling NH_3 into the solution.

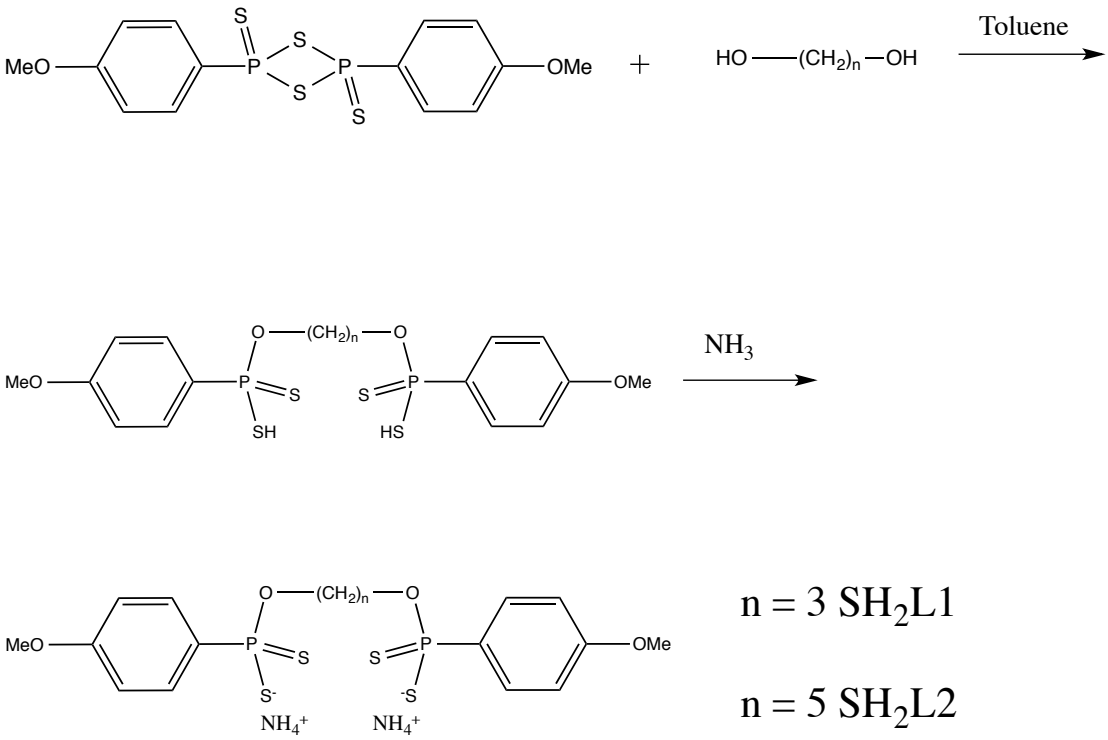

Scheme 2.1: Synthesis of the ligands

2.4 Extraction and Hydrolysis Studies

Two-phase extraction studies in methylene chloride/water (DCM/H_2O) were performed to determine the extraction capability for the removal of Cu^{2+} ions from aqueous solution. The ligands SH_2L1 and SH_2L2, which are quantitatively soluble in DCM, were used for extraction studies. Fresh solutions of $CuCl_2 \cdot 2H_2O$, $UO_2(NO_3)_2 \cdot 6H_2O$, or $GdCl_3$ were prepared in DI water, and the pH was adjusted with HNO_3 and KOH (±0.05). Simple extractions were tested at pH 4 with a ratio of 1:1 metal to ligand for compounds SH_2L1 and SH_2L2. The phases were agitated by stirring for the time periods indicated, then given 24 hours to equilibrate. After the equilibrium was complete, the organic layer drawn off into a separate vial.

2.5 Results and Discussion

The ligands SH_2L1 and SH_2L2 each possess four potential donor atoms to complex with metal atoms and are designed to take advantage of the chelate effect to enhance the efficiency of extractions. Although there are only a few examples of metal complexes of similar ligands, mass spectrometry has shown that the complexes can be either mononuclear or dinuclear.[9] Dithiophosphinate ligands without the

carbon bridge, such as Cyanex 301, can form many crystallographic species. Verani and co-workers reported crystal structure with Pt^{2+}, Pd^{2+}, and Ni^{2+}, were shown to have 1:2 metal to ligand complexes[10,11], whereas Karakus and co-workers have described a 2:4 metal to ligand crystal structure with cadmium in which two ligands have both donors coordinating to a single cadmium ion, while the other two ligands bridge the two metal centers.[12] Crystals suitable for X-ray diffraction were not able to be grown from SH_2L1 and SH_2L2.

Stock solutions of SH_2L1 and SH_2L2 were prepared by dissolving the respective ligand in DCM while an equivalent volume of an aqueous solution at pH 1-14 (± 0.05, adjusted with HNO_3 and KOH) was added to separate vials each containing SH_2L1 or SH_2L2 in DCM and shaken for 60 seconds. The solutions were left undisturbed over night, the organic layer isolated and the UV-Vis spectra taken. The extent of the hydrolysis was interpreted relative to the spectra for the ligand at neutral pH.

The two-phase hydrolysis study of SH_2L1 indicated the ligand hydrolyzes in the extreme pH conditions of 1-2 and 12-14 whereas SH_2L2 is hydrolyzed at pH 1-2 and 11-14. The UV-Vis spectra can be seen in Figures 2.2 and 2.3.

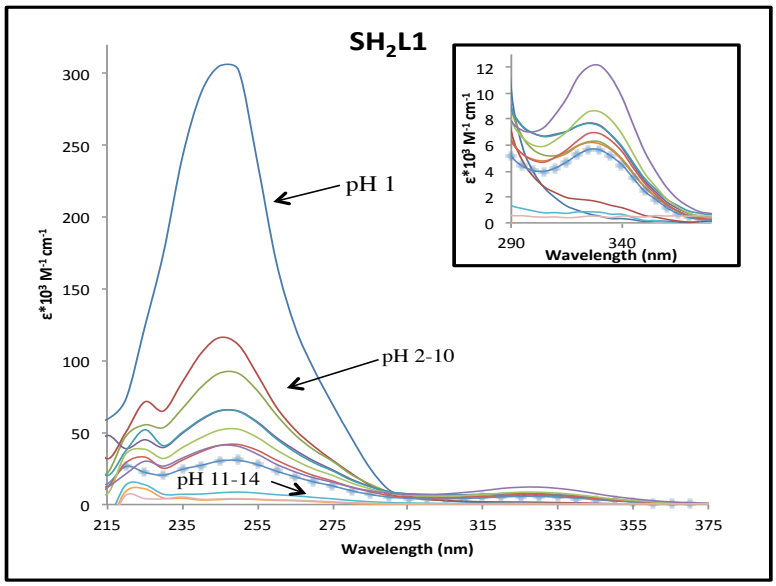

Figure 2.2: UV-Vis of the hydrolysis of SH_2L1. X indicates neutral pH

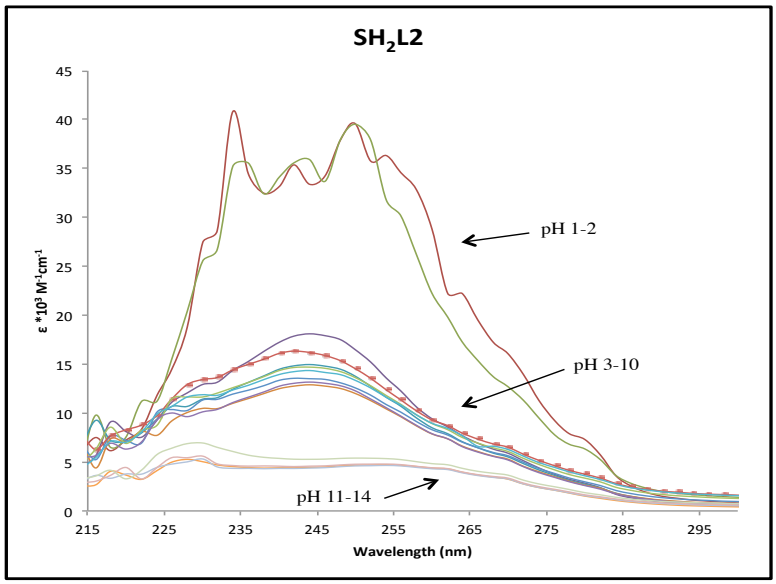

Figure 2.3: UV-Vis of the hydrolysis of SH_2L2. X indicates neutral pH.

The two phase extraction studies described herein were performed at pH 4.0 since the ligands only hydrolyze in extreme acidic conditions, typical of current extraction processes. The ligands were dissolved in DCM while the metal salts were dissolved in the aqueous phase, both at a concentration of 10 μM. The two phases were mixed by constant stirring on a magnetic stir plate for the indicated time. If the concentrations of the ligands went above 10 μM, a third layer could clearly be visible, therefore using UV-Vis spectroscopy to track extractions based on the uranyl peak was undesirable.

SH_2L1 was able to extract about 48% (± 0.5) of the copper ions after 8 hours and 57% (± 0.5) after 12 hours; however, after 24 hours, the metal ion concentration in the aqueous phase increased to about 50% (± 0.3) of the original solution, indicative of a third phase formation (Figure 2.5). The extraction of uranyl was a modest 41% (± 0.7) after 8 and 12 hours, and just as with copper, there was a increase in the uranyl concentration in the aqueous phase. As would be predicted by hard-soft acid base theory (HSAB), the soft base sulfur donors have a poor affinity for the hard acid gadolinium and only 17% (± 1) was extracted was after 8 hours.

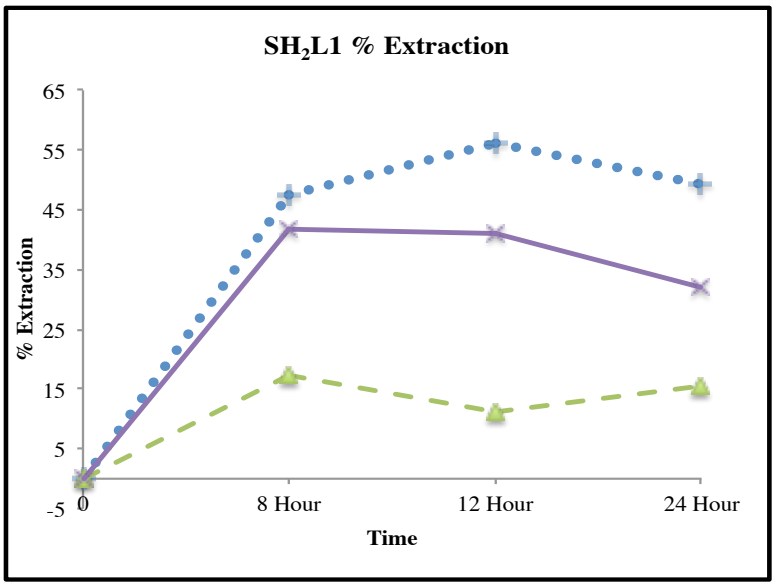

Figure 2.4: Percent extraction of copper (•), gadolinium (- -), and uranyl (-) by SH_2L1 at 8,12, and 24 hours.

The distribution ratio of copper with SH_2L1 was found to be ~1 but is much less for the other metal ions, meaning that approximately half the copper ions were extracted while less than half of other metal ions were extracted into the organic phase. However, the separation factor of uranyl over gadolinium is between 3-5, which indicates there is a extraction preference of uranyl over gadolinium for possible separation of trivalent actinides from lanthanides, with suitable modifications to the ligand.

Metal	8 Hour	12 Hour	24 Hour
Copper	0.91	1.28	0.98
Gadolinium	0.21	0.13	0.18
Uranyl	0.72	0.70	0.47

Table 2.1: Distribution of metal ions after extraction by SH_2L1 at 8,12, and 24 hours.

SH_2L2 has a five carbon linker chain and a bigger binding pocket for a metal ion complexation. After 8 hours, 80% (± 1) of the copper and after 24 hours, 95% (± 1) of the copper had been extracted into the organic phase. This proved interesting, so a shorter time scale was used to determine how quickly the copper could be extracted. After only 5 minutes of stirring, 87% (± 2) of the copper ions had been extracted from the aqueous phase. The extraction stays consistent at ~87% until about 8 hours before it drops to 80% (± 0.2) and increases again at 12 and 24 hours.

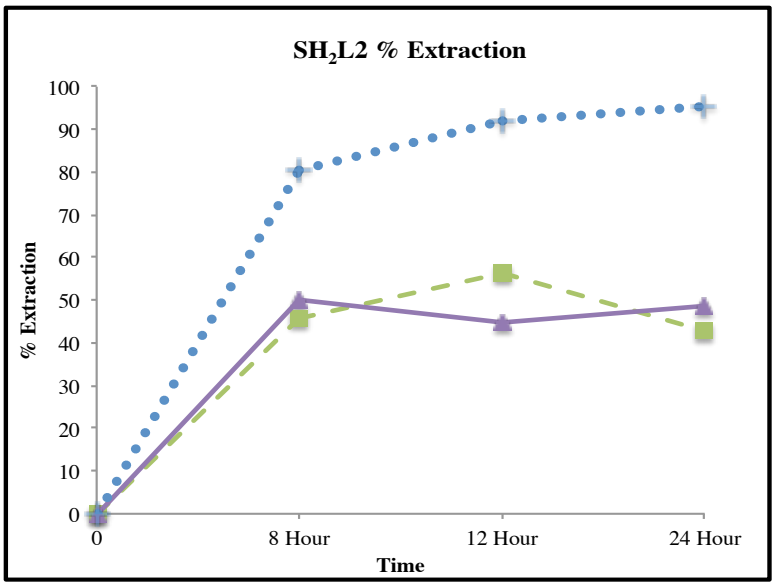

Figure 2.5: Percent extraction of copper (•), gadolinium (- -), and uranyl (-) by SH_2L2 at 8,12, and 24 hours.

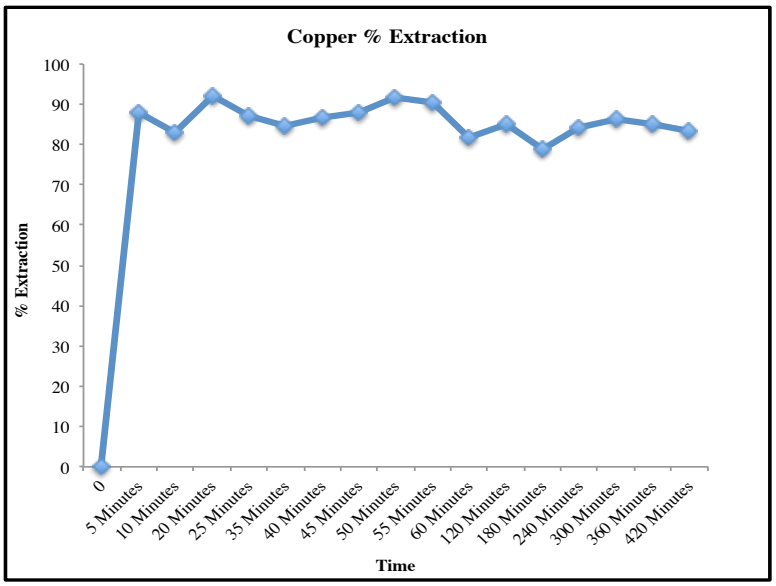

Figure 2.6: Copper % extraction at shorter time lengths for SH_2L2.

The bigger pocket of SH_2L2 does help the extraction of uranyl, gadolinium is also better extracted as it increases from ~20% with SH_2L1 to 50% SH_2L2. SH_2L2 also had issues of a third layer formation at higher concentrations, although not as severe as SH_2L1. The third phase caused many problems, most notably not being able to track extraction by UV-Vis.

Distribution of the copper ion increases after 8 hours to max of 20 after 24 hours, whereas gadolinium peaks at 12 hours and falls at 24 hours. The distribution of uranyl decreases between 8 and 12 hours, but then increases at 24 hours. The

separation factor for SH_2L2 for copper over uranyl increases with time. Although, it would be better to have uranyl bind over copper, this is still confirmation of a problem of uranyl and copper coordinating in the same binding pocket of a ligand.[13]

Metal	8 Hour	12 Hour	24 Hour
Copper	4.17	11.69	20.68
Gadolinium	0.85	1.30	0.76
Uranyl	1.00	0.81	0.95

Table 2.2: Distribution of metal ions after extraction by SH_2L2 at 8, 12, and 24 hours.

Separation Factors	8 Hours	12 Hours	24 Hours
D_{Cu}/D_U	4.18	14.52	21.85

Table 2.3: Separation factor of copper over uranyl for SH_2L2

2.6 Conclusions

Extractions were performed using three metals (Cu^{2+}, Gd^{3+}, and UO_2^{2+}) with two bisdithiophosphinate ligands SH_2L1 and SH_2L2. These ligands undergo

hydrolysis under very acidic conditions, unlike Cyanex 301, and therefore extractions were performed at pH 4. As expected, SH_2L1 was not good at extractions of gadolinium as anticipated from the Pearson theory of Hard and Soft Acids and Bases.[14] It did have moderate extraction of both copper and uranyl at 50 and 40% respectively. SH_2L2 with the two extra carbons for the linking chain, which increases the binding pocket, was a much better ligand for the extraction of all three metals. Copper had the highest extraction with nearly 100% extraction. More improvements to the ligands need to be made so that they are soluble in more common organic solvents such as kerosene, to deter the formation of a third phase that would hinder extractions.

2.7 References

(1) Musikas, C. *Inorg. Chim. Acta* **1987**, *140*, 197.

(2) Sole, K. C.; Hiskey, J. B. *Hydrometallurgy* **1992**, *30*, 345.

(3) Komasawa, I.; Otake, T. *J. Chem. Eng. Jpn.* **1984**, *17*, 417.

(4) Preston, J. S. *Hydrometallurgy* **1982**, *9*, 115.

(5) Hill, C.; Madic, C.; Baron, P.; Ozawa, M.; Tanaka, Y. *J. Alloys Compd.* **1998**, *271*, 159.

(6) Bhattacharyya, A.; Mohapatra, P. K.; Manchanda, V. K. *Sep. Purif. Technol.* **2006**, *50*, 278.

(7) Matloka, K. e. a. *C.R. Chimie* **2007**, *10*.

(8) Gataulina, A. R.; Safin, D. A.; Gimadiev, T. R.; Pinus, M. V. *Transition Met. Chem.* **2008**, *33*, 921.

(9) Karakus, M.; Yilmaz, H.; Bulak, E. *Russian Journal of Coordination Chemistry* **2005**, *31*, 316.

(10) Aragoni, M. C.; Arca, M.; Demartin, F.; Devillanova, F. A.; Graiff, C.; Isaia, F.; Lippolis, V.; Tiripicchio, A.; Verani, G. *Journal of the Chemical Society-Dalton Transactions* **2001**, 2671.

(11) Aragoni, M. C.; Arca, M.; Demartin, F.; Devillanova, F. A.; Graiff, C.; Isaia, F.; Lippolis, V.; Tiripicchio, A.; Verani, A. *Eur. J. Inorg. Chem.* **2000**, 2239.

(12) Karakus, M.; Yilmaz, H.; Ozcan, Y.; Ide, S. *Appl. Organomet. Chem.* **2004**, *18*, 141.

(13) Sessler, J. L.; Melfi, P. J.; Pantos, G. D. *Coord. Chem. Rev.* **2006**, *250*, 816.

(14) Pearson, R. G. *J. Am. Chem. Soc.* **1963**, *85*, 3533.

Chapter 3: Quinoxolinol salen ligands for colorimetric sensors

3.1 Introduction

Uranium is a naturally occurring element found at trace levels in the environment,[1,2] and it is a significant soil and water contaminant at sites associated with uranium mining, nuclear fuel production, and disposal.[3] Because uranyl is stable, water soluble, and mobile, it is readily transported through most soil matrices. The rate of uranyl migration depends on several parameters, including soil porosity and composition, water content, and temperature.[2-4] Methods that have been used for the detection of uranium include thin layer chromatography,[1,5] phosphorimetry,[6] fluorescence,[7,8] x-ray fluorescence,[9] inductively coupled mass spectrometry (ICP-MS),[10,11] surface enhanced Raman scattering (SERS),[12] and colorimetry.[13] Fluorimetry is a sensitive technique that is applicable even to low levels of uranium,[4,14] but the environment around a sensor or the presence of other naturally occurring metals could quench the fluorescence, and designing a selective turn-on sensor is difficult.[6,15-17] X-ray fluorescence, a wavelength dispersive method, is not sensitive enough for estimation at low levels. Phosphorimetry, SERS, and ICP are not readily mobile, are expensive, and often require a labor-intensive sequence of sampling, chemical treatment, preparation, measurement, and data treatment,[12,18-20] making on-site, real-time sensing difficult.[2]

Colorimetric sensors have the potential advantage of on-site, real-time sampling and determination without complicated separations or costly instruments. Spectrophotometry has been increasingly employed in process control since it is simple and adaptable technique.[4] UV-Vis units can be small and portable, and thus, only require the ligand to bind to the metal. Only a few sensors for uranium have been reported,[2,13] and these probes are not selective for uranyl over copper or other metal ions.[4,21-25] Here, we report the application of a previously synthesized ligand in the molecular recognition of uranyl.

3.2 Experimental

3.21 General Procedure

Dimethylformamide (DMF) was purchased and used without further purification. Uranyl(VI) acetate, copper(II) acetate, gadolinium(III) chloride, cobalt(II) nitrate, nickel(II) nitrate, and cerium(III) acetate were used without further purification. UV-Vis spectroscopy was performed on a Cary 50 UV-Vis spectrometer with a Xenon lamp with absorbance spectra from 200-1100 nm with a 1.0 cm width quartz cuvette. Fluorescence spectroscopy was performed on a Shimadzu RF-5301 PC fluorospectrophotometer with a 1.0 cm width quartz cuvette with an excitation wavelength of 350 nm and an emission spectrum of 375-900 nm.

3.22 Synthesis of Ligands[26]

The "salqu" ligand was synthesized as previously described by our group and dissolved in DMF.[26] 2,4-Difluoro-3,5-dinitro benzene was dissolved in THF and d-leucine methyl ester and 2.2 equiv. of DIPEA were mixed together. Ammonium hydroxide in water (3 equiv.), was employed in the substitution of the second fluorine. After reduction using wet Pd/C, the target intermediate was recrystallized from 95% ethanol (Scheme 1). For H_2L1 and H_2L2, 3,5-di-*tert*-butyl salicylaldehyde was dissolved in EtOH with the intermediate and 5 mol% trifluroacetic acid (TFA) at 80 ºC overnight to form the di-substituted ligand (Scheme 2). For H_3L3, 3,5-di-*tert*-butyl salicylaldehyde was dissolved in EtOH with the intermediate at 80 ºC for 24 hours to form the mono-substituted salqu ligand (Scheme 3).

3.23 Metal Titration and K_b Studies

The ligands, H_2L1 and H_3L2, were dissolved in DMF for metal titration and K_b studies. Fresh solutions of $Cu(OAc)_2 \cdot 2H_2O$, $UO_2(OAc)_2$, $Co(NO_3)_2 \cdot 4H_2O$, $Gd(OAc)_3$, $Ce(OAc)_3$, and $Ni(NO_3)_2$ were dissolved in deionized water and diluted to the appropriate concentrations with deionized water. Batch titrations were performed with constant ligand concentration and water content. Serial titrations were performed with no regard for dilution and final ligand concentration. K_b studies were undertaken using non-linear regression with a minimum sum of the least squares, by varying the

ligand concentration and keeping the metal concentration controlled. All individual metal UV-Vis spectra for the descibed experiments are located in Appendix 1.

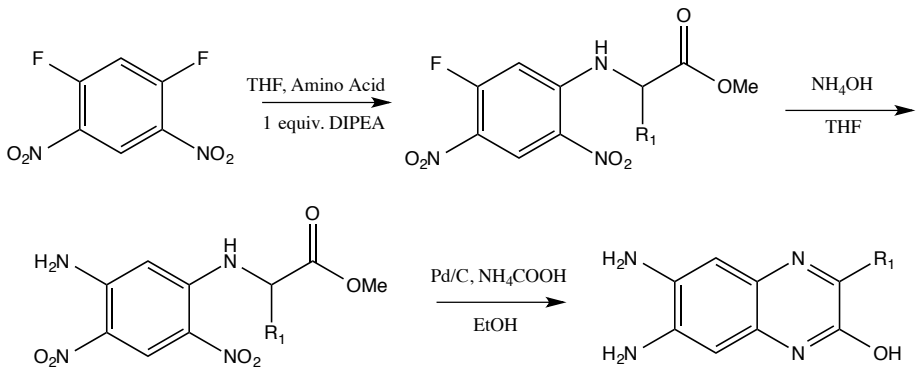

Scheme 3.1: Synthesis of quinoxolinol backbone

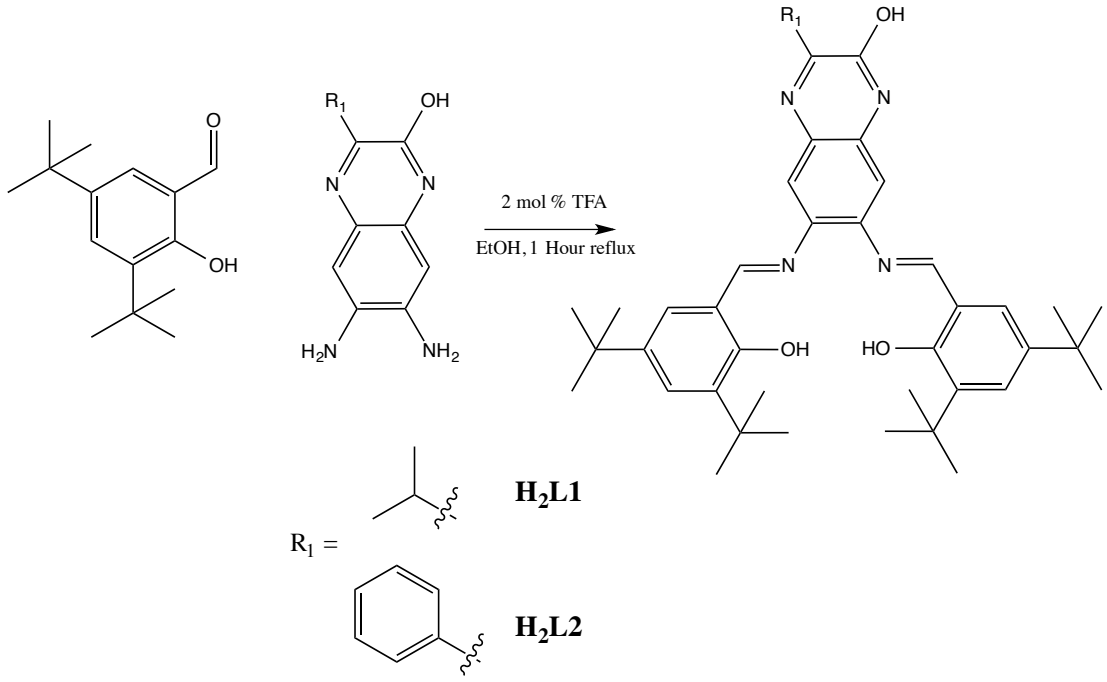

Scheme 3.2: Synthesis of di-substituted ligand

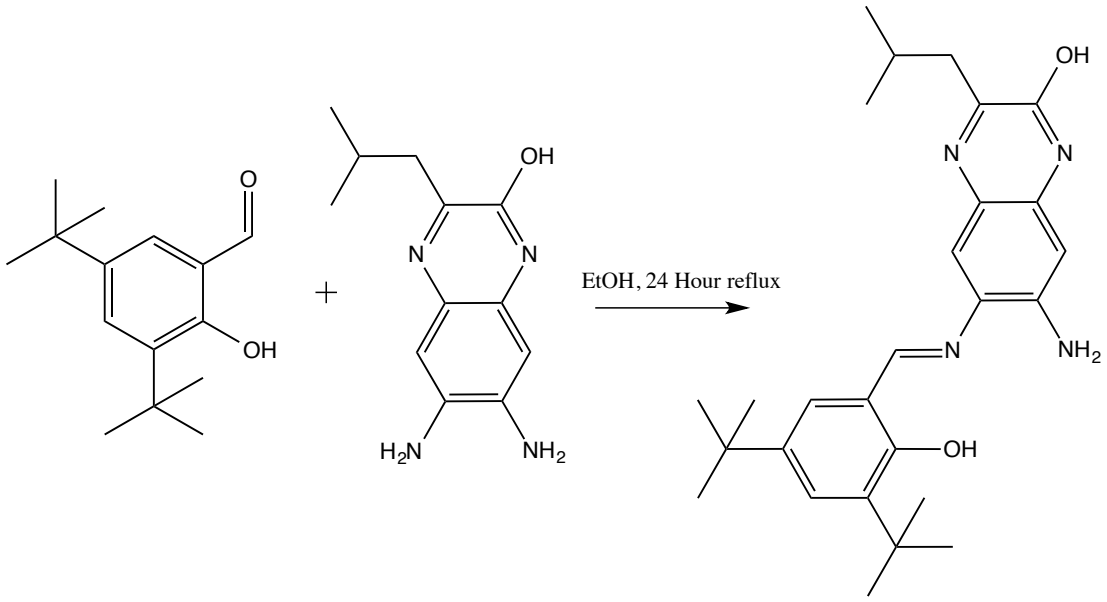

H_3L3

Scheme 3.3: Synthesis of mono-substituted ligand

3.3 Results

The advantage to using the quinoxolinol salen (Salqu) ligands is that the conjugated pi-system results in more intense UV-Vis spectra, thereby, allowing lower concentrations to be used in sensing experiments. Batch titrations were performed to determine the selectivity and photo-physical responses of the ligands for various metals, with special attention paid to distinguishing the differences between copper and uranyl, and uranyl and the ligand. Although the ligands themselves are not water-soluble, it was best to do as little pre-treatment to the metal solutions as possible. The

ligands were tested for solubility in water, acetonitrile, dimethylsulfoxide (DMSO), N,N'-dimethylformamide (DMF), pyridine, methylene chloride (DCM), methanol, hexane, toluene, tetrahydrofuran (THF) and octanol. THF had the highest solubility of the ligands and was chosen as the starting solvent. There were only slight changes in the UV-Vis spectra of the metal complexes, and there was also the problem of the solvent evaporating. This evaporation creates potential problems if this ligand is used as pre-made solutions that need to be stored for a long time. The next logical step was to characterize the ligands in a higher boiling point solvent, such as DMF, that is still miscible with water.

Batch and serial titrations were performed to determine any changes of the UV-Vis spectrum of the ligand as the metal concentrations increased. A batch titration was set up as ten vials all with the same ligand concentration and final water volume. Then, different concentrations of metal ranging from 20 μM metal (1:1 metal to ligand) to 200 μM (10:1 metal to ligand) were added to the vials labeled 1-10 respectively for the metal concentration they contained. The solutions were then stirred for 2 hours. During this time, the colors of the solutions changed, indicative of metal ion complexation. The procedure for the batch titration applied is detailed in Chart 3.1.

Metal to Ligand Ratio	Ligand in DMF(mL)	Metal in water (mL)	Water (mL)	DMF (mL)	Final Metal Concentration
1 : 1	5	0.2	1.8	3	20 uM
2 : 1	5	0.4	1.6	3	40 uM
3 : 1	5	0.6	1.4	3	60 uM
4 : 1	5	0.8	1.2	3	80 uM
5 : 1	5	1	1	3	100 uM
6 : 1	5	1.2	0.8	3	120 uM
7 : 1	5	1.4	0.6	3	140 uM
8 : 1	5	1.6	0.4	3	160 uM
9 : 1	5	1.8	0.2	3	180 uM
10 : 1	5	2	0	3	200 uM

Chart 3.1: Batch titration set up for 20% water/DMF solution and 40 μM ligand stock and 1 mM metal stock solution for final concentrations of 20 μM ligand and the desired final concentration of metal. Total volume for each solution is 10 mL.

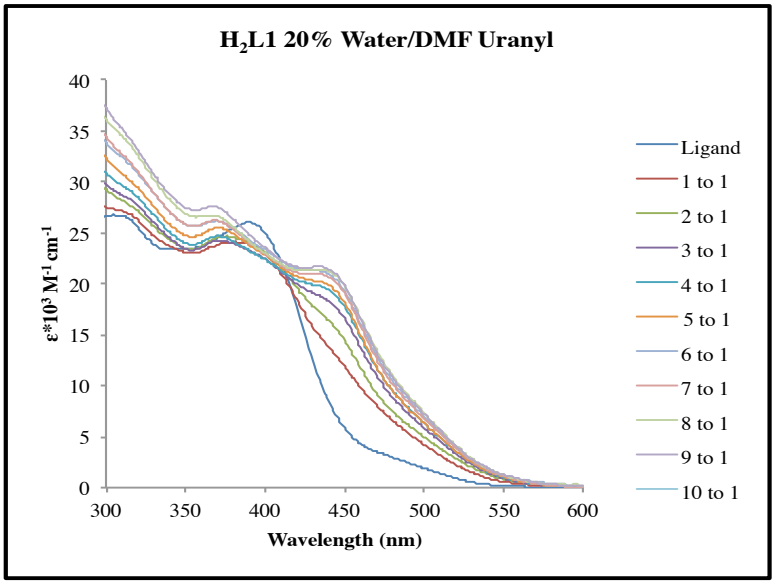

Figure 3.1: Example of batch titration with uranyl and H_2L1. The uranyl concentration was increased from a 1:1 metal to ligand ratio to a 10:1 metal to ligand ratio.

To determine additional real-time data, serial titrations were performed. A typical procedure would start with a solution of ligand, to which an aliquot of aqueous metal solution would be added (0.1:1 metal to ligand for each aliquot). The resulting solution would be stirred for 5 minutes, measured, and then, the next aliquot added. This however, gives no regard as to the concentration of the water, and thus it had to be performed at low final water percentage to prevent the ligand from precipitating.

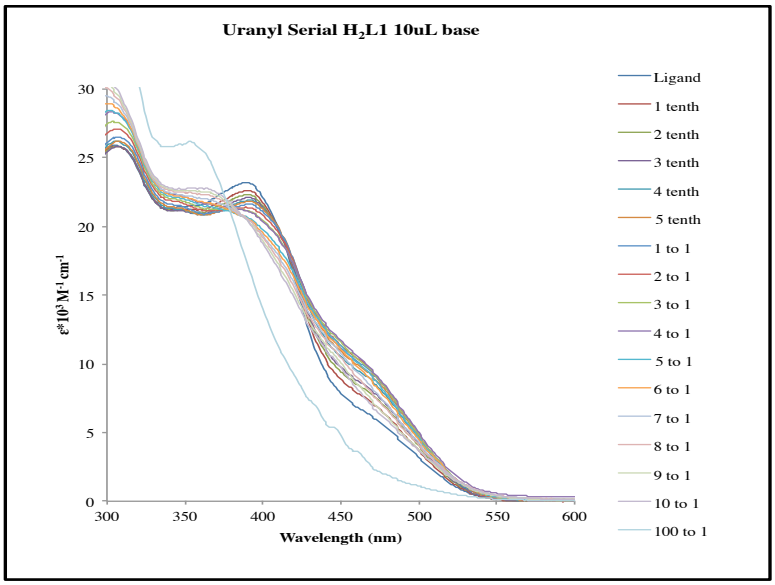

Figure 3.2: Example of serial titration with uranyl and H_2L1. Uranyl concentration was increased from a 0.1:1 metal to ligand to 100:1 metal to ligand ratio

The first method tested was to perform the UV-Vis characterization with solute and chromophore dissolved in DMF. This, of course, would require first concentrating whatever water sample was obtained, and then adding DMF to it and

assuming all trace metal dissolves. While the full approach was not taken, the metals were dissolved in a small amount of water, and then diluted to the appropriate concentrations with DMF a few times to have less than 1% water in the total system with no precipitate observed. The graph for H_2L1, with copper, and with uranyl can be seen in Figure 3.3. The ligand had a maximum absorbance at 387 nm with an extinction coefficient of 2.6 x 10^4 M^{-1} • cm^{-1}. There is a substantial increase in absorption upon reaction with copper(II) acetate at 450 nm and 328 nm, with molar extinction coefficients of 3.9 x 10^4 M^{-1} • cm^{-1} and 2.9 x 10^3 M^{-1} • cm^{-1}, respectively. Concomitant with these increases, the band attributed to the free ligand decreases in intensity. Uranyl had a maximum absorbance peak at 376 nm, with an extinction coefficient of 2.8 x 10^4 M^{-1} • cm^{-1}, a shift of 11 nm from the ligand peak. This separation between the ligand and uranyl, and between uranyl and copper, could be used to differentiate the metals and distinguish actinides in the environment from other metals.

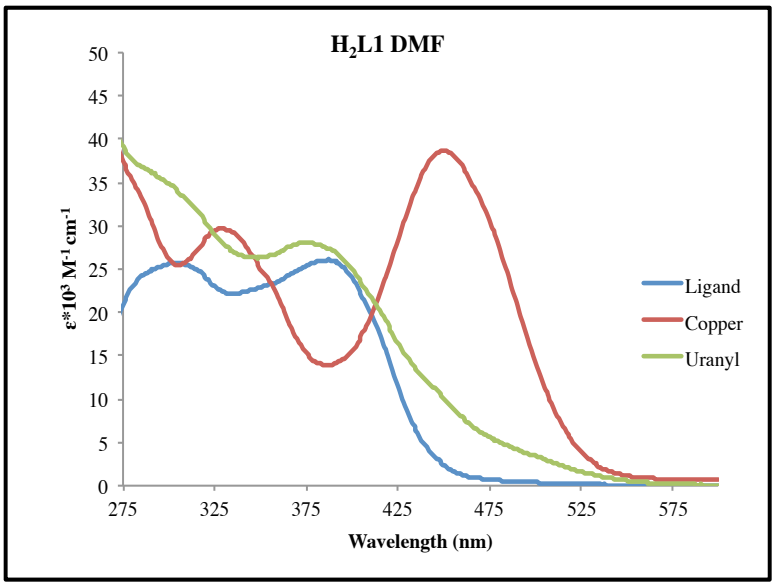

Figure 3.3: Combined UV-Vis spectra of H_2L1 (20 μM) with copper (20 μM) and uranyl (200 μM) in DMF after 2 hour stir.

The water concentration was slowly increased by 5% until 25%, at which point, the ligand precipitated from solution. At 5% water/DMF, the ligand maximum absorbance is at 386 nm, a difference of 1 nm from <1% water. The uranyl peak has a maximum at 369 nm, a shift of 17 nm from the ligand, while the copper and cobalt peaks are at 448 nm and 430 nm respectively.

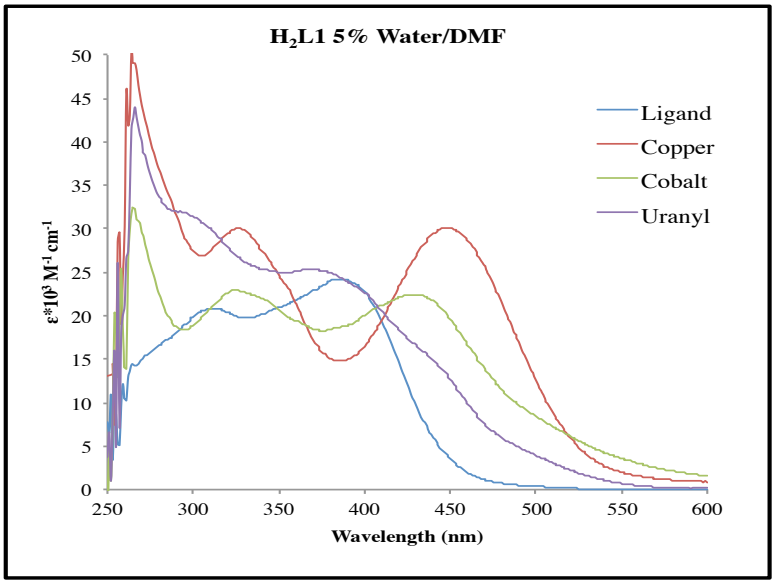

Figure 3.4: Combined batch metal titration for copper (40 μM), uranyl (120 μM), and cobalt (40 μM) with H_2L1 (20 μM) in 5% Water/DMF (v/v)

At 10% water/DMF, the ligand has a maximum absorbance at 385 nm, a shift of 2 nm from the previous 5% water/DMF. Copper had a maximum absorbance at 450 nm, with a $3.2x10^4$ M^{-1} • cm^{-1} extinction coefficient. Cobalt had an absorbance maximum of 429 nm, with an extinction coefficient of 2.5 $x10^4$ M^{-1} • cm^{-1}, while uranyl had an absorbance maximum peak of 367 nm, with a 2.5 $x10^4$ M^{-1} • cm^{-1} extinction coefficient.

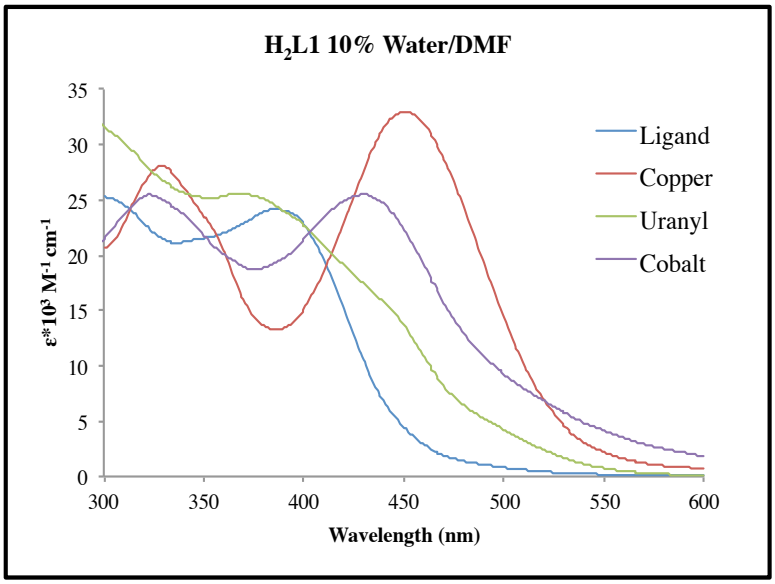

Figure 3.5: Combined batch metal titration for copper (40 μM), uranyl (200 μM), and cobalt (100 μM) with H_2L1 (20 μM) in 10% Water/DMF (v/v)

For 15% water/DMF the ligand maximum absorbance peak was at 389 nm, with an extinction coefficient of 2.5 $x10^4$ M^{-1} • cm^{-1}. The copper absorbance maximum increased to 452 nm, with a fairly consistent 3.2 $x10^4$ M^{-1} • cm^{-1} extinction coefficient. The cobalt complex had a higher energy increase in absorbance maximum to 417 nm, and an extinction coefficient of 2.3 $x10^4$ M^{-1} • cm^{-1}. Uranyl had a maximum absorbance at 369 nm, and an extinction coefficient close to that of the ligand of 2.6 $x10^4$ M^{-1} • cm^{-1}.

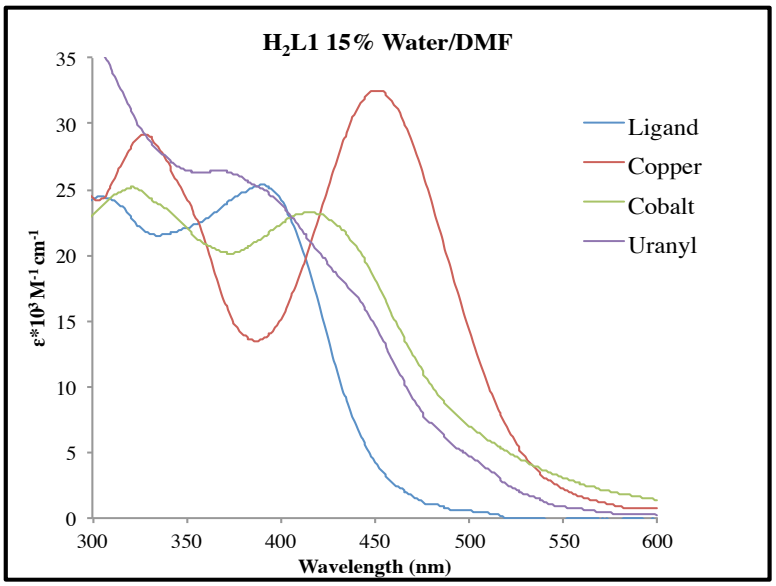

Figure 3.6: Combined batch metal titration for copper (40 μM), uranyl (100 μM), and cobalt (60 μM) with H_2L1 (20 μM) in 15% Water/DMF (v/v)

H_2L1 in 20% water/DMF (v/v) had a maximum extinction coefficient for uranyl of 2.6 $x10^4$ M^{-1} • cm^{-1}, at 367 nm. The cobalt complex has a peak at 436 nm, with an extinction coefficient of 2.1 $x10^4$ M^{-1} • cm^{-1}. The copper complex has an extinction coefficient of 2.4 $x10^4$ M^{-1} • cm^{-1}, at 450 nm. The other metals in figure 3.7 have little to no shift from the ligand peak, at 390 nm, in the spectrum.

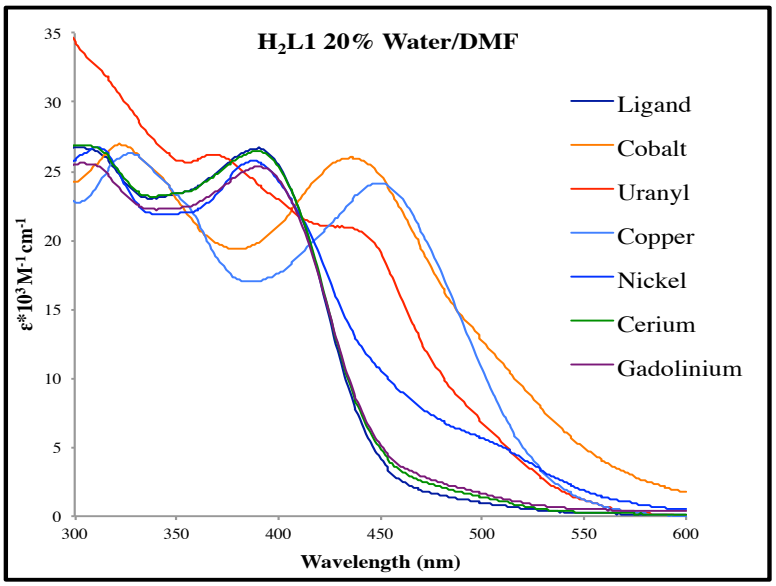

Figure 3.7: H_2L1 with various metals in 20% water/DMF (v/v). 20 μM ligand concentrations, 80 μM metal concentration

% water	H_2L1	ε*10⁴ M^{-1} cm^{-1}	Copper	ε*10⁴ M^{-1} cm^{-1}	Uranyl	ε*10⁴ M^{-1} cm^{-1}	Cobalt	ε*10⁴ M^{-1} cm^{-1}
< 1%	387	2.6	450	3.9	376	2.8	-	-
5%	386	2.4	448	3.0	369	2.5	430	2.2
10%	385	2.4	450	3.2	367	2.5	429	2.5
15%	389	2.5	452	3.2	369	2.6	417	2.3
20%	390	2.7	450	2.4	367	2.6	436	2.1

Table 3.2: Maximum absorbance and extinction coefficient for H_2L1, copper and uranyl summary based on % water/DMF.

H_2L1 was also tested in acetone to determine if a different solvent could improve the kinetics of binding and/or alter the UV-Vis absorption. The ligand in acetone was not shown to improve, with either an increase in signal selectivity nor separation of the peaks, on any of the previous work performed in DMF, and was

actually worse for kinetics. The first complexation of the metals by a color change took place after constantly stirring for 24 hours, indicating that the kinetics of the binding was greatly slowed, or possibly affected by the decrease in pH between DMF and acetone. Secondly, because the kinetics had slowed, the UV-Vis spectra did not show as significant of a change from the ligand maximum absorbance. After 5 hours, the copper peak at ~450 nm still appears, but uranyl and cobalt give rise to spectra that are similar to that of the free ligand. Acetone also evaporates quickly at ambient conditions, and it is difficult to maintain the specific concentrations of stock solutions over long periods of time.

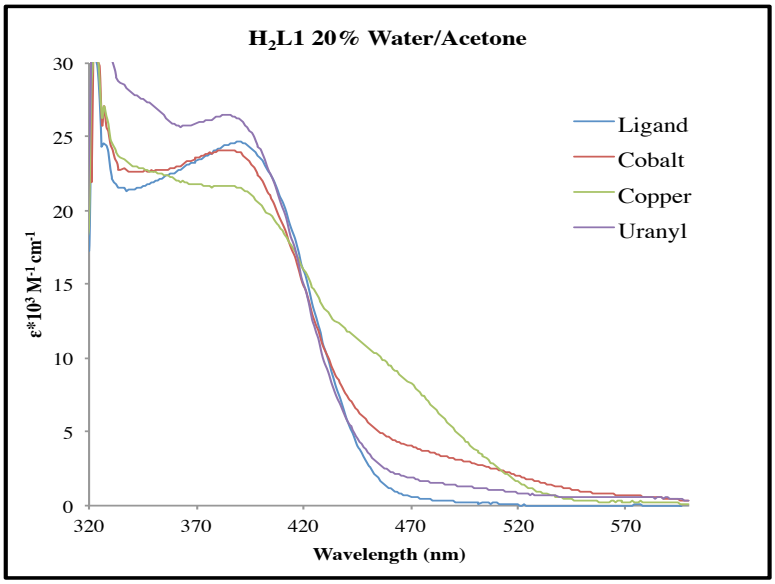

Figure 3.8: H_2L1 with various metals in 20% water/Acetone (v/v). 20 μM ligand concentrations, 80 μM metal concentration after a 5 hour stir

The di-substituted ligand with phenyl alanine (H_2L2) was also tested at 20% water/DMF (v/v). The hypothesis was that the extra phenyl ring on the backbone could increase the sensitivity of the ligand and lower the detection limit of the metals It was observed that the shoulder in the spectra for H_2L1 became a distinct peak at 450 nm for H_2L2, conversely the peak for H_2L1 at 367 nm is a shoulder for H_2L2. The cobalt complex's maximum absorbance shifted from 430 nm in H_2L1 to 466 nm for H_2L2, and the copper complex shifted only 6 nm from H_2L1 to 456 nm for H_2L2.

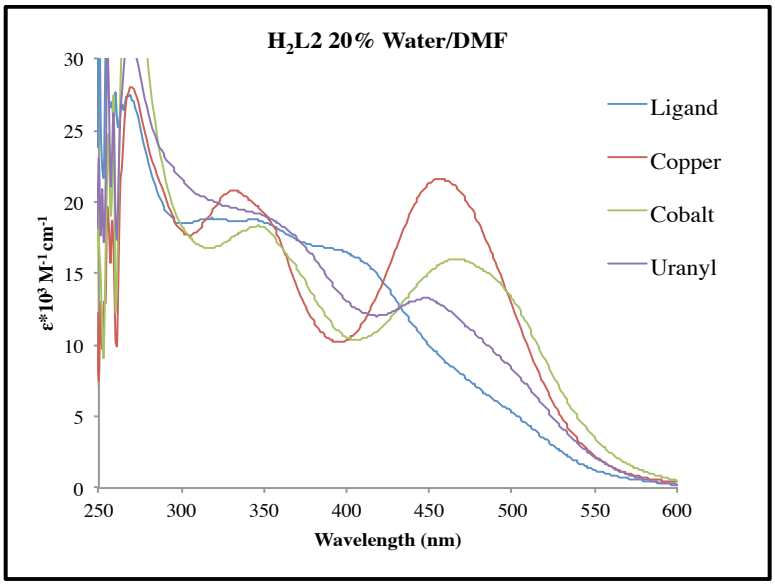

Figure 3.9: H_2L2 with various metals in 20% water/DMF (v/v). 20 μM ligand concentrations, 80 μM metal concentration

The mono-substituted ligand (H_3L3) was also investigated. This ligand was able to withstand up to 40% water without precipitating; however, the batch titration with uranyl at >1% water provided no evidence of uranyl binding due to no color

change or a shift in the absorbance maximum. The lack of a distinct peak could be a solvent interaction, or a dimerization preventing the change in absorbance, or it could be that the three donor atoms are not sufficient to bind the metal strongly. The least likely explanation is that the uranyl ion is too big to fit in the three donor binding pocket effectively. Copper did bind, but at a higher concentration as compared to the di-substituted ligand, H_2L1. Copper had a maximum absorbance at 406 nm, a shift of 30 nm to lower energy from the ligand peak.

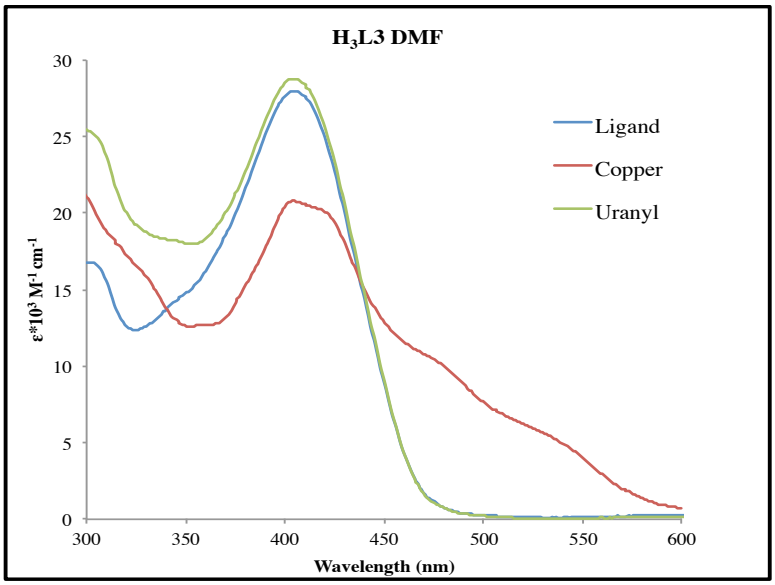

Figure 3.10: H_3L3 with various metals in DMF. 20 μM ligand concentrations, 80 μM metal concentration

The water content was increased to 10% for the mono-substituted ligand, because it should at least be able to match the di-substituted ligand before precipitation. At 10% water/DMF (v/v), uranyl did not have any signs of binding, as

there was no change in the UV-Vis absorbance. The main ligand peak at 406 nm was still present for the copper complex, but there were broad peaks for equivalents 1-4 that turned into two shoulders as the concentration of the copper increased above 80 uM (Figure A3.24). The broad peaks are at 518 nm, whereas the shoulders are around 530 nm and 450 nm. Cobalt exhibited only a small shift in the absorbance maximum at 412 nm, a shift of about 6 nm.

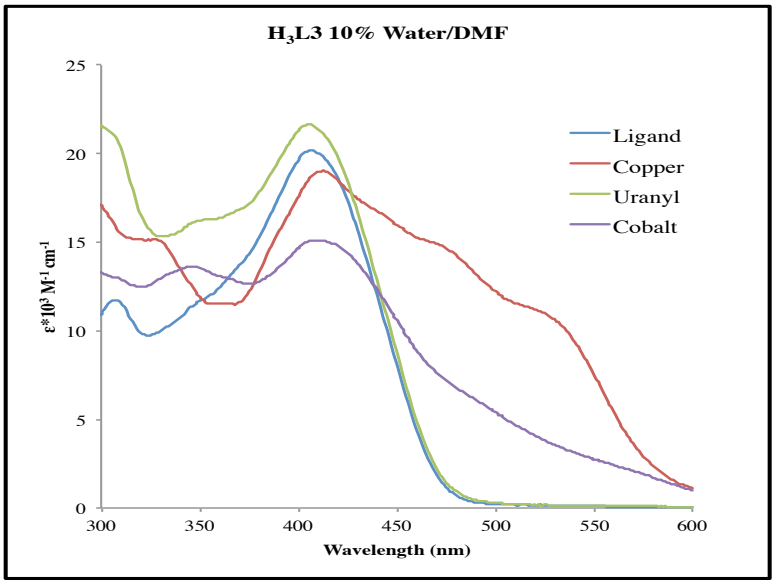

Figure 3.11: H_3L3 with various metals in 10% water/DMF (v/v). 20 μM ligand concentrations, 200 μM metal concentration

After it became apparent that uranyl was not going to cause changes to the UV-Vis spectra with H_3L3, further titrations were investigated with just copper and cobalt. The idea was that a two-ligand system could be used in a sample. H_3L3 would be used first to bind to metals such as copper or cobalt, and then extracted. While it is

preferred to avoid pre-purification, a similar ligand with good extraction kinetics that could be used on-site could be useful. Then, the analysis on the water sample for actinides could be preformed with H_2L1. This leads to a pre-treatment of the sample of sorts, but it is a simple pre-treatment as compared to ion exchange resins or other techniques that may be used.

For the 20% water/DMF (v/v) with H_3L3, the copper spectrum was in general, much the same as it was for the 10% water/DMF. There are broad peaks all the way up to 7 equivalents, more equivalents than for 10% water/DMF. For 8, 9, and 10 equivalents, there is a shoulder at lower, and a peak at higher in energy than the broad peaks. The broad peaks have a maximum absorbance at ~508 nm. The shoulder is at ~520 nm while the peaks are at 463 nm. The cobalt complex spectrum is nothing like the 10% water/DMF spectra, the only major peak is obscured the by the main ligand peak. There is an increase in absorbance between 450 and 600 nm, indicating a charge-transfer band, but there is not a distinct absorbance peak like before.

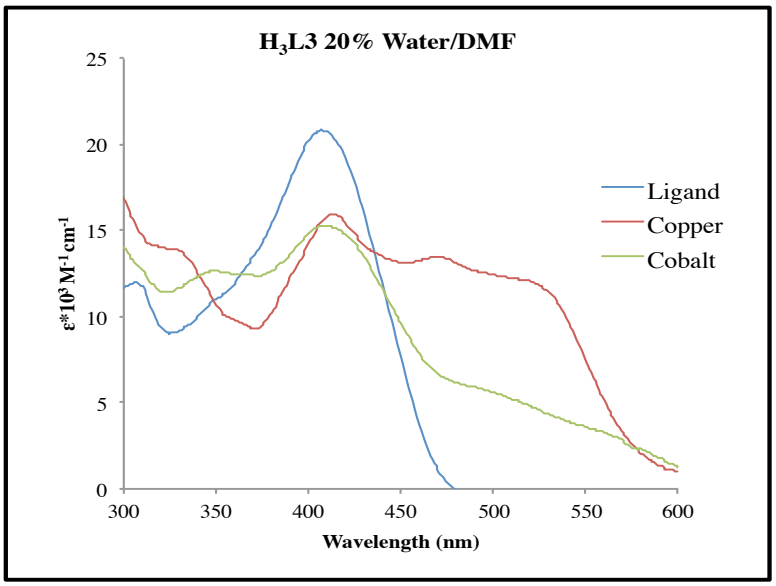

Figure 3.12: H_3L3 with various metals in 20% water/DMF (v/v). 20 μM ligand concentrations, 200 μM metal concentration

The copper complex with H_3L3 in 30% water/DMF (v/v), had broad peaks up to 4 equivalents with shoulders and a higher energy peak for all the other equivalents up to 10 equivalents. The broad peaks have a maximum absorbance of ~496 nm, whereas the shoulders are at about ~520 nm, and the higher energy peaks have a maximum absorbance ~463 nm. For the cobalt complex, the UV-Vis spectrum follows the same structure as was seen for the 20% water/DMF. The charge-transfer band, and a color change indicate the ligand did bind to copper. The cobalt complex has a small shift off the ligand peak, with a shoulder around 500 and 550 nm.

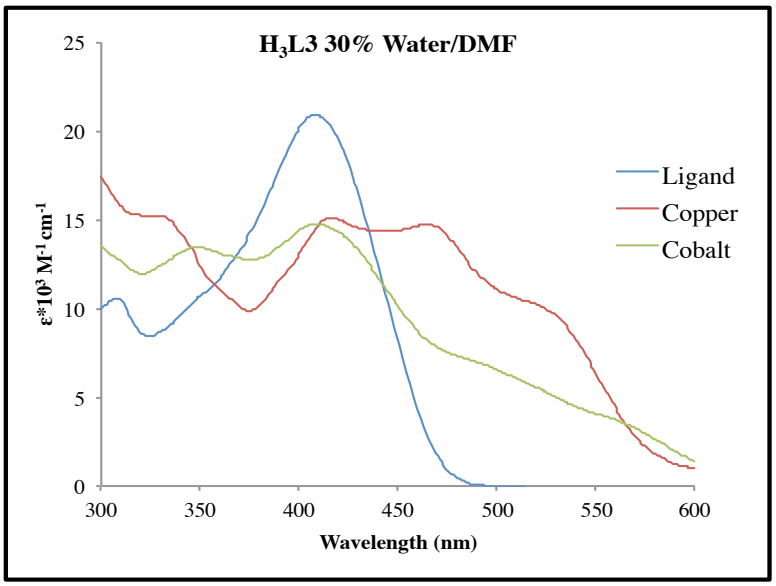

Figure 3.13: H_3L3 with various metals in 30% water/DMF (v/v). 20 μM ligand concentration, 200 μM metal concentration

The highest percentage of water that could be tolerated without ligand precipitation was 40%. All the metals tested with H_2L1 in 20% water/DMF were also tested with H_3L3 in 40% water/DMF (v/v). Uranyl with the H_3L3 ligand shows no change in the UV-Vis spectra, indicative of uranyl not bonding to the ligand, or not bonding strongly. Even the addition of up to 50 μL (~18 equiv.) of triethylamine does not elicit a UV-Vis response from the uranyl complex. Gadolinium, cerium, and nickel, likewise, do not appear to bind H_3L3 either, as evidenced by the lack of change in the UV-Vis spectrum with up to 10 equivalents of metal. One reason this could be the case is that Ni^{2+} prefers to be in a square planar geometry and the ligand may not be able to accommodate that, whereas Cu^{2+} can bind in square planar or in a

tetrahedral. The maximum absorbance peak for the copper complex is 459 nm, a shift of 50 nm from the ligand. Cobalt has a shoulder located at ~ 480 nm.

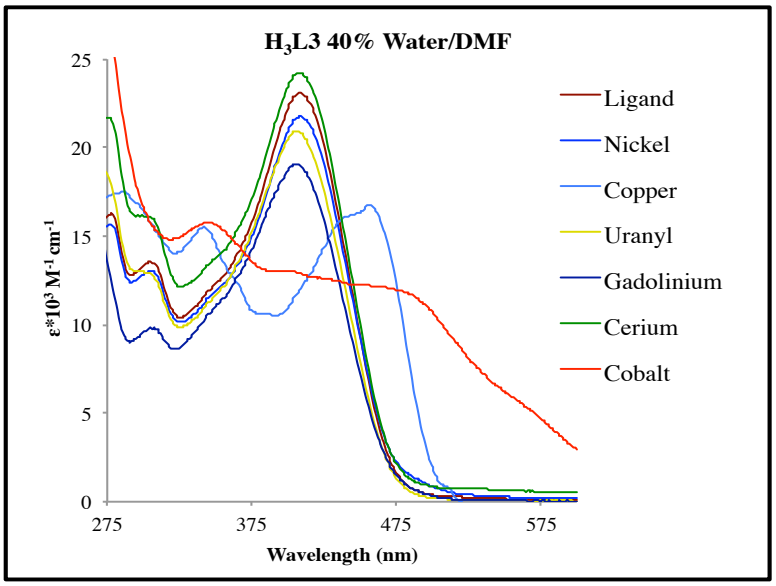

Figure 3.14: H_3L3 with various metals in 40% water/DMF (v/v). 20 μM ligand concentration, 200 μM metal concentration

% water	H_3L3	ε*10⁴ M⁻¹ cm⁻¹	Copper	ε*10⁴ M⁻¹ cm⁻¹	Uranyl	ε*10⁴ M⁻¹ cm⁻¹	Cobalt	ε*10⁴ M⁻¹ cm⁻¹
< 1%	405	2.8	405	2.1	405	2.8	-	-
10%	406	2.4	413	1.9	406	2.2	310	1.5
20%	407	2.1	413, 470	1.6, 1.3	-	-	410	1.5
30%	408	2.1	416, 464	1.5, 1.5	-	-	408	1.5
40%	408	2.3	457	1.7	-	-	399	1.3

Table 3.3: Maximum absorbance and extinction coefficient for H_2L1 and metals summary based on % water/DMF.

One possibility is that aggregation of the ligands could hinder the kinetics. In an attempt to limit aggregation of the ligand and improve the complexation kinetics, the use of HEPES (2-4[-(2-hydroxyethyl)piperazine-1-yl]ethanesulfonic acid) buffer was employed. HEPES is an inexpensive phosphate containing buffer component that has an effective pH range between 6.8-8.2, more typical of what you might find in a natural water flow from a river. Metals are also unlikely to bind the HEPES anion even at a 50 μM total concentration. It was added to the individual metal solution before addition of ligand and adjusted to pH 7. In acetone, the addition of HEPES buffer greatly improved the kinetics over no buffer. Copper complexation took place in about 6 hours; whereas the uranyl and cobalt complexation took about 12 hours. The buffer also made the copper complex peak at 450 nm more defined. The cobalt peak can be seen increasing absorbance, whereas the uranyl peak shows a slight shift to higher energy from the ligand peak.

For the HEPES buffer metal solution with the H_2L1 in DMF, complexation of uranyl occurred in 1 hour, as opposed to the 2 hours required without the buffer. The addition of copper and cobalt still elicited the same color change immediately after addition, as before. The uranyl complex peak was further shifted to 349 nm, but this would be overlapped by the copper complex peak at 355 nm. The main copper peak from before at 450 nm, was also higher energy shifted to 446 nm.

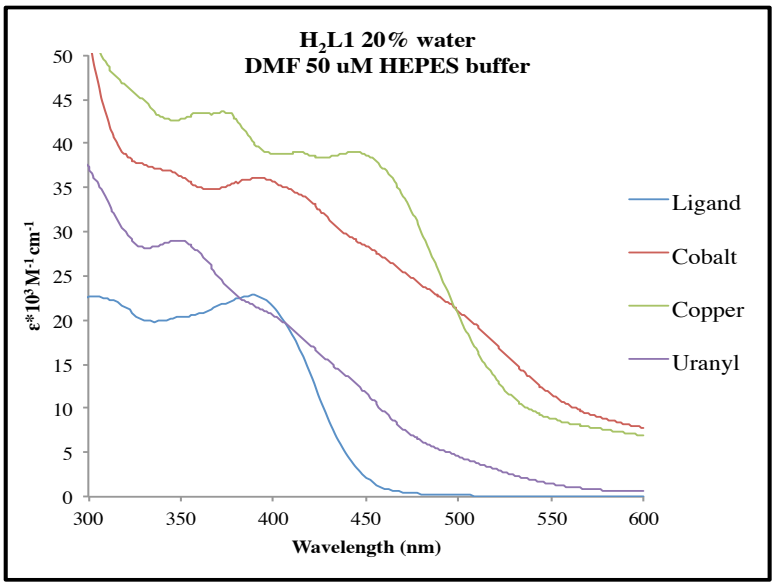

Figure 3.15: H_2L1 (20 μM) with various metals (80 μM) in 20% water/DMF (v/v) with 50 μM HEPES buffer.

3.4 Fluorescence

Fluorescence spectroscopy is a valuable technique used in the detection of trace metals due to its sensitivity.[7] H_2L1 and H_3L3 both fluoresce at 350 nm wavelength excitation to give peaks at ~565 nm and 525 nm respectively. Within 5 seconds, quenching of the fluorescence was seen upon the addition of copper in both H_2L1 and H_3L3 whereas only a decrease in the emission was seen upon the addition of uranyl within 5 seconds. It took one equivalent of copper to cause a complete quench of H_2L1 and two equivalents to cause a complete quench of H_3L3. The uranyl intensity does not change after 2 hours. Such a significant rapid quenching of the copper signal would be useful to use in the distinguishing between copper and uranyl

ions in the sample or in combination with UV-Vis to detect metal and fluorescence to confirm the contribution of uranyl. There could be a problem of a small amount of copper could that cause incomplete quenching, and therefore mimic the uranyl signal. This should be investigated further.

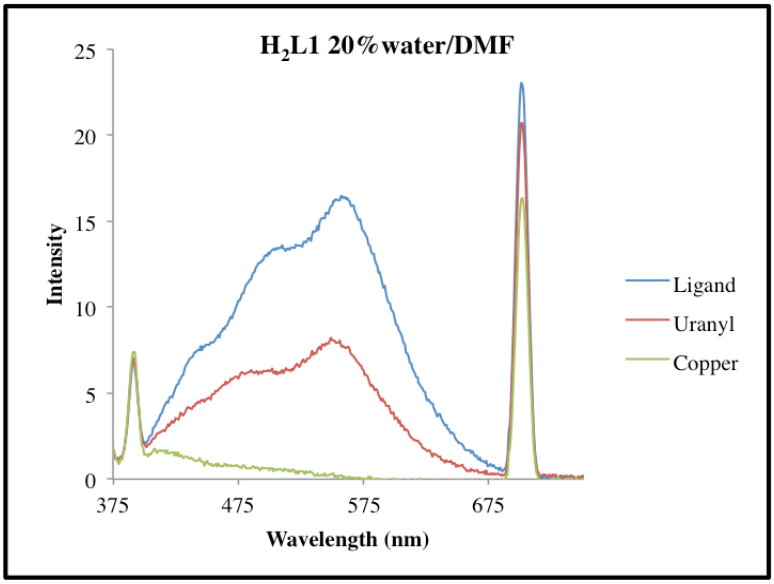

Figure 3.16: Fluorescence of H_2L1 with uranyl complex and copper complex after 2 hour stirring in 20% water/DMF (v/v) at 350 nm excitation

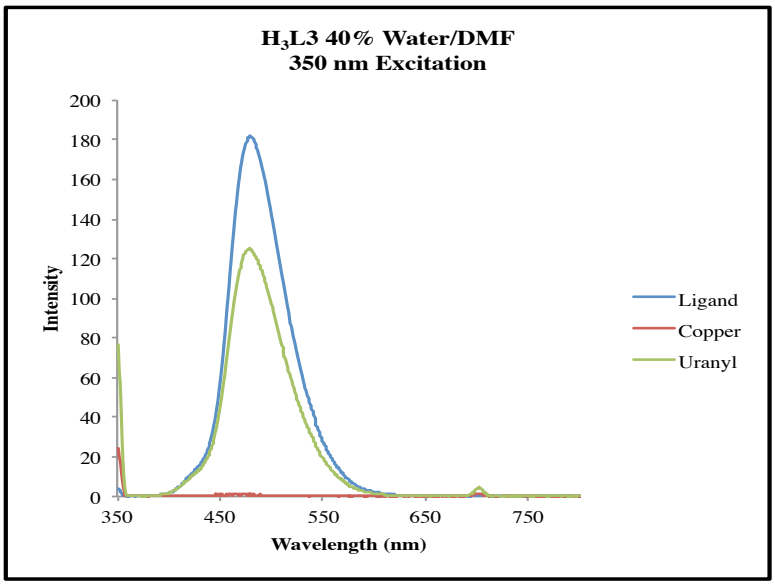

Figure 3.17: Fluorescence of H_3L3 with uranyl complex and copper complex after 2 hour stirring in 40% water/DMF (v/v) at 350 nm excitation

3.5 Calculations

Calculations in Gaussian 09[27] were used to determine the interactions between the HOMO and LUMO at the excitations that are causing the shifts seen in the spectra. The calculations were optimized using B3LYP[28] at the 6-31g(d) basis set and solvated in DMF, followed by time-dependent DFT (TDDFT) to determine the excitations and a predicted UV-Vis in Gaussview. Although the calculated UV-Vis does not exactly match up to the experimental spectra (figure 3.19), the overall shape of the spectra is very similar with respect to the shifts of the complexes to higher and lower energies. Natural Transition Orbitals (NTO)[29] were used to identify the contributing orbitals in the HOMO-LUMO interaction.

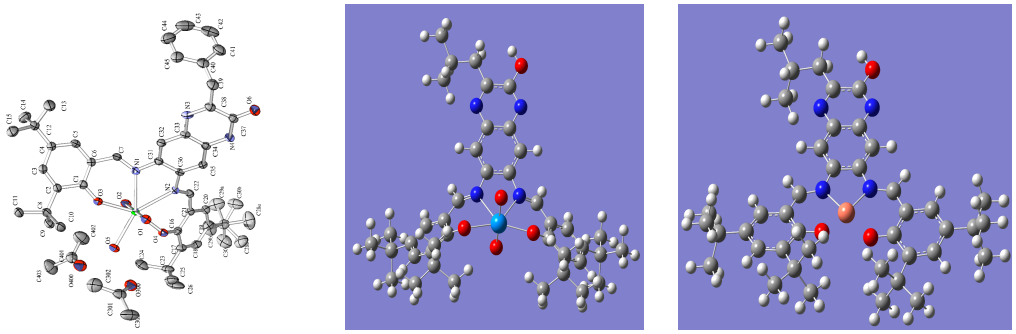

U-N1 2.551(3)	U-N1 2.539	Cu-N1 1.940
U-N2 2.577(3)	U-N2 2.550	Cu-N2 1.941
U-O1 2.254(2)	U-O1 2.257	Cu-O1 1.904
U-O2 2.255(2)	U-O2 2.255	Cu-O2 1.906
$U\text{-}O3_{yl}$ 1.774(2)	$U\text{-}O3_{yl}$ 1.794	
$U\text{-}O4_{yl}$ 1.779(2)	$U\text{-}O4_{yl}$ 1.790	

Figure 3.18: Optimized structures for uranyl and copper complex with bond distances comparing the uranyl crystal structure.[30]

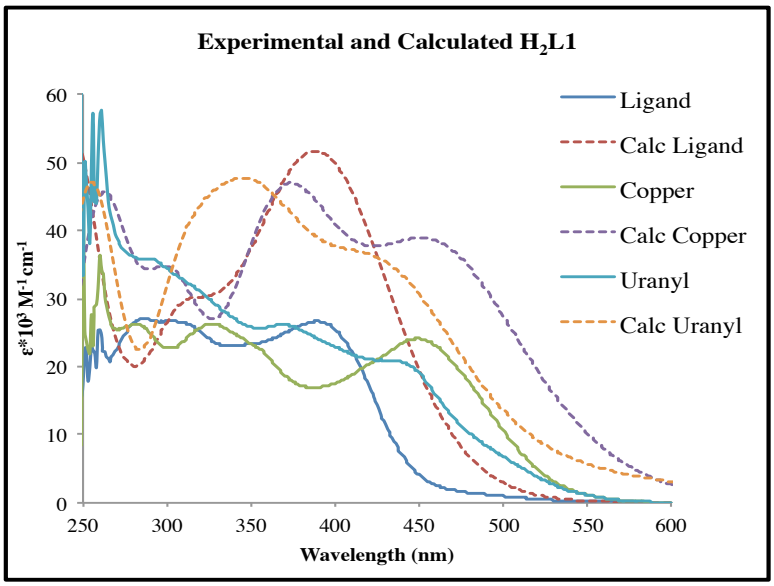

Figure 3.19: Combined experimental and calculated UV-Vis spectra for H_2L1. Calculated has a 30 nm shift to better match up with experimental spectrum.

For the uranyl complex, the HOMO orbital's major contribution was from the ligand with a single electron going into the LUMO *f*-orbital on the metal. This higher energy excitation caused the absorbance to blue shift from the ligand peak. For the copper complex, the HOMO orbital was the d-orbital on the metal going to the ligand LUMO orbital, causing the lower energy shift from the ligand.

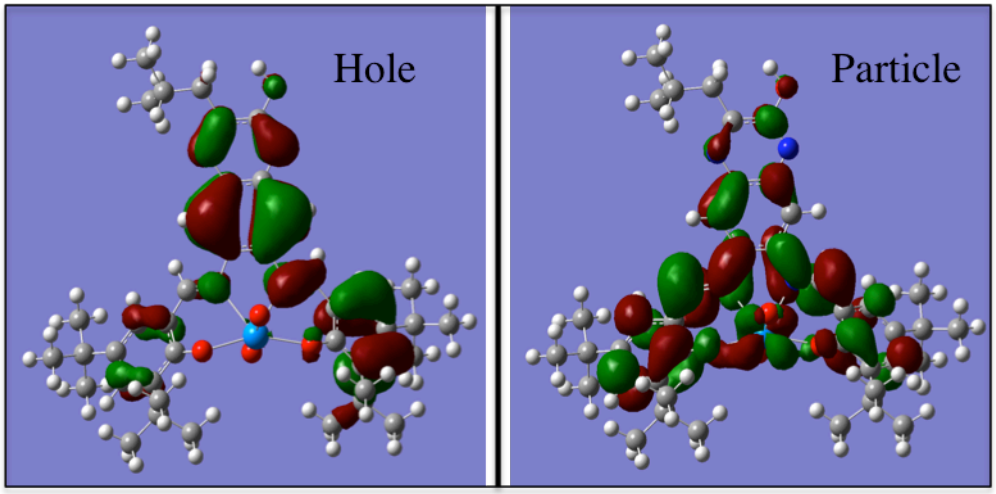

Figure 3.20: Hole (HOMO) and particle (LUMO) for NTO analysis of the uranyl complex.

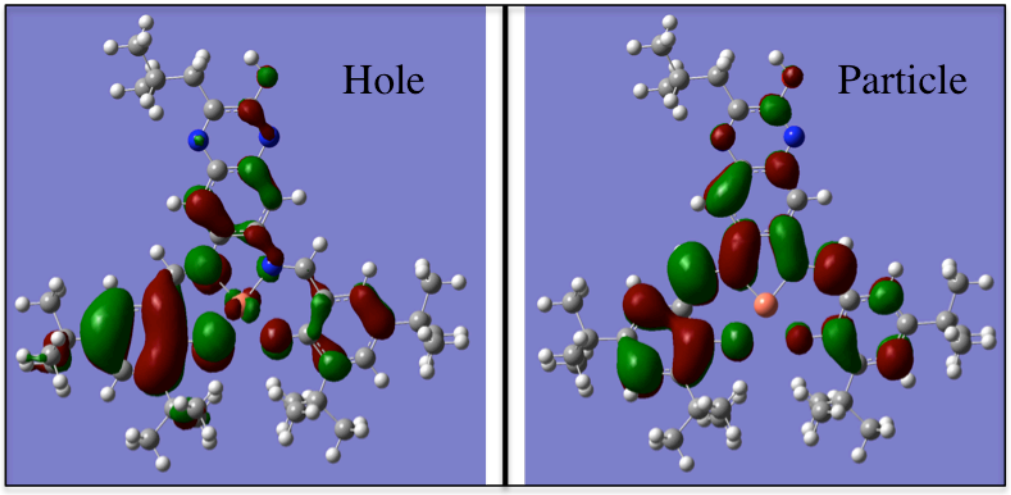

Figure 3.21: Hole (HOMO) and particle (LUMO) for NTO analysis of the copper complex

These different excitations are caused as the two metals interact with the ligand, and is a step to predicting the best ligand for selectivity and sensing. Other ligands detailed in Chapter 4 that were not selective, all had the same interaction with the metals whether it was metal to ligand, or ligand to metal in the HOMO to LUMO.

3.6 Binding Constants

H_2L1	DMF		5% Water		10% Water		20% Water	
	Log K	ε	Log K	ε	Log K	ε	Log K	ε
Uranyl	3.88	3.20E+04	3.57	6.50E+04	3.80	2.97E+04	3.52	3.38E+04
Copper	4.22	4.43E+04	4.16	4.16E+04	4.27	3.90E+04	4.28	2.99E+04
Cobalt	3.77	4.31E+04	3.83	5.89E+04	3.62	8.29E+04	3.79	5.52E+04

Table 3.4: Average of binding constants from two replications of data collection and extinction coefficients for H_2L1 with uranyl copper and cobalt

	DMF		10% water	
	Log K	ε	Log K	ε
Copper	3.74	4.78E+04	3.04	2.13E+05
Cobalt	3.09	2.30E+05	3.44	2.93E+04

Table 3.5: Average of binding constants from two replications of data collection and extinction coefficients for H_3L3 complexes with copper and cobalt.

The binding constants and extinction coefficients were calculated using non-linear regression with the sum of the least squares of the UV-Vis spectra, changing the ligand concentration with the metal concentration remaining constant. The

titrations were allowed to stir for 24 hours to ensure complete complexation. The solver program in Excel was used to determine the smallest number for the sum of the squares and have the model fit the experimental data as best as it could. The data gave a K and extinction coefficient in the answer.

3.7 Colorimetry

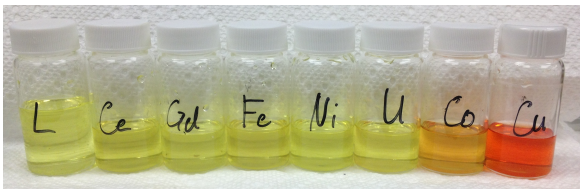

Figure 3.22: H_3L3 colorimetry 40% water/DMF

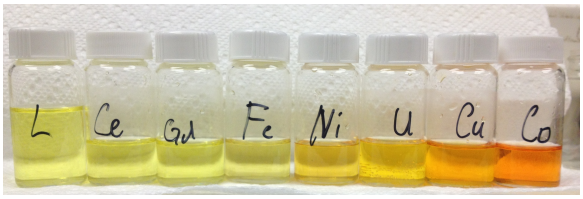

Figure 3.23: H_2L1 colorimetry 20% water/DMF

The other advantage of the Quinoxolinol salen ligands is that upon metal complexation, the ligand changed from a light green-yellow to a yellow, orange, or red color depending on the ligand and metal coordinated. Ni has a small shift in

maximum absorbance from the ligand and an increasing absorbance at ~450 nm that caused the color change.

3.8 Conclusion

A series of batch and serial titrations were analyzed at varying metal concentrations with two ligands, H_2L1 and H_3L3. H_2L1 was shown that it could be used as a UV-Vis sensor for uranyl due to the higher energy shift of the absorbance peak in the uranyl complex, compared to copper, which gave a lower energy shift in the spectrum relative to the ligand. The uranyl peak was also separated from the ligand by ~20 nm. The ligand could be used in up to 20% water before precipitation. Other metals such as gadolinium, nickel, and cerium gave little to no shift from the ligand peak.

H_3L3, while able to withstand a higher water content (40%), was not a good sensor for uranyl. The spectrum did not change between the ligand and uranyl. The same metals tested by titration with H_2L1 were also tested with H_3L3 and only copper and cobalt gave any change in the UV-Vis spectrum.

Calculations were performed to determine the viability of the current ligand system (H_2L1), and to also determine what modifications to the quinoxolinol and binding pocket could be made to improve either, the selectivity or sensitivity of the

ligand, or both. NTO analysis on the current ligand system showed that the uranyl peak is caused by an excitation from the ligand HOMO to a LUMO *f*-orbital of uranyl, while the copper excitation was caused by a HOMO *d*-orbital on the metal being excited to the ligand LUMO. Further calculations for the modifications of the ligand are reported in Chapter 4.

3.9 References

(1) Hodisan, T.; Curtui, M.; Haiduc, I. *J. Radioanal. Nucl. Chem.* **1998**, *238*, 129.

(2) Lee, J. H.; Wang, Z. D.; Liu, J. W.; Lu, Y. *J. Am. Chem. Soc.* **2008**, *130*, 14217.

(3) Pestov, D.; Chen, C. C.; Nelson, J. D.; Anderson, J. E.; Tepper, G. *Sens. Actuators, B* **2009**, *138*, 134.

(4) Lutfullah; Alam, M. N.; Rahman, N.; Azmi, S. N. H. *J. Haz. Materials* **2008**, *155*, 261.

(5) Hodisan, T.; Curtui, M.; Cobzac, S.; Cimpoiu, C.; Haiduc, I. *J. Radioanal. Nucl. Chem.* **1998**, *238*, 179.

(6) Brina, R.; Miller, A. G. *Anal. Chem.* **1992**, *64*, 1413.

(7) Hong, K. B.; Jung, K. W.; Jung, K. H. *Talanta* **1989**, *36*, 1095.

(8) Nivens, D. A.; Zhang, Y. K.; Angel, S. M. *J. Photochem. Photobiol., A* **2002**, *152*, 167.

(9) Mcmahon, A. W. *Sci. Total Environ.* **1993**, *130*, 285.

(10) Aydin, F. A.; Soylak, M. *Talanta* **2007**, *72*, 187.

(11) Tamborini, G.; Donohue, D. L.; Rudenauer, F. G.; Betti, M. *J. Anal. At. Spectrom.* **2004**, *19*, 203.

(12) Ruan, C. M.; Luo, W. S.; Wang, W.; Gu, B. H. *Anal. Chim. Acta* **2007**, *605*, 80.

(13) Sessler, J. L.; Melfi, P. J.; Seidel, D.; Gorden, A. E. V.; Ford, D. K.; Palmer, P. D.; Tait, C. D. *Tetrahedron* **2004**, *60*, 11089.

(14) Murty, B. N.; Jagannath, Y. V. S.; Yadav, R. B.; Ramamurty, C. K.; Syamsundar, S. *Talanta* **1997**, *44*, 283.

(15) Rakicioglu, Y.; Young, M. M.; Schulman, S. G. *Anal. Chim. Acta* **1998**, *359*, 269.

(16) Hayes, N. W.; Tremlett, C. J.; Melfi, P. J.; Sessler, J. D.; Shaw, A. M. *Analyst* **2008**, *133*, 616.

(17) Xu, Z. C.; Xiao, Y.; Qian, X. H.; Cui, J. N.; Cui, D. W. *Org. Lett.* **2005**, *7*, 889.

(18) Tarancon, A.; Garcia, J. F.; Rauret, G. *Anal. Chim. Acta* **2005**, *538*, 233.

(19) Ganjali, M. R.; Memari, Z.; Norouzi, P.; Shaabani, B.; Emamalizadeh, M.; Hanifehpour, Y.; Faridbod, F. *Anal. Lett.* **2010**, *43*, 2220.

(20) Mlakar, M.; Branica, M. *Anal. Chim. Acta* **1989**, *221*, 279.

(21) Sadeghi, S.; Doosti, S. *Dyes and Pigments* **2009**, *80*, 125.

(22) Collins, G. E.; Lu, Q. *Anal. Chim. Acta* **2001**, *436*, 181.

(23) Rohwer, H.; Rheeder, N.; Hosten, E. *Anal. Chim. Acta* **1997**, *341*, 263.

(24) Suresh, A.; Patre, D. K.; Srinivasan, T. G.; Rao, P. R. V. *Spectrochim. Acta, Part A* **2002**, *58*, 341.

(25) Gray, H. N.; Jorgensen, B.; McClaugherty, D. L.; Kippenberger, A. *Ind. Eng. Chem. Res.* **2001**, *40*, 3540.

(26) Wu, X.; Gorden, A. E. V. *J. Comb. Chem.* **2007**, *9*, 601

(27) M. J. Frisch, G. W. T., H. B. Schlegel, G. E. Scuseria, M. A. Robb, J. R. Cheeseman, G. Scalmani, V. Barone, B. Mennucci, G. A. Petersson, H. Nakatsuji, M. Caricato, X. Li, H. P. Hratchian, A. F. Izmaylov, J. Bloino, G. Zheng, J. L. Sonnenberg, M. Hada, M. Ehara, K. Toyota, R. Fukuda, J. Hasegawa, M. Ishida, T. Nakajima, Y. Honda, O. Kitao, H. Nakai, T. Vreven, J. A. Montgomery, Jr., J. E. Peralta, F. Ogliaro, M. Bearpark, J. J. Heyd, E. Brothers, K. N. Kudin, V. N. Staroverov, R. Kobayashi, J. Normand, K. Raghavachari, A. Rendell, J. C. Burant, S. S. Iyengar, J. Tomasi, M. Cossi, N. Rega, J. M. Millam, M. Klene, J. E. Knox, J. B. Cross, V. Bakken, C. Adamo, J. Jaramillo, R. Gomperts, R. E. Stratmann, O. Yazyev, A. J. Austin, R. Cammi, C. Pomelli, J. W. Ochterski, R. L. Martin, K. Morokuma, V. G. Zakrzewski, G. A. Voth, P. Salvador, J. J. Dannenberg, S. Dapprich, A. D. Daniels, Ö. Farkas, J. B. Foresman, J. V. Ortiz, J. Cioslowski, and D. J. Fox; A.1 ed.; Gaussian Inc.: Wallingfor CT, 2009.

(28) Becke, A. D. *J. Chem. Phys.* **1993**, *98*, 5648.

(29) Martin, R. L. *J. Chem. Phys.* **2003**, *118*, 4775.

(30) Wu, X.; Hubbard, H. K.; Tate, B. K.; Gorden, A. E. V. *Polyhedron* **2009**, *28*, 360.

Chapter 4: Quinoxolinol based sensors for molecular recognition: A TDDFT computational study

4.1 Introduction

Since the 1950s, nuclear weapons, power reactors, medical, and research activities have introduced many different radionuclides into the environment.[1] It is important to fundamentally study the actinides because of their use in nuclear energy and nuclear materials, where such issues as long-term storage of nuclear waste, environmental cleanup, and actinide separations need to be addressed.[2] The development of sensors for the detection of metal ions is an ongoing challenge that is attracting the attention of researchers across a range of disciplines.[3] In the case of chemical agents that trigger an easy-to-monitor response (e.g., optical, fluorescent, electrochemical), otherwise known as chemosensors (sensors for short), both sensitivity and selectivity are critical elements of a successful design.[3] This is particularly true for sensors developed for *f*-elements, since specific action recognition is critical to identifying species that might be present in the environment as the result of a radioactive spill or a terrorist attack involving a dirty bomb.[3]

Typical analytical methods used include inductively coupled plasma mass-spectrometry (ICP-MS),[4,5] capillary electrophoresis, fluorescence,[6] X-ray fluorescence

(XRF),[7] phosphorimetry,[8] and colorimetry.[9] These methods tend to be costly, involve multiple sample manipulations, and often have insufficient selectivity and/or sensitivity.[3,10-12] One of the methods proposed for nuclear waste treatment and actinide separation involves the coordination of actinide ions with polydentate ligands, exploiting this chelate effect.[2,13] Previous ligands proposed as chemosensors for actinides include expanded porphyrins[14,15] and related Schiff-base macrocycles[16], calixarenes[17], crown-ethers[18-20], aza-crowns[21], and Arsenazo III.[3,22] With this study, we sought to use a two fused ring system (quinoxaline) to increase the binding and modify the coordination pocket to increase the selectivity for uranyl over copper. This backbone also fluoresces, providing an additional means of identifying a sensor, but those calculations are not performed or described here.

4.2 Methods

Calculations in Gaussian 09[23] to determine the source of the shifts of H_2L1 were performed using the hybrid DFT B3LYP[24] basis set and solvated using the SCRF keyword with N,N'-dimethylformamide. The Stuttgart effective core potential basis set was used for uranium, replacing 60 core electrons to account for scalar-relativistic effects.[25,26] The 6-31g(d)[27,28] basis set was used for all carbon, nitrogen, oxygen, hydrogen and copper atoms. All structures were converged with the default self-consistent-field (tight) convergence cutoffs.[29] The optimized structure of the uranyl complex was in close relation to the published uranyl crystal structure. After optimization, time-dependent DFT (TDDFT)[30-37] was used to determine the excited

states and predicted UV-Vis spectra for the ligand and metal complex. The calculated UV-Vis did match the general spectrum shape but was shifted to higher energies. Natural transition orbitals (NTO)[38] were investigated to determine the HOMO to LUMO interaction causing the changes in the absorbance maximum and the differences between the metal complexes.

4.3 Results

This series of calculations was undertaken to try to characterize how the quinoxolinol ligand system UV-Vis spectra differentiates between the copper and uranyl complexes and to predict the spectroscopic signal response generated. Further, it was investigated as to how this system might be modified to further improve the separation of the peaks and increase the extinction coefficient, thus improving the sensitivity. The current salqu system has a shift to higher energy excitations from the ligand peak for uranyl, whereas there is a shift to lower energy excitations for copper as seen below in Figure 4.1. The uranyl complex has a peak at 370 nm and a shoulder at 450 nm corresponding to extinction coefficients of 2.6 $x10^4$ M^{-1} • cm-1 and 1.9 $x10^4$ M^{-1} • cm^{-1} respectively for those peaks. Copper has peaks at 450 nm and 327 nm corresponding to a 2.5 $x10^4$ M^{-1} • cm-1 extinction coefficient for both peaks.

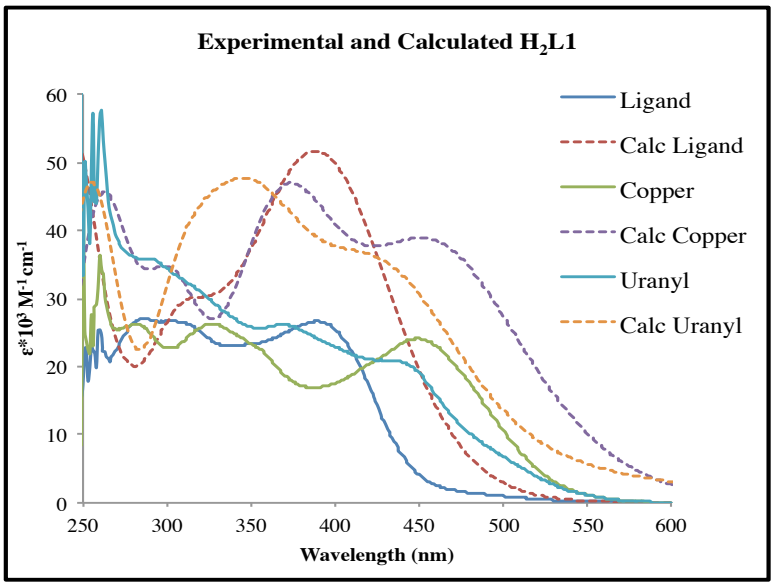

Figure 4.1: Experimental salqu with copper and uranyl complex

The calculated absorbance spectrum (figure 4.1), although shifted to slightly higher energies (~30 nm), matches the general shape of the spectrum found in the experimental. The uranyl extinction coefficient is 4.8 x10^4 M^{-1} • cm^{-1} at the peak and 3.7 x10^4 M^{-1} • cm^{-1} at the shoulder. The most influential excitation for the peak at 343 nm is an excitation at 308 nm. The copper extinction coefficient is 4.7 x10^4 M^{-1} • cm^{-1} at 343 nm and 3.9 x10^4 M^{-1} • cm^{-1} at 421 nm. For copper, the most influential excitation is at 421 nm.

To begin to understand the excitations causing the shift in the spectra, natural transition orbitals were applied to the excitation states. These would provide information as to what singlet excitation was causing the shifts, whether it was simply a pi to pi*, metal to ligand, or ligand to metal transitions. According to the NTO calculations, the carbon atoms on carbons on the lower quinoxolinol ring and on the

phenyl rings occupy the majority of the hole and the uranium f-orbital atom occupies over 70% of the particle orbital. Looking at the next orbitals of the hole – 1 and particle + 1 it is even more of a ligand to metal transition with uranium *f*-orbital occupying over 90% orbital particle + 1 orbital. The copper complex has the opposite singlet excitation. Copper occupies >70% of the *d*-orbital in the hole and the ligand occupies the majority of the particle orbital. Hole -1 and particle +1 also show a more defined metal to ligand transition.

Three rules were developed to determine if the modified ligands were acceptable; (1) the copper complex peak must not overlap with the uranyl complex peak, (2) the uranyl complex peaks needs to be at least 10-15 nm from any other peak, (3) a higher extinction coefficient of the uranyl complex over any other peaks should be considered as this is a measure or sensitivity. The H_2L1 ligand by itself has a pi to pi* transition as would be expected. For the uranyl complex with H_2L1, there is a ligand to metal excitation into the *f*-orbital of the uranium. The copper(II) complex with H_2L1 has a *d*-orbital metal to ligand excitation from the HOMO to the LUMO.

4.31 Salicylaldehydes

The first series of calculations to modify the ligand was to incorporate different salicylaldehyde moieties and thereby determine if the difference was electronic in nature. The first test was for no substituents on the salicylaldehyde, and

then these results were used to determine what additional modifications to make. A range of commercially available salicylaldehydes was with electron-donating and electron-withdrawing groups in the 3, 4, 5, and 6 positions, including some with substituents on multiple positions was characterized. These included 3-ethoxy, 3,5-dichloro, 4-amino, 4-chloro, 4-hydroxy, 4-methoxy, 4,6-hydroxy, 5-amino, 5-hydroxy, 5-methyl, and 5-*t*-butyl. Of these, none were more selective or sensitive than the experimental ligand, with the salicylaldehyde being the best of the computed ligands. The 4-chlorosalicylaldheyde is a possible improvement as it has a higher extinction coefficient at higher energy than the free ligand, which would need to be further probed experimentally.

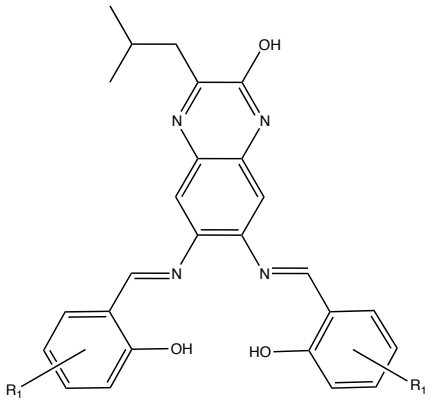

Figure 4.2: Salicylaldehyde representation

R1	λmax Abs (nm)					
	Ligand	ε*10⁴ M^{-1} cm^{-1}	Copper	ε*10⁴ M^{-1} cm^{-1}	Uranyl	ε*10⁴ M^{-1} cm^{-1}
H	220, 257, 353	4.0, 3.7, 4.1	220, 336, 404	4.9, 4.2, 4.1	220, 320	4.4, 4.1
3-ethoxy	219, 357	5.7, 4.9	231, 358	5.4, 5.5	226, 334	5.5, 4.7
3,5-dichloro	223, 367	6.2, 4.2	236, 347, 403	5.4, 4.6, 4.0	231, 266, 336	4.6, 3.6, 4.1
4-amino	218, 334	3.9, 5.6	216, 393	4.5, 6.8	221, 376	2.6, 5.9
4-chloro	220, 260, 362	4.1, 4.1, 4.5	223, 399	4.7, 5.3	224, 276, 368	4.0, 3.8, 4.8
4-hydroxy	217, 264,351	4.0, 3.4, 4.7	221, 388	4.3, 5.7	224, 365	3.4, 5.0
4-methoxy	218, 271, 353	3.9, 3.5, 5.1	222, 383	4.7, 6.3	224, 363	3.4, 5.6
4,6-hydroxy	322, 359	4.5, 4.5	225, 383	5.2, 6.6	225, 275, 355	3.0, 2.9, 5.3
5-amino	235, 362	6.0, 3.6	242, 344, 506	5.0, 4.9, 2.1	217, 266, 325	5.6, 3.9, 4.5
5-hydroxy	219, 288, 377	4.1, 3.2, 4.3	227, 341, 465	4.9, 4.7, 2.6	222, 264, 341	3.5, 3.7, 4.6
5-methyl	217, 278, 363	4.3, 2.9, 4.7	225, 336, 417	5.4, 4.3, 3.7	222, 268,344	4.0, 3.6, 4.5
5-*t*-butyl	216, 277, 361	4.7, 3.0, 4.0	227, 340, 411	5.6, 4.8, 3.5	226, 268, 343	3.9, 4.0, 4.7

Table 4.1: Salicylaldehyde derivatives with absorbance maximums. Green highlight is the best and yellow is a possibility.

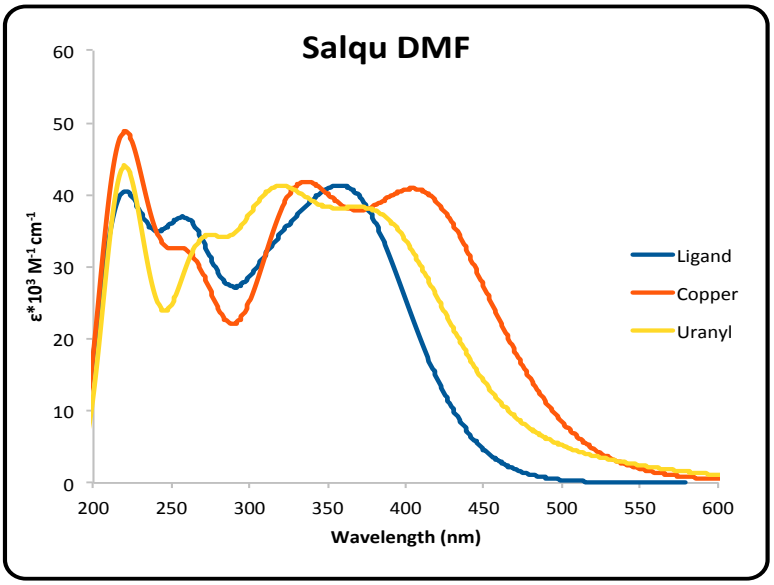

Figure 4.3: Calculated salicylaldehyde spectrum with copper and uranyl complex in DMF

4.32 Schiff Bases

Changing the substituents on the phenyl rings did not appear to improve upon the selectivity already established with the experimental ligand. One additional point of diversity to change is the binding pocket while keeping the imine to keep the synthesis simple. To make a comparable series, the components chosen for the binding pocket are all softer base-donating nitrogens, from pyrroles, pyridines, bipyridines, 2-amionobenzaldehyde. Softer donors were chosen as they have been recently shown by k-edge XAS to better interact with the 5*f*-orbitals of the actinides, creating more covalent bonds.[39] Also, softer donors are being considered as both a replacement and a co-extractant in Europe for the PUREX process.[40] The European system dubbed SANEX uses bis-triazines attached to a softer donor backbone, such as pyridines[41], bi-pyridines[42], and phenanthrolines.[43]

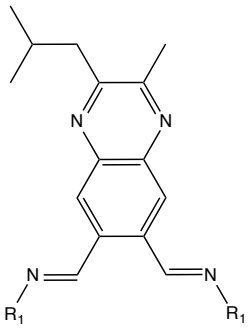

Figure 4.4: Schiff base changes to the ligand

R1	λmax Abs (nm)					
	Ligand	$\varepsilon*10^4$ M^{-1} cm^{-1}	Copper	$\varepsilon*10^4$ M^{-1} cm^{-1}	Uranyl	$\varepsilon*10^4$ M^{-1} cm^{-1}
pyrrole	204, 262, 346	2.8, 2.4, 5.8	234, 362	3.6, 5.3	364	5.5
pyridine	211, 287, 358	3.2, 3.9, 3.3	215, 245, 388	3.0, 3.5, 5.7	214, 270, 387	2.7, 3.1, 5.4
bipyridine	249, 359	7.0, 4.6	246, 383	5.3, 5.5	239, 395	5.5, 5.6
2-amino benzaldehyde	222, 374	4.3, 4.0	226, 282, 507	3.8, 5.3, 5.1	225, 265, 331, 464	4.8, 3.7, 5.3, 1.6

Table 4.2: Schiff base derivatives with their maximum absorption peaks.

The 2-aminobenzaldehyde based salqu ligand (Figure 4.4) was the best of the Schiff bases measured and it is the candidate to replace the 3,5-di-tert-butylsalicylaldehyde currently in use. While 2-aminobenzaldehyde is expensive, 2-nitrobenzaldehyde is not and can be easily reduced to the amine by catalytic hydrogenation by palladium on carbon, or ferrous sulfate and ammonia before being distilled off as pure product.[44] As can been seen in the figure below, the copper, uranyl, and ligand peaks are separated at ~280 – 380 nm. The copper complex has a higher energy peak that could be used to help differentiate it from the uranyl complex at 530 nm.

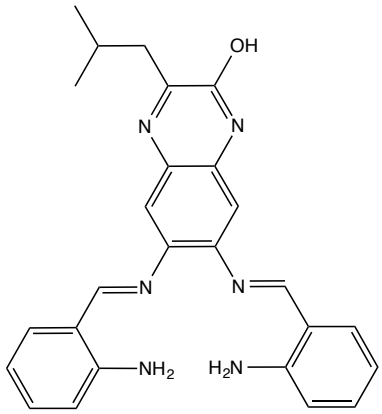

Figure 4.4: 2-aminobenzaldehyde with quinoxolinol backbone

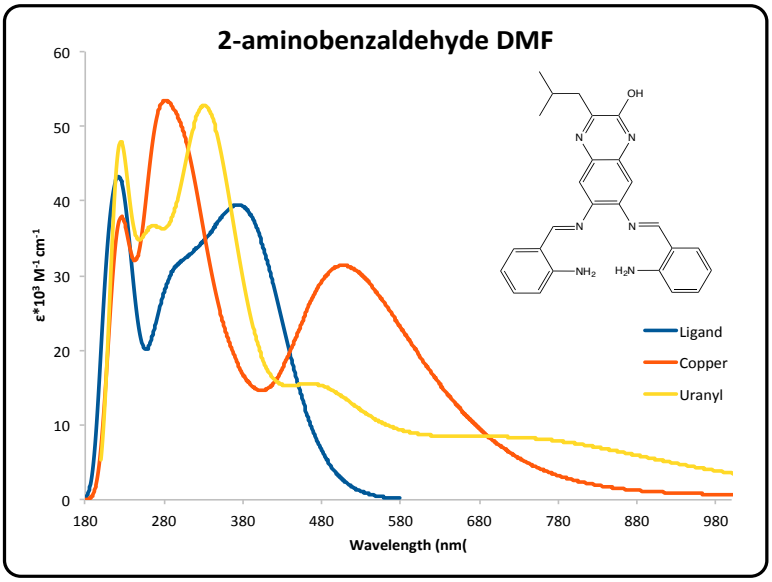

Figure 4.5: Calculated 2-aminobenzaldehyde Schiff base spectrum with the copper and uranyl complex.

4.33 Triazine

To continue the investigation with ligands based on those used in the SANEX process, 2,3,6-triazine groups were incorporated with the quinoxolinol backbone for comparison. Synthetically, this adds four steps to the synthesis. The first step is a Sandmeyer reaction to replace the amines with nitriles. Hydrazine hydrate is then used to add two nitrogens, followed by an α-diketone addition to complete the rings. Because of the pyridine rings, only one nitrogen on each triazine binds to the metal, but since pyridines are not incorporated into the quinoxolinol, the calculations were done with the 1,2 nitrogens of the triazine both binding the metals. The procedure for making this synthetically is very challenging and has not been completed to date for the quinoxolinol backbone. The coordination shown in figure 4.6 is not currently in the literature. Any coordination to the 1,2,4-triazine is coordinated to the 2-N and a pyridine or some other coordinating molecule attached to the triazine by a linker is also bound to the metal.[45,46] Since there is not another group attached, for the purpose of these calculations, the 1,2-nitrogens to help fill the coordination sphere. Future experiments will determine if this coordination is feasible and calculations can be modified to reflect the changes.

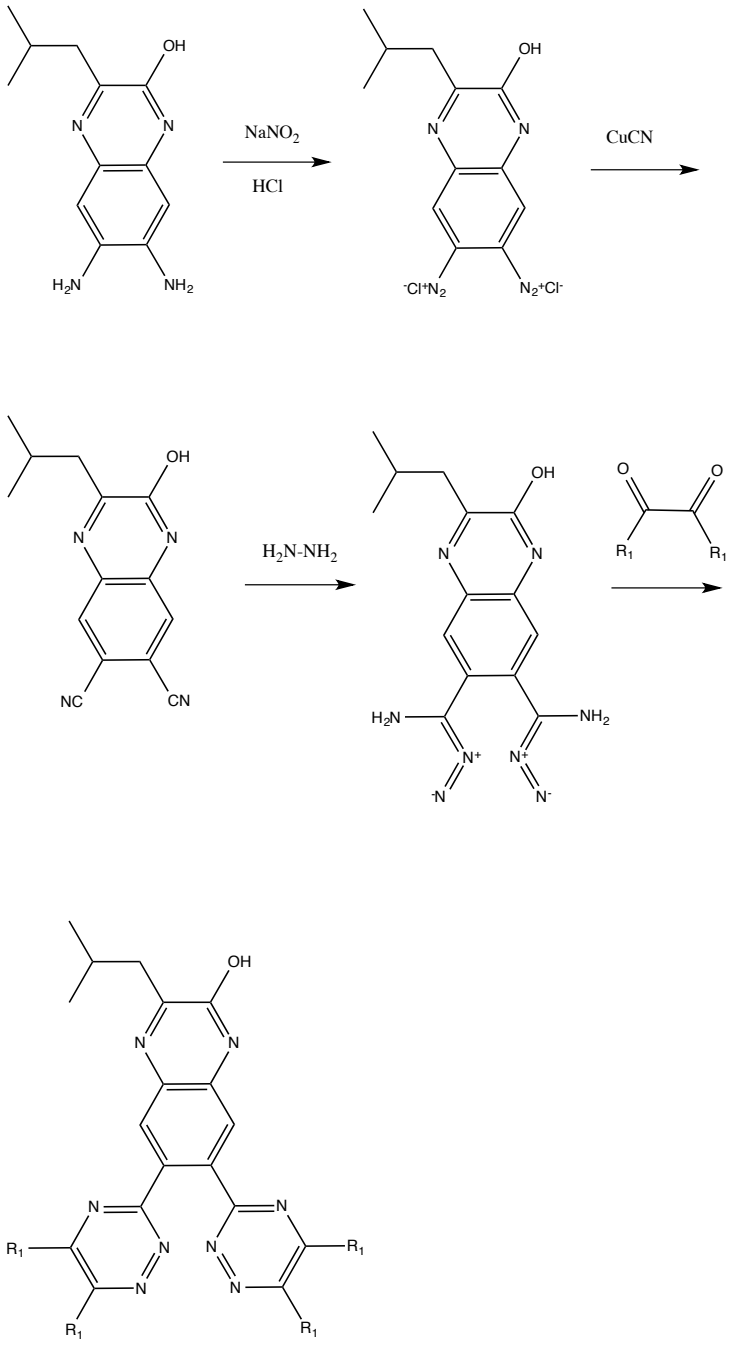

Scheme 4.1: Synthesis of triazine from quinoxaline

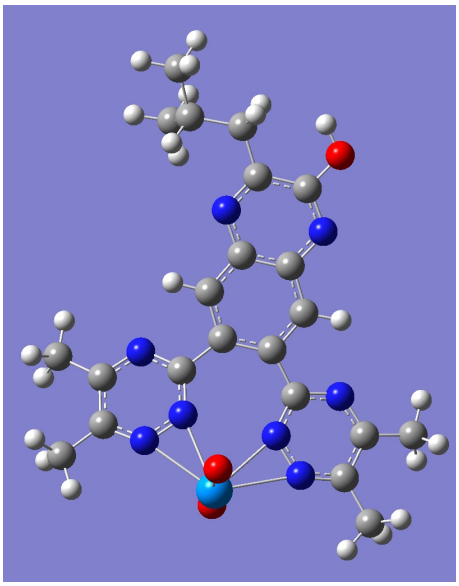

Figure 4.7: Showing the binding with two of the three triazine nitrogens for uranyl in the calculations. Copper is bound the same way for the calculations.

R1	λmax Abs (nm)					
	Ligand	ε*10⁴ M^{-1} cm^{-1}	Copper	ε*10⁴ M^{-1} cm^{-1}	Uranyl	ε*10⁴ M^{-1} cm^{-1}
H	240, 304	1.0, 5.4	314, 486	3.8, 0.3	309	5.6
t-butyl	201, 277	4.0, 6.8	225, 303, 521	3.3, 5.4, 0.3	239, 308	2.8, 6.2
i-butyl	257, 326	6.7, 3.5	260, 490	9.9, 0.6	265, 572	9.4, 0.7
methyl	275	6.8	242, 302, 500	2.3, 6.7, 0.1	222, 303, 442	2.8, 6.8, 0.2
phenyl	222, 298	4.3, 7.6	342	7.6	336	8.4
hexyl	275	6.9	231, 301, 499	2.7, 5.2, 0.5	229, 303	2.8, 6.9
1,2-cylcohexane	274	6.8	234, 299, 509	2.7, 5.6, 0.4	242, 302	2.3, 6.7

Table 4.3: R_1 groups to complete the triazine, maximum absorbance and extinction coefficient.

The best α-diketone was diacetyl to complete the triazine ring. Copper and uranyl both give the same shift away from the ligand, but the difference is around 225 nm when uranyl has a higher energy peak as compared to the copper complex. At 450

nm, both complexes have a shoulder but the uranyl has a higher extinction coefficient, so that could possibly be another way to differentiate the two metals. The diketone consisting of iso-butyl groups and a di-aldehyde would be worth pursuing for synthesis and further characterization by experiment.

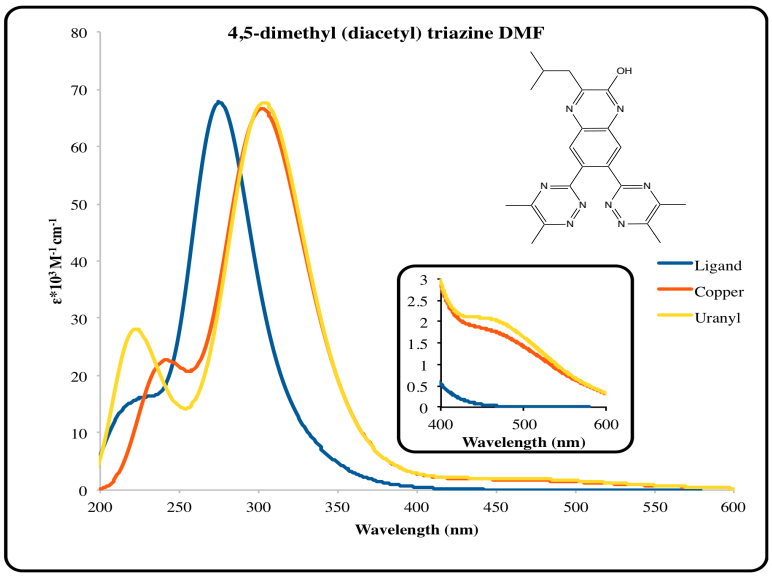

Figure 4.8: Calculated di-acetyl spectrum for triazine quinoxolinol with copper and uranyl complex.

4.34 Pyridine Amides

Macrocycles such as crown ethers, aza-crowns, and expanded porphyrins have long been proposed for selective coordination to actinide metal ions.[2,3] In keeping with the commonly held premise that the softer donors are more selective for actinides, a 2,6-pyridine-dicarboxylic acid or the di-acid chloride could be used to

potentially create a 6-N macrocycle, with the size big enough to fit the actinides, but would force a twist in the ligand to bind to transition metals. Although the goal is the macrocycle, three other ligands could be made as well; a mono-substituted with one pyridine and one quinoxolinol, a di-substituted around the quinoxolinol and a di-substituted around the pyridine (Figure 4.). These macrocycles are also known for being anion receptors for ions such as chlorine, fluorine, and nitrate.[47]

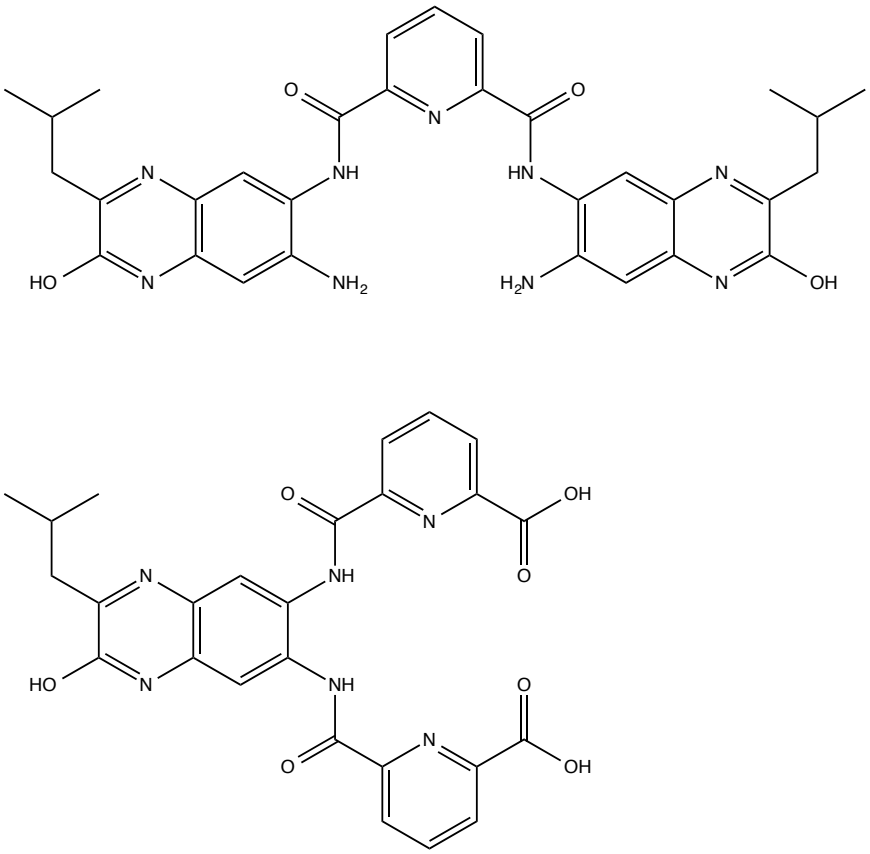

Figure 4.9: Pyridine-amide ligand designes

After optimization of the coordinated geometry of the complexes, actinides fit into the macrocycle much better than the transition metals. The transition metals only

bind to one side of the macrocycle and to fill a 4th coordination site if needed, the ligand twists under itself. This may not happen experimentally because of the strain (not calculated here) on the molecule, thus the last coordination site would likely be filled with a solvent molecule. The actinides fit with only a slight twist of the macrocycle to accommodate the later actinides such as plutonium and americium

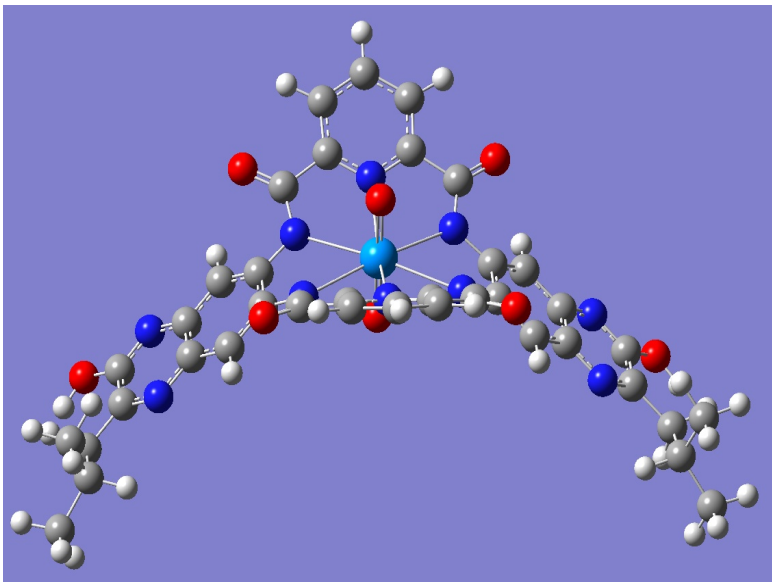

Figure 4.10: Optimized geometry of uranyl complex of pyridine amide macrocycle

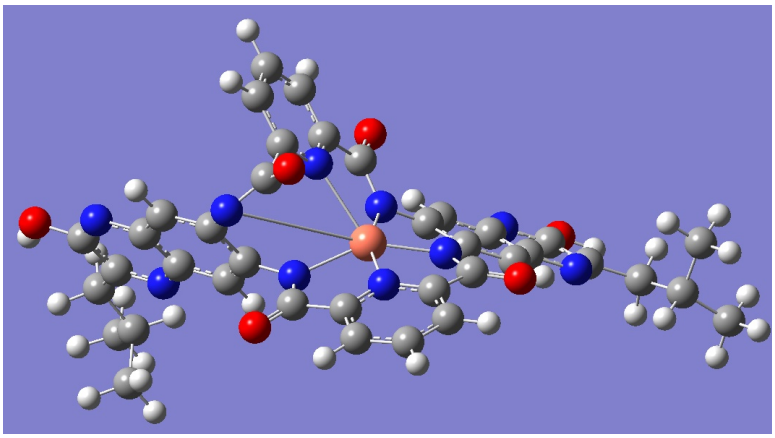

Figure 4.11: Optimized geometry of copper complex of pyridine amide macrocycle

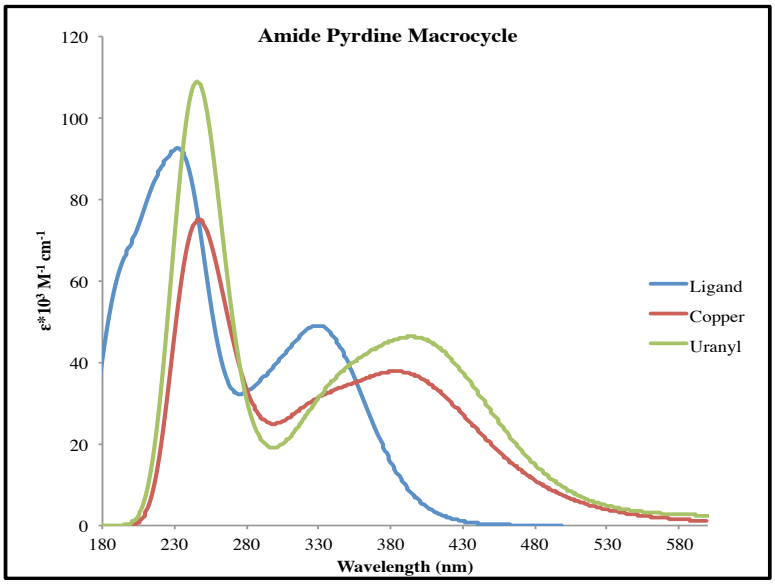

Figure 4.12: Calculated spectrum of amide pyridine macrocycle with copper and uranyl complex

While the uranyl and copper complex peaks overlap, the uranyl has a higher extinction coefficient which could be one way to distinguish between the two metals.

There is a small difference between the peaks at 379 for copper and 387 for uranyl. The di-substituted ligand on the pyridine has the potential to be a good ligand depending on experimental outcomes. In this case, the uranyl peak also has a higher extinction coefficient than the copper complex, and there is an absorbance maximum unique to the copper complex. The di-substituted on the quinoxolinol is a different story. The uranyl complex has less extinction coefficient and the peaks overlap with the copper complex. Future work will continue with the mono-substituted ligand.

4.35 Isopththaldehyde

A second macrocycle was proposed using isophthaldehyde. The geometry of the complexes was questionable for actinides, with the metal being either above or below the macrocycle. The transition metals fit in the middle of the macrocycle perfectly. There is not bending other than the backbone when the transition metal is bound.

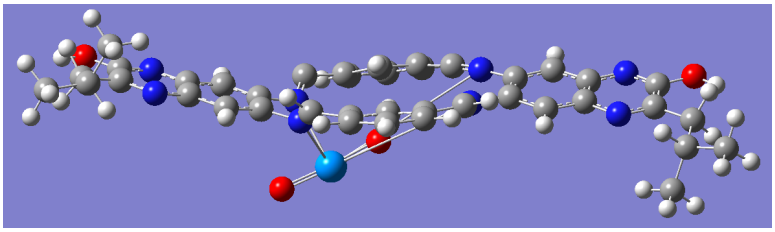

Figure 4.13: Optimized geometry of isophthaldehyde macrocycle with uranyl.

4.4 Conclusions

After preliminary examination of H_2L1 to see if the calculations would be satisfactory, a number of ligands were investigated for their use as potential UV-Vis sensors for uranyl and compared to a known interference metal, copper for comparison. The first calculations were to modify the existing salicylaldehyde, with different substituents and see if the electronics could enhance selectivity or sensitivity. These calculations did not improve upon either the selectivity or sensitivity as compared to the calculated spectra for H_2L1. Next different salicylaldehydes with softer N-donors were tested with the quinoxolinol backbone. These were chosen to enhance the ligand to metal excitation and would hopefully give better selectivity, with sensitivity remaining about the same as compared to H_2L1. The calculations predict that 2-aminobenzaldehyde with the quinoxolinol backbone would give the best separation of absorbance peaks between the uranyl complex, copper complex, and the ligand. Finally, following the SANEX process for nuclear fuel separations in Europe, triazines was investigated with different substituents in the 4,5 positions. The best was methyl groups at the 4,5-position to improve selectivity, sensitivity appeared to decrease. Other ligands that would be of interest would include the pyridine amide macrocycle (Figure 4.14) the pyridine amide disubstituted on the pyridine (Figure 4.15), and the diacetyl triazine (Figure 4.6). The diacetyl triazine provides a greater extinction coefficient at lower energies, but the limits of detection would not be lower to do the lower overall extinction coefficient. The diacetyl also has a uranyl complex peak at very high energy that

could differentiate it from the ligand or copper complex. Whereas a normal salicylaldehyde would be comparable to the experimental 3,5-di-tert-butyl salicylaldehyde, it does not appear to be better than the ones currently being experimentally used. Further experimental work should focus on softer donor ligands such as the triazine and the 2-aminobenzaldehyde.

4.5 References

(1) Tarancon, A.; Garcia, J. F.; Rauret, G. *Anal. Chim. Acta* **2005**, *538*, 233.

(2) Shamov, G. A.; Schreckenbach, G.; Martin, R. L.; Hay, P. J. *Inorg. Chem.* **2008**, *47*, 1465.

(3) Vargas-Zúñiga, G. I.; Sessler, J. L. In *The Rare Earth Elements*; John Wiley and Sons: 2012.

(4) Aydin, F. A.; Soylak, M. *Talanta* **2007**, *72*, 187.

(5) Tamborini, G.; Donohue, D. L.; Rudenauer, F. G.; Betti, M. *J. Anal. At. Spectrom.* **2004**, *19*, 203.

(6) Hong, K. B.; Jung, K. W.; Jung, K. H. *Talanta* **1989**, *36*, 1095.

(7) Mcmahon, A. W. *Sci. Total Environ.* **1993**, *130*, 285.

(8) Brina, R.; Miller, A. G. *Anal. Chem.* **1992**, *64*, 1413.

(9) Sessler, J. L.; Melfi, P. J.; Seidel, D.; Gorden, A. E. V.; Ford, D. K.; Palmer, P. D.; Tait, C. D. *Tetrahedron* **2004**, *60*, 11089.

(10) Lutfullah; Alam, M. N.; Rahman, N.; Azmi, S. N. H. *J. Haz. Materials* **2008**, *155*, 261.

(11) Ruan, C. M.; Luo, W. S.; Wang, W.; Gu, B. H. *Anal. Chim. Acta* **2007**, *605*, 80.

(12) Ganjali, M. R.; Memari, Z.; Norouzi, P.; Shaabani, B.; Emamalizadeh, M.; Hanifehpour, Y.; Faridbod, F. *Anal. Lett.* **2010**, *43*, 2220.

(13) Gorden, A. E. V.; Xu, J.; Raymond, K. N.; Durbin, P. W. *Chem. Rev.* **2003**, *103*, 4207

(14) Sessler, J. L.; Gorden, A. E. V.; Seidel, D.; Hannah, S.; Lynch, V.; Gordon, P. L.; Donohoe, R. J.; Tait, C. D.; Keogh, D. W. *Inorg. Chim. Acta* **2002**, *341*, 54.

(15) Sessler, J. L.; Vivian, A. E.; Seidel, D.; Burrell, A. K.; Hoehner, M.; Mody, T. D.; Gebauer, A.; Weghorn, S. J.; Lynch, V. *Coord. Chem. Rev.* **2001**, *222*, 275.

(16) Sessler, J. L.; Mody, T. D.; Dulay, M. T.; Espinoza, R.; Lynch, V. *Inorg. Chim. Acta* **1996**, *246*, 23

(17) Thuéry, P.; Nierlich, M.; Souley, B.; Asfari, Z.; Vicens, J. *J. Chem. Soc. Dalton Trans* **1999**, *2589 -2594.*

(18) Rogers, R. D.; Bond, A. H.; Hipple, W. G.; Rollins, A. N.; Henry, R. F. *Inorg. Chem.* **1991**, *30*, 2671

(19) Deshayes, L.; Keller, N.; Lance, M.; Navaza, A.; Nierlich, M.; Vigner, J. *Polyhedron* **1994**, *13*, 1725

(20) Clark, D. L.; Keogh, D. W.; Palmer, P. D.; Scott, B. L.; Tait, C. D. *Angew. Chem., Int. Ed. Eng.* **1998**, *37*, 164

(21) Thuery, P.; Keller, N.; Lance, M.; Vigner, J. D.; Nierlich, M. *New J. Chem.* **1995**, *19*, 619.

(22) Khan, M. H.; Warwick, P.; Evans, N. *Chemosphere* **2006**, *63*, 1165.

(23) M. J. Frisch, G. W. T., H. B. Schlegel, G. E. Scuseria, M. A. Robb, J. R. Cheeseman, G. Scalmani, V. Barone, B. Mennucci, G. A. Petersson, H. Nakatsuji, M. Caricato, X. Li, H. P. Hratchian, A. F. Izmaylov, J. Bloino, G. Zheng, J. L. Sonnenberg, M. Hada, M. Ehara, K. Toyota, R. Fukuda, J. Hasegawa, M. Ishida, T. Nakajima, Y. Honda, O. Kitao, H. Nakai, T. Vreven, J. A. Montgomery, Jr., J. E. Peralta, F. Ogliaro, M. Bearpark, J. J. Heyd, E. Brothers, K. N. Kudin, V. N. Staroverov, R. Kobayashi, J. Normand, K. Raghavachari, A. Rendell, J. C. Burant, S. S. Iyengar, J. Tomasi, M. Cossi, N. Rega, J. M. Millam, M. Klene, J. E. Knox, J. B. Cross, V. Bakken, C. Adamo, J. Jaramillo, R. Gomperts, R. E. Stratmann, O. Yazyev, A. J. Austin, R. Cammi, C. Pomelli, J. W. Ochterski, R. L. Martin, K. Morokuma, V. G. Zakrzewski, G. A. Voth, P. Salvador, J. J. Dannenberg, S. Dapprich, A. D. Daniels, Ö. Farkas, J. B. Foresman, J. V. Ortiz, J. Cioslowski, and D. J. Fox; A.1 ed.; Gaussian Inc.: Wallingfor CT, 2009.

(24) Becke, A. D. *J. Chem. Phys.* **1993**, *98*, 5648.

(25) Feller, D. *J. Comput. Chem.* **1996**, *17*, 1571.

(26) Schuchardt, K. L.; Didier, B. T.; Elsethagen, T.; Sun, L. S.; Gurumoorthi, V.; Chase, J.; Li, J.; Windus, T. L. *J. Chem. Inf. Model.* **2007**, *47*, 1045.

(27) Petersson, G. A.; Al-Laham, M. A. *J. Chem. Phys.* **1991**, *94*, 6081.

(28) Petersson, G. A.; Bennett, A.; Tensfeldt, T. G.; Al-Laham, M. A.; Shirley, W. A.; Mantzaris, J. *J. Chem. Phys.* **1988**, *89*, 2193.

(29) Bacskay, G. B. *Chem. Phys.* **1981**, *61*, 385.

(30) Bauernschmitt, R. A., Reinhart *Chem. Phys. Lett.* **1996**, *256*, 454.

(31) Casida, M. E.; Jamorski, C.; Casida, K. C.; Salahub, D. R. *J. Chem. Phys.* **1998**, *108*, 4439.

(32) Furche, F.; Ahlrichs, R. *J. Chem. Phys.* **2002**, *117*, 7433.

(33) Furche, F.; Ahlrichs, R. *J. Chem. Phys.* **2004**, *121*, 12772.

(34) Scalmani, G.; Frisch, M. J.; Mennucci, B.; Tomasi, J.; Cammi, R.; Barone, V. *J. Chem. Phys.* **2006**, *124*, 94107.

(35) Stratmann, R. E.; Scuseria, G. E.; Frisch, M. J. *J. Chem. Phys.* **1998**, *109*, 8218.

(36) Van Caillie, C. A., Roger D. *Chem. Phys. Lett.* **1999**, 249.

(37) Van Caillie, C. A., Roger D. *Chem. Phys. Lett.* **2000**, 159.

(38) Martin, R. L. *J. Chem. Phys.* **2003**, *118*, 4775.

(39) Minasian, S. G.; Keith, J. M.; Batista, E. R.; Boland, K. S.; Clark, D. L.; Kozimor, S. A.; Martin, R. L.; Shuh, D. K.; Tyliszczak, T. *Chem. Sci.* **2014**.

(40) Hudson, M. J.; Harwood, L. M.; Laventine, D. M.; Lewis, F. W. *Inorg. Chem.* **2013**, *52*, 3414.

(41) Drew, M. G. B.; Guillaneux, D.; Hudson, M. J.; Iveson, P. B.; Madic, C. *Inorg. Chem. Commun.* **2001**, *4*, 462.

(42) Drew, M. G. B.; Foreman, M. R. S. J.; Hill, C.; Hudson, M. J.; Madic, C. *Inorg. Chem. Commun.* **2005**, *8*, 239.

(43) Lewis, F. W.; Harwood, L. M.; Hudson, M. J.; Drew, M. G. B.; Desreux, J. F.; Vidick, G.; Bouslimani, N.; Modolo, G.; Wilden, A.; Sypula, M.; Vu, T. H.; Simonin, J. P. *J. Am. Chem. Soc.* **2011**, *133*, 13093.

(44) Foy, B. D.; Smudde, R. A.; Wood, W. F. *J. Chem. Educ.* **1993**, *70*, 322.

(45) Geist, A.; Hill, C.; Modolo, G.; Foreman, M. R. S. J.; Weigl, M.; Gompper, K.; Hudson, M. J. *Solvent Extr. Ion Exch.* **2006**, *24*, 463.

(46) Jian, F. F.; Ren, P. *Acta Crystallogr. Sect. Sect. E: Struct. Rep. Online* **2010**, *66*, O427.
(47) Gale, P. A. *Chem. Commun.* **2011**, *47*, 82.

Chapter 5: Uranyl vs. Europium extractions from nitric acid

5.1 Introduction

Nuclear fuel reprocessing is going to play an important part in the future, as more and more reactors are built to provide the necessary electricity demanded by society, and renewable energy still as yet cannot keep up with the demand for energy. At present, over half of the world's spent nuclear fuel is produced in a "once-through cycle."[1,2] There are two approaches considered when managing the radioactive byproducts of nuclear fission: the open fuel cycle in which spent fuel elements are managed as waste, and the closed-loop fuel cycle in which spent fuel undergoes separation to recover byproducts for reuse and recycle (leaving the less useful materials for disposal as waste).[3] In the open loop (once-through) fuel cycle, the fuel elements remain intact and are the waste form, stored in concrete and steel casks till geological disposal.[3] Currently practiced in France, the closed loop fuel cycle recycles U and Pu isotopes only using tri-n-butyl phosphate, while all other materials are converted to glass for disposal.[3] The current problem with this recycling is the separation and isolation of weapons grade plutonium (^{239}Pu) in any separations process, leading to proliferation and security issues,[4] as well as the minor actinides left in the processed waste.[5]

The processed nuclear fuel could be stored in a deep geological depository but the fuel will remain radioactive for millions of years, and storage is not favored by the public.[6] There is an alternative method to the leftover spent fuel after the recycling process that could render the fuel safer and more suitable for geological storage. Of the transuranium elements, the minor actinides americium and curium have especially high radiotoxicities, making them desirable to remove them from spent nuclear fuel and deal with them separately.[7,8] The removal of U and Pu reduced the radiotoxicity significantly as is, but the additional removal of the minor actinides would reduce the storage time to 300 years, from 9000 years.[6] It is still important to separate Am and Cm from the lanthanides because of the neutron capture ability of the lanthanides is 40 times greater than the actinides.[6] One possible future scenario is the conversion or transmutation of these long-lived minor actinides, into short-lived isotopes by irradiation with neutrons in a fast reactor.[9,10]

Many extraction processes have been studied as indicated in chapter 1, such as PUREX,[11] DIAMEX,[12] TRUEX,[13] TALSPEAK,[3] and SANEX[14] but there remains room for improvement, and it is the hope that the ligands used in sensing could have a dual use in extractions. The research below was to test the sensing ligand "Salqu" as an extractant for uranyl versus europium, as a model for actinides versus lanthanides.

5.2 Experimental

The Salqu (H_2L1) ligand was synthesized as previously described and dissolved in 1-octanol to the desired concentration (See figure 5.1.) The extractions were performed by shaking equal volumes of aqueous ($0.1 – 1.0 \times 10^{-5}$ M HNO_3) and organic phase for 1 minute and allowing the phases 2 hours to settle. The aqueous phase was removed and taken to ICP-OES to determine the metal concentration. The ligand was also compared to a normal Salen ligand, and the quinoxalinol backbone dissolved in 1-octanol at the same molar concentrations. Distribution and separation factors were calculated to determine the extraction ability and selectivity of the ligands for the two metals. Distribution (D) is defined as the concentration of the organic phase divided by the concentration in the aqueous phase. Separation factor (SF) is defined as D_U / D_{Eu}.

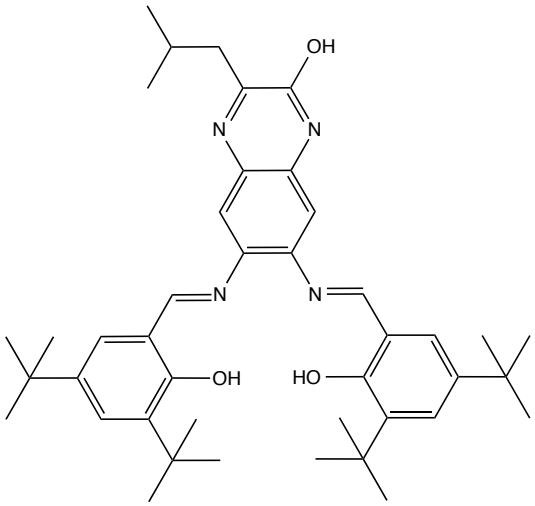

H_2L1

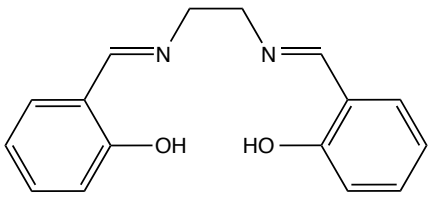

Salen

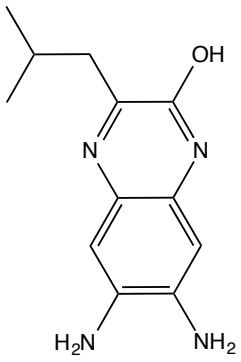

2-quinoxalinol backbone

Figure 5.1: Ligands used in extractions

5.3 Results

With the selectivity for uranyl over lanthanides according to the UV-Vis spectra, this H_2L1 ligand should be a good step towards ideas of future ligands for the reprocessing of nuclear fuel. The first test was to determine if the ligand would not decompose in 3 M nitric acid, the concentration of the aqueous phase at which current separations of nuclear fuel take place. There was an immediate color change of the ligand in octanol from yellow to red as the two phases were shaken and mixed. This would typically indicate the double bond of the Schiff base breaking down to a single bond and would hinder binding. Thus, the ligand was decomposing and would not be useable under extreme acidic conditions. The highest concentration of nitric acid able to be used was 0.1 M HNO_3 and extractions were tested all the way to 1 x 10^{-5} M HNO_3, typical of a mixed N-, O-donor extractant.[6]

At a 1 to 1 molar ratio of metal to ligand, all three ligands are increase the extraction of both metals as the nitric acid concentration decreases with the highest increases between 0.01 and 0.0001 M HNO_3. Unexpectedly, the softer donors of the amines on the quinoxalinol increased the europium extraction as well, as nitrogens do not typically form strong bonds with lanthanides. The separation factors were within the same range between 5 and 7 and the majority is below 10, which is a general threshold for good selectivity. The only one above 10 is the quinoxalinol at a very low nitric acid concentration, which is not suitable for nuclear fuel waste extractions. To increase the extraction efficiency and amount of uranyl extracted, higher

concentrations of ligands were used: 0.5 mM, 0.75 mM, and 1.0 mM. This should increase the distribution of uranyl with the same distribution for europium, thereby increasing the separation factor.

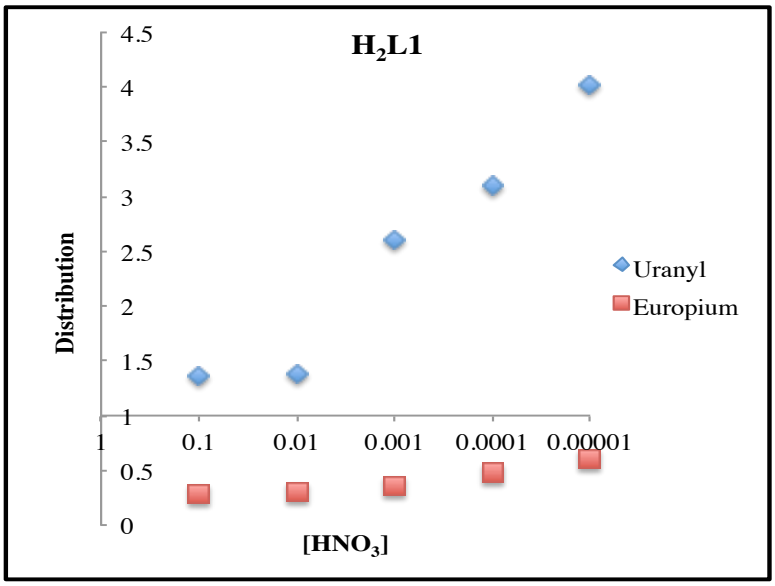

Figure 5.2 a: H_2L1 distribution of uranyl and europium at 1 to 1 molar concentrations

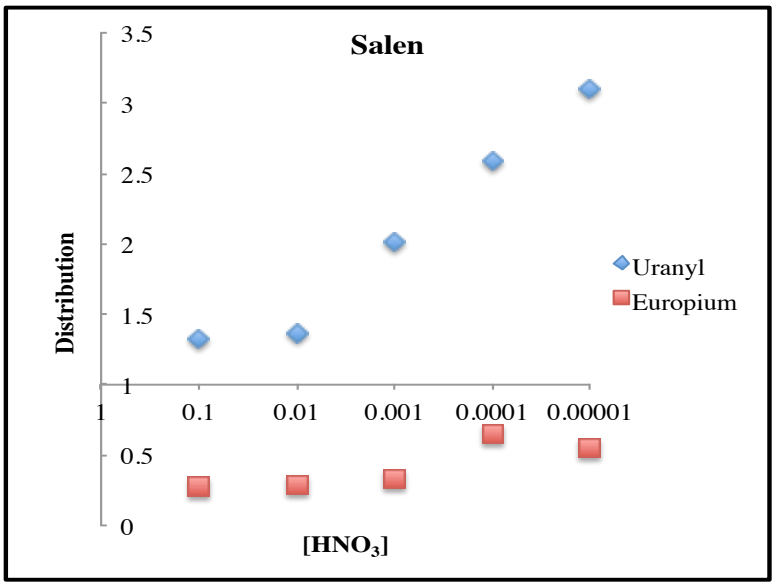

Figure 5.2 b: Salen distribution of uranyl and europium at 1 to 1 molar concentrations

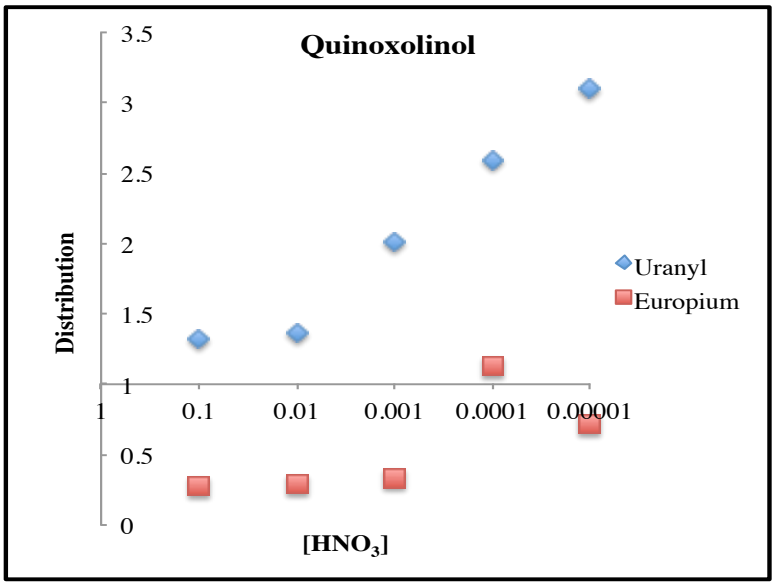

Figure 5.2 c: Quinoxalinol distribution of uranyl and europium at 1 to 1 molar concentrations

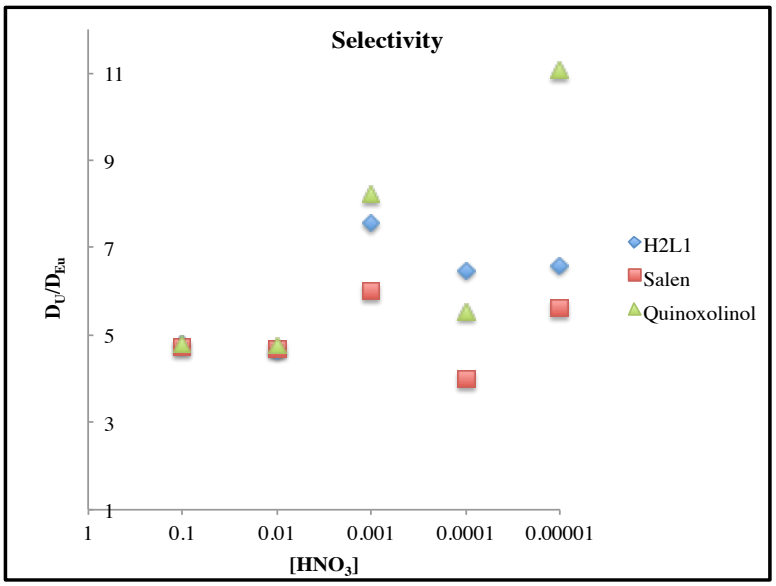

Figure 5.3: Separation factor for the three ligands at 1 to 1 molar ratio

5.31 0.5 mM ligand concentration

Much like what was seen with a 1 to 1 molar ratio of ligand to metal, the efficiency of the extraction increases for H_2L1 as the concentration of nitric acid decreases. The europium extraction greatly increases at 1.0 x 10^{-4} M HNO_3, even being extracted more than uranyl. The uranyl extraction was less with more ligand than compared to the 1 to 1 extractions, especially at lower concentrations of nitric acid. Salen had the opposite effect of what has been seen previously. The uranyl extraction becomes less whereas the europium extraction stays the same or slightly increases. The uranyl decreasing in distribution ratio will cause the separation factor to decrease as well making the selectivity poor. Why is it that europium was extracted more for H_2L1 than salen at the same nitric acid concentration. Could the backbone

play a role in binding? One would not expect that the quinoxalinol alone would be very good for extraction in general, but it should still extract more uranyl than europium, because the amines would act more favorably as donors to uranyl than europium. By looking at 0.75 mM of quinoxalinol, the same increase in europium extraction occurred so maybe the quinoxalinol really did do the extractions that well at that concentration of nitric acid. Perhaps, at the lower concentrations of nitric acid, the metal salt is being stripped of the nitrates and able to bind more tightly to the ligands.

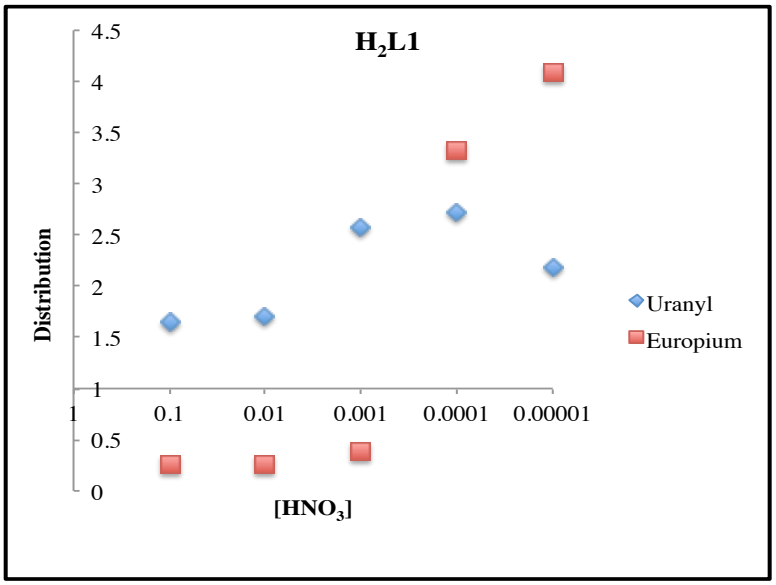

Figure 5.4 a: H_2L1 (0.5 mM) distribution ratio for uranyl and europium

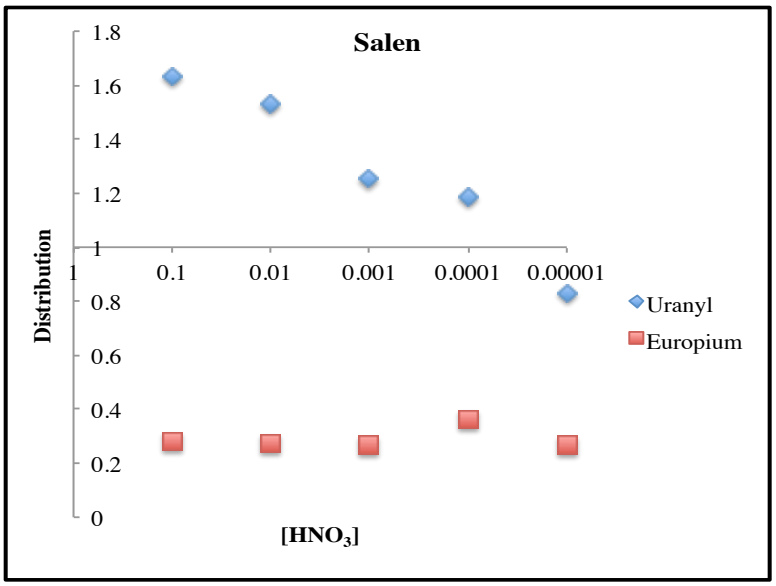

Figure 5.4 b: Salen (0.5 mM) distribution ratio for uranyl and europium

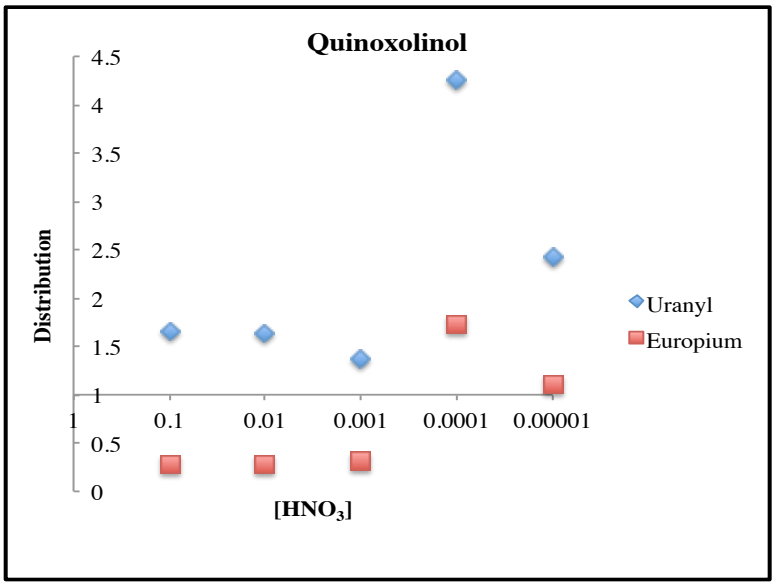

Figure 5.4 c: Quinoxalinol backbone (0.5 mM) distribution ratio for uranyl and europium.

As would be expected with the increasing extraction of europium by all the ligands as the nitric acid concentration became less, but was still in the range for higher nitric acid concentrations as with the 1:1 metal to ligand ratio. No ligand had less selectivity than H_2L1 as it greatly increased the extraction of europium at lower nitric acid concentrations. As of this point, increasing the ligand concentration does not increase the extraction of uranyl, nor does it increase the selectivity.

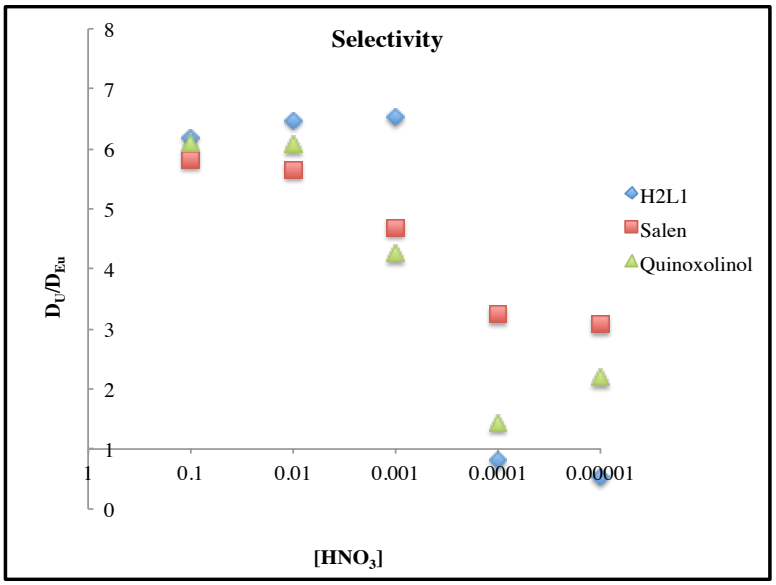

Figure 5.5: Separation factors for the three ligands at 0.5 mM concentration

5.32 0.75 mM ligand concentration

Increasing the H_2L1 ligand concentration to 0.75 mM also did not improve the extraction of uranyl, but greatly increased the extraction of europium at lower concentrations of nitric acid, to a point that the selectivity of uranyl is less than for

europium (Figure 5.6a). Unlike the other extractions seen so far, but what seems typical for salen, is that the extraction ability stayed relatively the same at about a distribution of 3. The europium was extracted more at lower nitric acid concentrations to around 0.6. The higher nitric acid concentrations only had a distribution of 0.5 (Figure 5.6b). The quinoxalinol follows the same trend as at 0.5 mM concentration but there is more europium than uranyl extracted at $1x10^{-4}$ but decreases at $1x10^{-5}$ M HNO_3 (Figure 5.6c). The uranyl was extracted more as well as can be seen at the higher distribution at those concentrations, but quinoxalinol is not a good ligand for separating the groups at these nitric acid concentrations. It is still odd that the uranyl does not have a higher distribution ratio than europium due to the hard soft acid base theory.

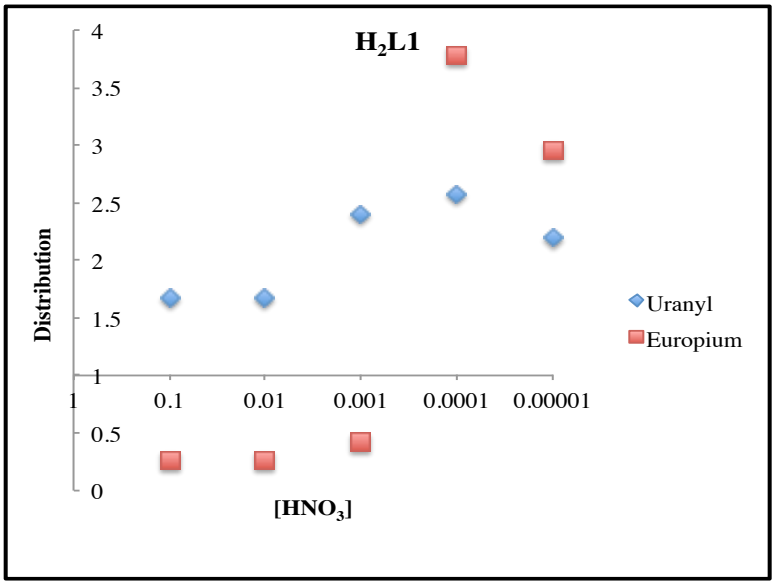

Figure 5.6 a: H_2L1 (0.75 mM) distribution ratio for uranyl and europium

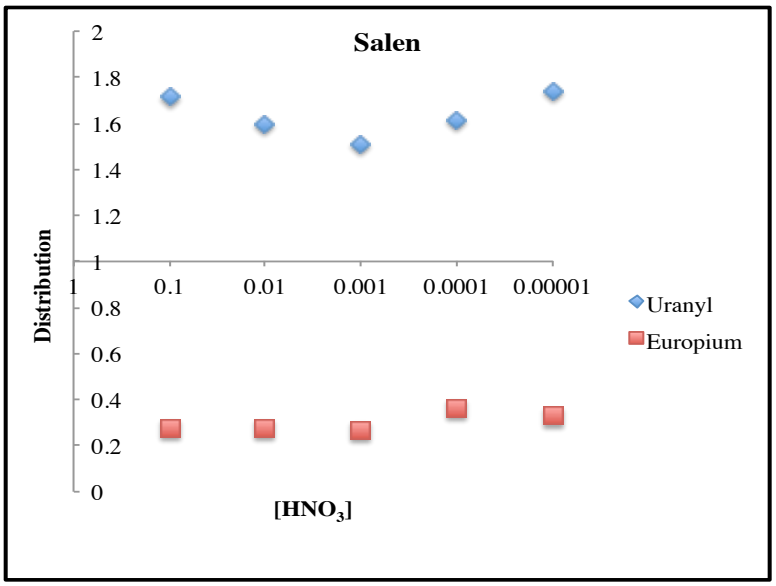

Figure 5.6 b: Salen (0.75 mM) distribution for uranyl and europium

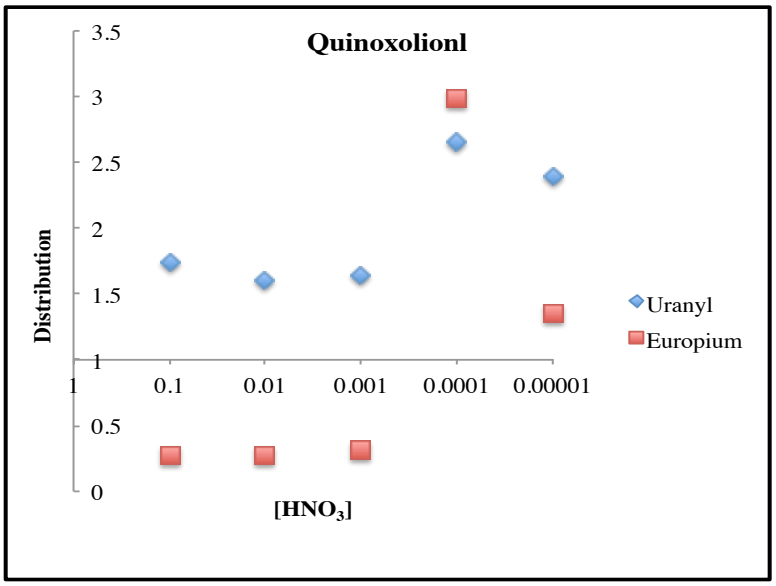

Figure 5.6 c: Quinoxalinol backbone (0.75 mM) distribution of uranyl and europium.

As the graph below suggests (Figure 5.7), there is a downward trend in selectivity, as the concentration of nitric acid decreases. This is because more europium is being extracted at those concentrations limiting the selectivity. The quinoxalinol had the worst at the $1x10^{-5}$ M HNO_3 while the separation is similar for 0.1 to $1x10^{-3}$ M HNO_3.

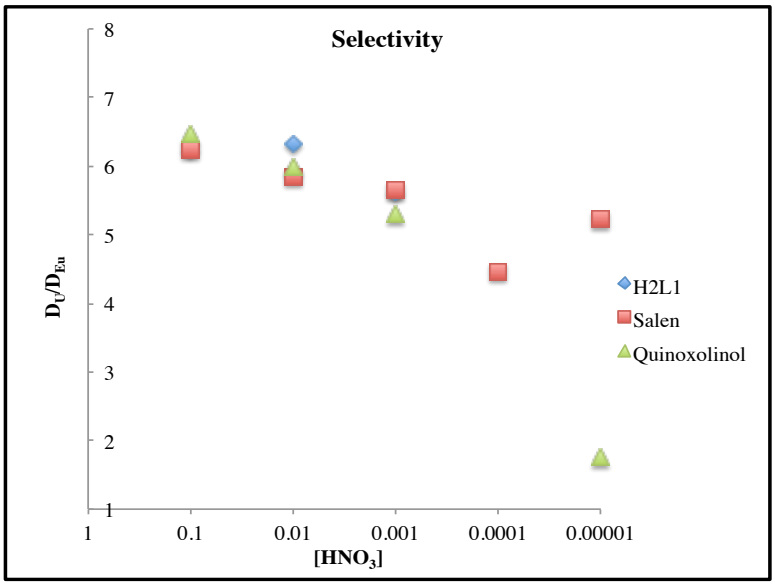

Figure 5.7: Separation factors for the three ligands at 0.75 mM concentration

5.33 1.0 mM ligand concentration

Following the current trends with an excess of ligand, the H_2L1 ligand is increasing extraction of europium at lower concentrations of nitric acid, with a general increase in the extraction of uranyl (Figure 5.8a). It was expected that at such a high concentration of ligand compared to the metal, that the uranyl would be greatly

more extracted but this is shown to not be the case. Salen extraction of uranyl remained roughly the same as the nitric acid concentration changed (Figure 5.8b). The europium extraction was also very close to being the same except at 0.0001 M HNO_3. For the first time with quinoxaline, the europium extraction does not have a distribution ratio greater than 1 (Figure 5.8c). The uranyl extraction is relatively steady till 0.00001 M HNO_3 concentration where it increases up to around 3.5, much higher than the ~1.5 from higher nitric acid concentrations.

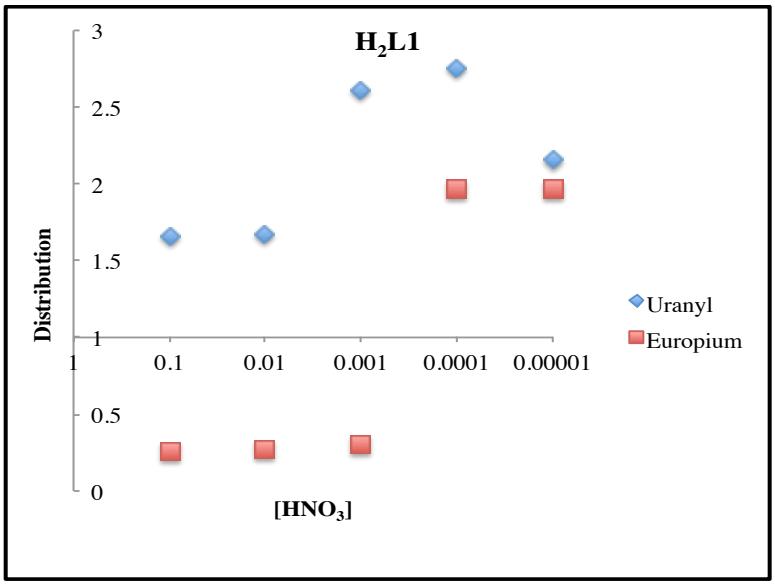

Figure 5.8 a: H_2L1 (1.0 mM) distribution of uranyl and europium

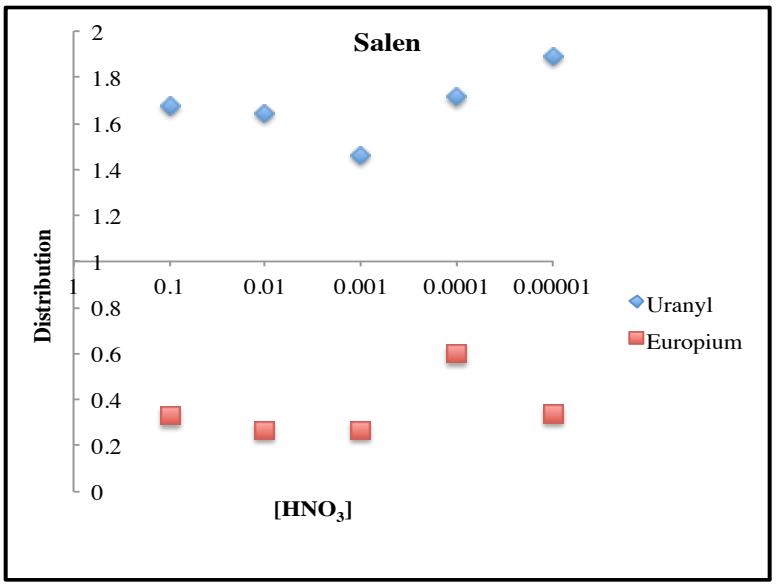

Figure 5.8 b: Salen (1.0 mM) distribution ratio for uranyl and europium

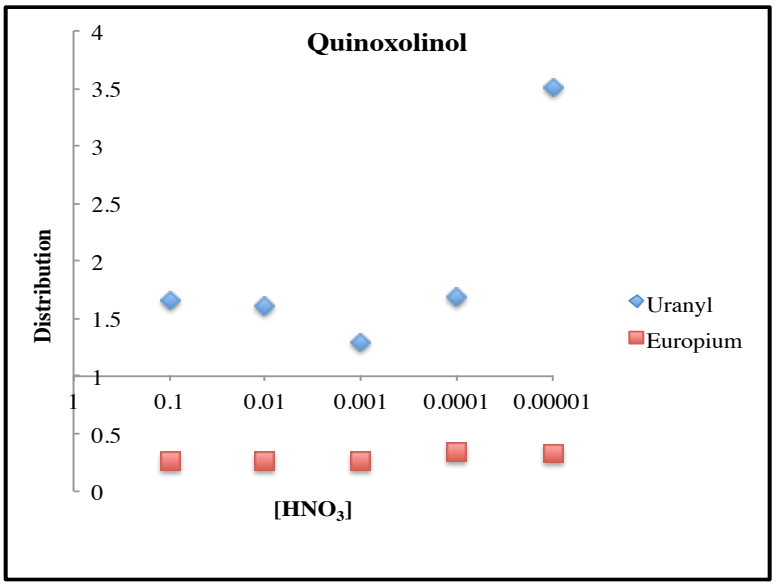

Figure 5.8 c: Quinoxalinol (1.0 mM) distribution for uranyl and europium

The H_2L1 ligand has a sharp decrease in selectivity as more europium was extracted at lower concentrations of nitric acid (Figure 5.9). The Salen ligand remained relatively unchanged except for at 0.0001 M HNO_3 due to the increase in europium extraction and unchanged uranyl extraction at that concentration. The quinoxalinol ligand was unchanged until the lowest nitric acid concentration when it reaches above 10 for the separation factor. This is due to the greater extraction of uranyl with a low extraction of europium. Further study into improved systems and new ligands with the calculations will be discussed in the next chapter.

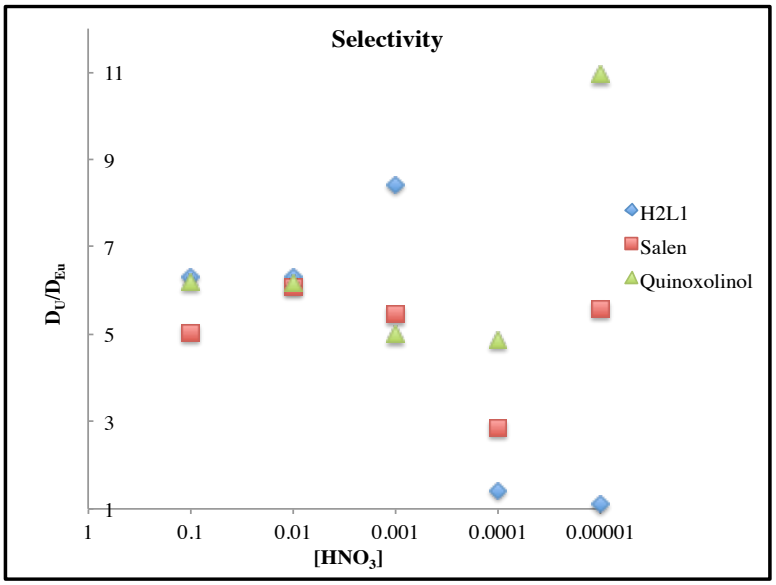

Figure 5.9: Separation factors for H_2L1, Salen, and Quinoxalinol at concentration of 1.0 mM

Extractions with this mixed N- and O- donor ligands are typical of other N- and O- donor ligands where the extraction increases as the nitric acid concentration

decreases. The increasing europium extraction was something unexpected that happened with all the ligands. These ligands are not suitable for nuclear fuel extractions.

5.4 Conclusions

The ability of H_2L1 and salen to extract more uranyl at lower concentrations of nitric acid is consistent with other mixed N, O – donor ligands from previous extractants. This hinders these ligands as nuclear fuel waste extractants because they cannot be used at 3M nitric acid concentrations. Across the board the extractions were similar for every experiment with the uranyl distribution above 1 and the europium distribution below 1. The only exceptions was for europium having a distribution greater than 1 was for increased concentrations of H_2L1, and lower nitric acid concentrations for the quinoxalinol backbone. The separation factors, although above 1, were not above 10, which is considered the threshold of good selectivity for separations. The next step if so desired, would be to use H_2L1 as a stripping agent from a loaded organic phase. Much work still needs to be done to increase the selectivity of these ligands for use as nuclear fuel extractants.

5.5 References

(1) Mathur, J. N.; Murali, M. S.; Nash, K. L. *Solvent Extr. Ion Exch.* **2001**, *19*, 357.

(2) Schaffer, M. B. *Energy Policy* **2011**, *39*, 1382.

(3) Nilsson, M.; Nash, K. L. *Solvent Extr. Ion Exch.* **2007**, *25*, 665.

(4) Ewing, R. C. *Comptes Rendus Geoscience* **2011**, *343*, 219.

(5) Lewis, F. W.; Harwood, L. M.; Hudson, M. J.; Drew, M. G. B.; Wilden, A.; Sypula, M.; Modolo, G.; Vu, T.-H.; Simonin, J.-P.; Vidick, G.; Bouslimani, N.; Desreux, J. F. *Procedia Chemistry* **2012**, *7*, 231.

(6) Hudson, M. J.; Harwood, L. M.; Laventine, D. M.; Lewis, F. W. *Inorg. Chem.* **2013**, *52*, 3414.

(7) Choppin, G. R.; Liljenzin, J.-O.; Rydberg, J. *Radiochemistry and Nuclear Chemistry*; 3rd ed.; Butterworth-Heinemann: Woburn, Massachussets, 2002.

(8) Birkett, J. E.; Carrott, M. J.; Fox, O. D.; Jones, C. J.; Maher, C. J.; Roube, C. V.; Taylor, R. J.; Woodhead, D. A. *Chimia* **2005**, *59*, 898.

(9) Boubals, N.; Drew, M. G. B.; Hill, C.; Hudson, M. J.; Iveson, P. B.; Madic, C.; Russell, M. L.; Youngs, T. G. A. *J. Chem. Soc., Dalton Trans.* **2002**, 55.

(10) Sakamoto, Y.; Garnier, J.-C.; Rouault, J.; Grandy, C.; Fanning, T.; Hill, R.; Chikazawa, Y.; Kotake, S. *Nucl. Eng. Des.* **2013**, *254*, 194.

(11) Mckibben, J. M. *Radiochimica Acta* **1984**, *36*, 3.

(12) Serrano-Purroy, D.; Baron, P.; Christiansen, B.; Malmbeck, R.; Sorel, C.; Glatz, J. P. *Radiochimica Acta* **2005**, *93*, 351.

(13) Mincher, B. J.; Schmitt, N. C.; Case, M. E. *Solvent Extr. Ion Exch.* **2011**, *29*, 247.

(14) Whittaker, D. M.; Griffiths, T. L.; Helliwell, M.; Swinburne, A. N.; Natrajan, L. S.; Lewis, F. W.; Harwood, L. M.; Parry, S. A.; Sharrad, C. A. *Inorg. Chem.* **2013**, *52*, 3429.

Chapter 6 Conclusions and Future Work

Much research has focused on creating sensors for the selective recognition of actinide metals that is inherently difficult due to the strong coordination of transition metal ions to the same sorts of binding pockets. Perhaps, it is better investigate ligands that would provide a unique signal for the actinides as they would for other metals, a green light for actinides, and a red light for transition metals, and yellow light for lanthanides. The other way to differentiate them is through UV-Vis spectroscopy, where the ligand when bound to the metal, would give a maximum absorbance that is different from the ligand and any competing metals. It would be fine if all the actinide absorbencies overlapped so long as they were different than the ligand and competing metals.

This investigation began with the ligand H_2L1, a quinoxolinol salen ligand. With many pi-bonds, this ligand should create a high signal to noise ratio to help with sensitivity. H_2L1 proved to be a good sensor for uranyl over copper and other metals that were tested. This ligand dissolved in dimethylformamide (DMF), had a maximum absorbance of ~389 nm depending on the concentration of water in the sample with an extinction coefficient of 2.6×10^4 $M^{-1} \cdot cm^{-1}$ at a ligand concentration of 20 μM. Maximum water concentration could only be 20% before precipitation. Upon the addition of 1 equivalent of copper acetate solution, the ligand color would

change from a fluorescent yellow to a orange-yellow and the UV-Vis spectrum would indicate a maximum absorbance at 450 nm with an extinction coefficient of ~3.2 x10^4 M^{-1} • cm^{-1} across all concentrations of water. The detection limit for copper with this ligand was ~1 ppm. With the addition of 4 equivalents of uranyl, after two hours of constant stirring, the ligand would change in color from a fluorescent yellow to a more dull yellow. Equivalents 1-3 show no color change to the naked eye but the UV-Vis spectrum would show an increasing shoulder at 450 nm and a small higher energy shift from the ligand. The higher energy shift reached a maximum at 4 equivalents of uranyl, with a maximum absorbance of ~368 nm and an extinction coefficient of 2.6x10^4 M^{-1} • cm^{-1}, giving a detection limit of ~20 ppm. The addition of 1 equivalent of cobalt solution causes a change in the ligand solution color to an orange with a maximum absorbance at ~433 nm and an extinction coefficient of 2.1x10^4 M^{-1} • cm^{-1}, with a detection limit equal to copper, of ~1 ppm. Other metals such as nickel, cerium and gadolinium, have < 3 nm or no shift from the ligand and only nickel has a color change due to an increasing absorbance ~450 nm.

The mono-substituted ligand H_3L3 was also investigated in DMF with varying metals and percentage of water. This ligand could withstand up to 40% water in solution. The ligand, however, was not a good sensor for uranyl. This could be due to binding not being strong enough, or it doesn't bind at all. Copper and cobalt were still investigated for increasing concentrations of water, and all metals that were tested for H_2L1 were tested at 40% water/DMF for H_3L3. Copper and cobalt had color changes and changes in the UV-Vis spectrum. Uranyl did not exhibit a color change and there

was not a change in the UV-Vis spectrum after 24 hours of stirring. Future mono-substituted ligands, should be investigated as potential sensors, but this ligand is not one of them. A mono-substituted bi-pyridine would fill the coordination sphere of uranyl better than a salicylaldehyde can, and thus should be investigated.

H_2L1 became the starting point to design new ligand to test as sensors for actinides. In order to understand H_2L1 and facilitate any new ligand designs, computational chemistry of the ligands was explored and in particular time-dependent density functional theory (TD-DFT) was used to predict the UV-Vis spectrum of the free ligand, with uranyl, and with copper. While the calculations do not agree with the experiment 100%, they have proven to be fairly useful tool in this research. The calculations can be performed generally in less than a week using the supercomputer and are a quick way to determine if a particular ligand could be useful for detection of actinides versus other metals in the UV-Vis. The calculations have drawbacks such as the use of a mixed solvent system. A true mixed solvent system explicitly adds to the cost of the calculation, greatly decreasing efficiency. Even the interaction of just three solvent molecules increases the computational complexity and cost significantly.

From the calculations, it was determined that the ligand by itself was a pi to pi* interaction as would be expected of the system. The uranyl complex absorbance peak at 369 nm was the cause of a ligand to metal *f*-orbital singlet excitation from the HOMO to the LUMO. The copper complex absorbance at 450 nm was the cause of a metal *d*-orbital to the ligand excitation from the HOMO to the LUMO. The first

attempts to try to increase this shift were purely electric in changing the substituents around the salicylaldehyde from *t*-butyl groups to other electron donating and withdrawing groups, with a normal salicylaldehyde having no other substituents being the best, but not better than the original ligand. Next, using ligands known for their ligand to metal excitations such as bi-pyridine and other soft nitrogen containing donors were tested. The best of this group was the 2-aminobenzaldehyde providing the best separation of absorbance peaks. The final test was to try to mimic the SANEX extraction process by using 2,3,6-triazines. The best was the 4,5-dimethyl-2,3,6-triazine but the ligand synthesis has been complicated and thus has not been prepared. Studies are currently underway to attach the 2-aminobenzaldehyde to the 2-quinoxolinol backbone after synthesizing the 2-aminobenzaldehyde from 2-nitrobenzaldehyde using ferrous sulfate and ammonia.

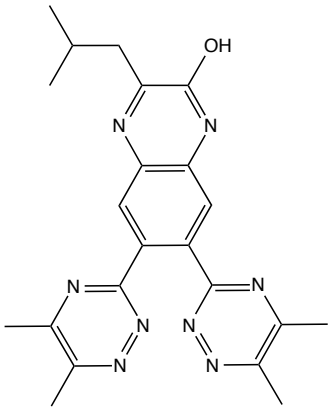

bis-4,5-dimethyl-2,3,6-triazine

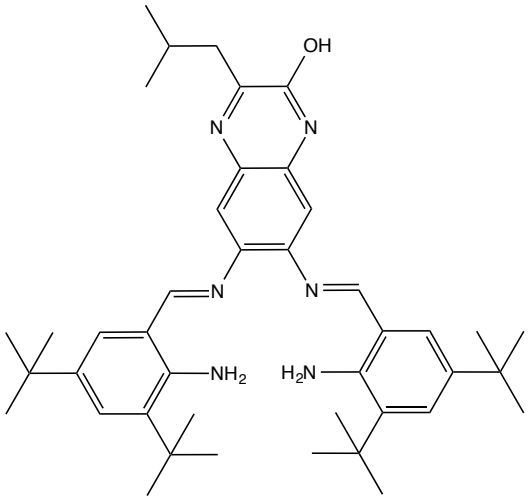

2-aminobenzaldehyde with quinoxolinol backbone

Figure 6.1: Best ligands according to the calculations.

While H_2L1 did not improve upon current extraction strategies, the mixed N,O-donor ligand was typical of other ligands of the same type in that their best

extraction was at lower nitric acid concentrations (< 0.1 M). The ligand did extract more uranyl than europium that is needed of an extractant for nuclear fuel waste, but the selectivity determined by the separation factor was below 10, considered the threshold for a good extractant. Excess ligand caused problems at the lowest nitric acid concentration ($1x10^{-5}$ M) tested, when as much europium was extracted as uranyl, causing the separation factor to decrease to 1. This does not support a case for extractants being good sensors and vice versa, nor do it dispel it, having a dual sensor/extractant does not work with this ligand.

6.1 Future Work

The sensors and computational component of them have the best potential for the future. Sensors for actinides are being studied much less than for extractants of nuclear fuel waste. Any new ligands synthesized should be tested for both molecular recognition and extractions, even if the ligand decomposes in stronger nitric acid (> 1 M).

The next group should be have the utmost concern with decreasing the detection limit from ~25 ppm to ~20 ppb. This can be achieved by increasing the number of conjugated pi-bonds in the ligand system, which will increase the signal to noise ratio, increasing the selectivity. A good starting point would be to use 2,3-diaminosphenazine or 2,3-diaminoanthracene with 3,5-di-*t*-butylsalicylaldehyde or 2-aminobenzaldehyde. Calculations on these ligands should only take a couple of extra

days due to the larger system. The synthesis would be similar to H_2L1 by adding 3,5-di-*t*-butylsalicylaldehyde to the diamino in ethanol and heating to reflux.

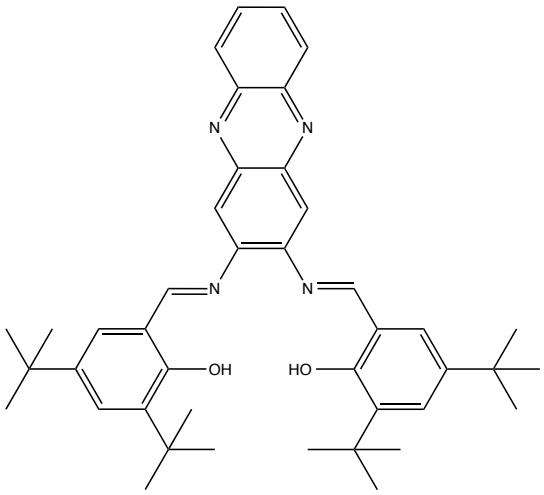

Figure 6.2: Salazine with 3,5-di-*t*-butylsalicylaldehyde

If that does not reduce the detection limit enough, macrocycles would be the best way to go before the ligand precipitates, and doesn't dissolve in any solvent.. The macrocycles need to be big enough to accommodate the actinides which should make any competing transition metals only bind to one side of the macrocycle if at all. Early attempts to make the free macrocycle have failed. A chlorine anion was determined to be bound in the pyridine amide macrocycle (Figure 6.2). Attempts to template around uranyl to form the macrocycle have also been unsuccessful. Calculations show that this could be a promising ligand. Pyridine dicarboxylic acid should form an amide with the amines for the backbones, but the conversion of the carboxylic acids to acid chlorides is a better starting to point to achieve the desired

amides. An increase in sensitivity for the macrocycles could be to use phenazine as backbone (Figure6.3).

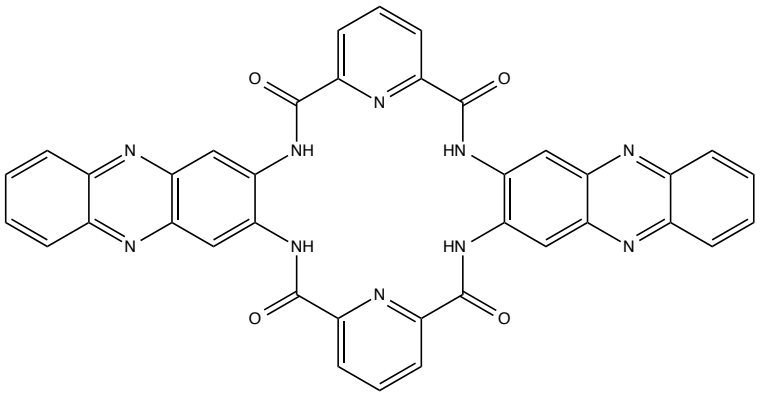

Figure 6.3: Phenazine with pyridine amides to form a 6N-donor macrocycle.

Appendix 1 for Chapter 3

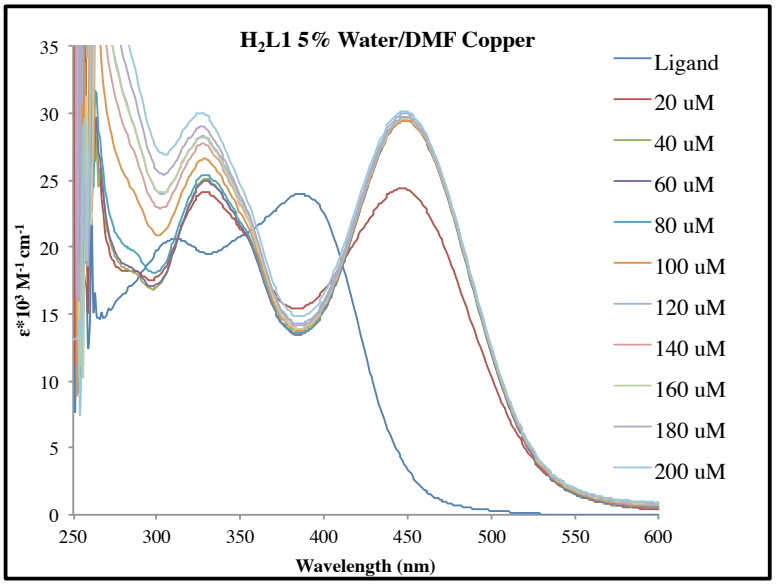

Figure A3.1: Batch copper titration for H_2L1 (20 μM) in 5% water/DMF (v/v). Concentrations shown are final concentrations of metal.

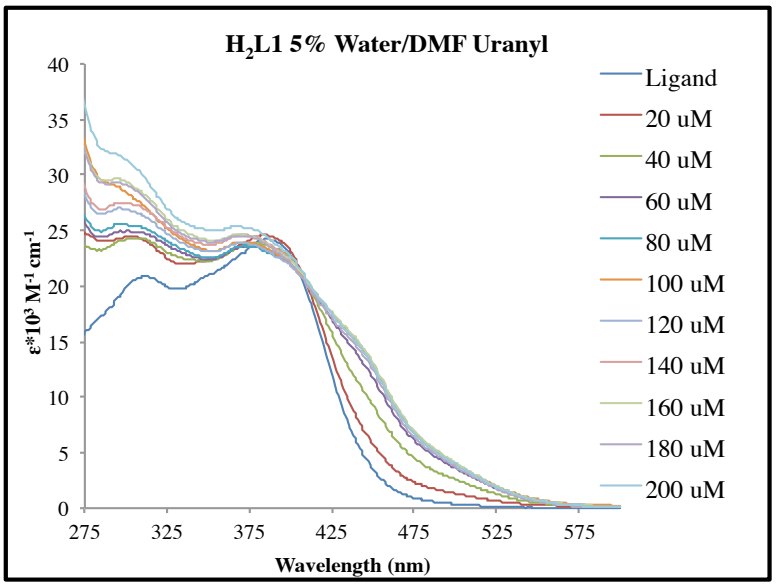

Figure A3.2: Batch uranyl titration for H_2L1 (20 μM) in 5% water/DMF (v/v). Concentrations shown are final concentrations of metal.

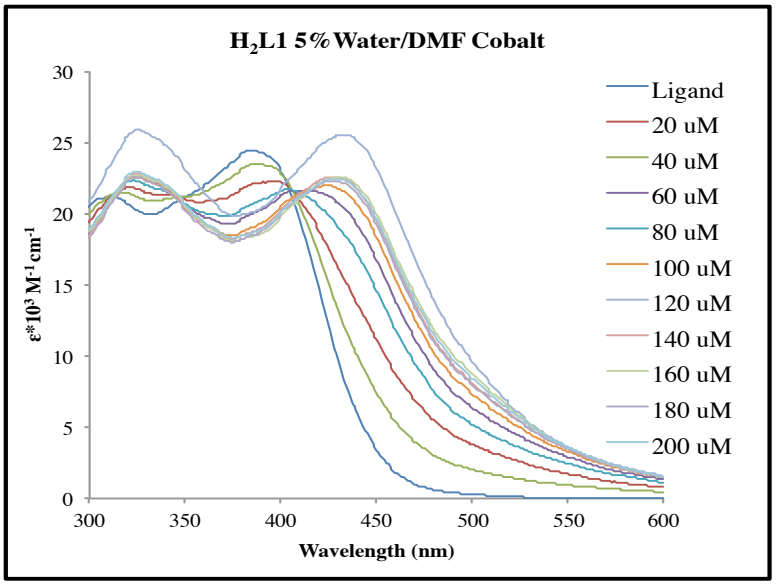

Figure A3.3: Batch cobalt titration for H_2L1 (20 μM) in 5% water/DMF (v/v). Concentrations shown are final concentrations of metal.

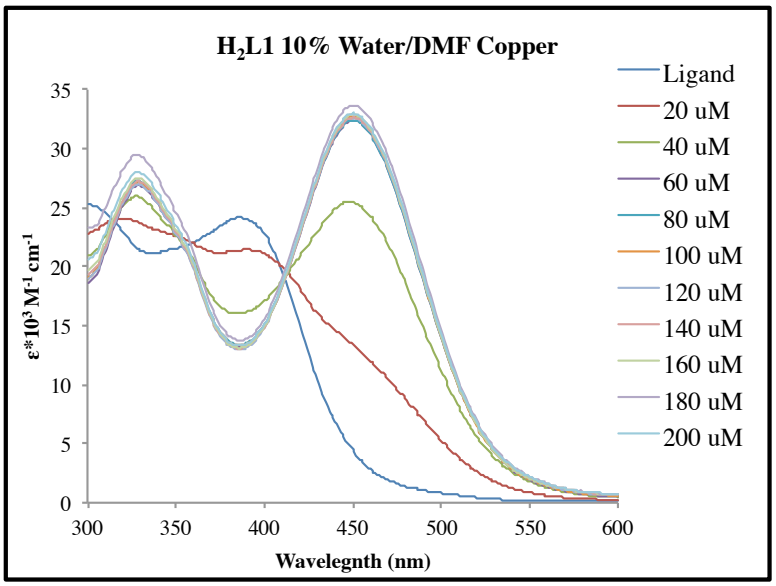

Figure A3.4: Batch copper titration for H_2L1 (20 μM) in 10% water/DMF (v/v). Concentrations shown are final concentrations of metal.

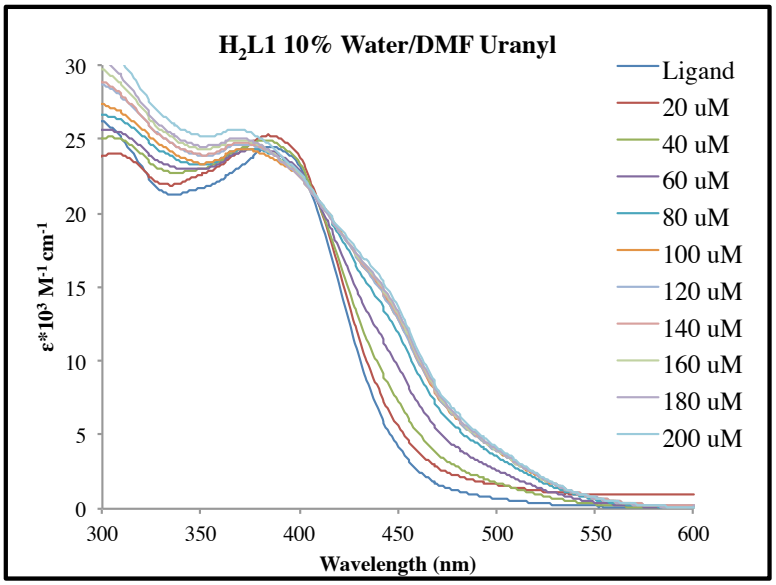

Figure A3.5: Batch uranyl titration for H_2L1 (20 μM) in 10% water/DMF (v/v). Concentrations shown are final concentrations of metal.

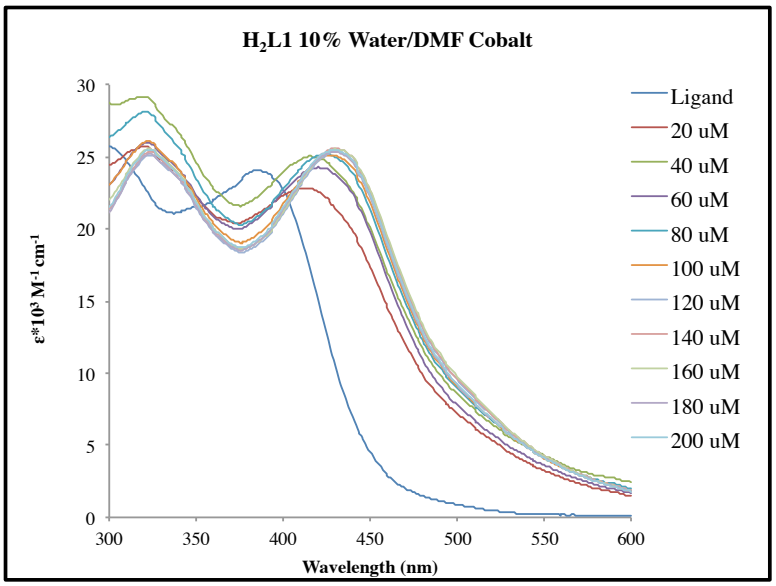

Figure A3.6: Batch cobalt titration for H_2L1 (20 μM) in 10% water/DMF (v/v). Concentrations shown are final concentrations of metal.

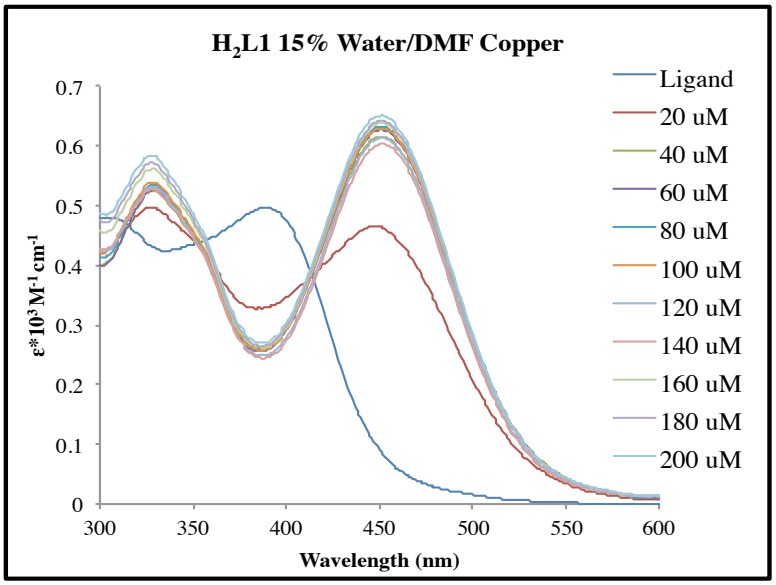

Figure A3.7: Batch copper titration for H_2L1 (20 μM) in 15% water/DMF (v/v). Concentrations shown are final concentrations of metal.

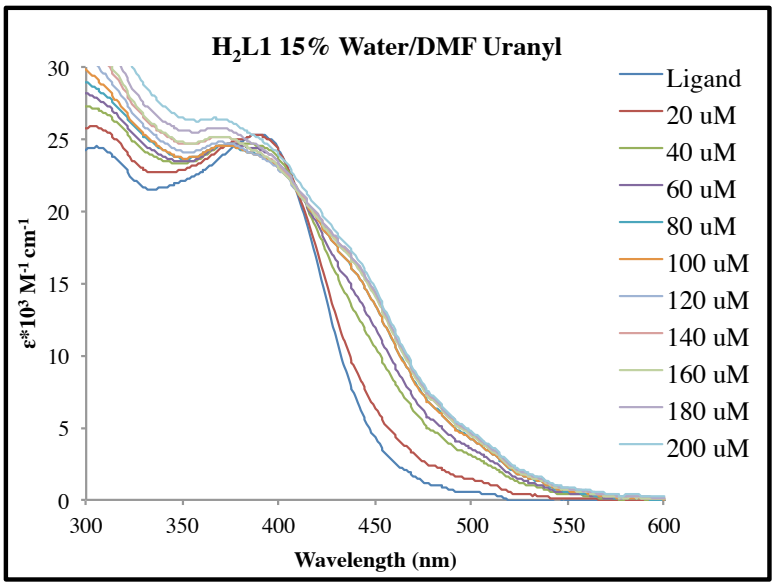

Figure A3.8: Batch uranyl titration for H_2L1 (20 μM) in 15% water/DMF (v/v). Concentrations shown are final concentrations of metal.

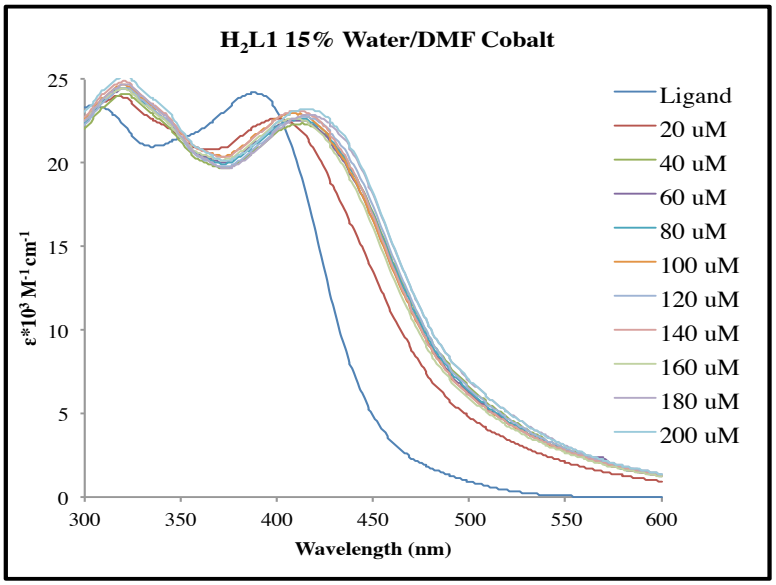

Figure A3.9: Batch cobalt titration for H_2L1 (20 μM) in 15% water/DMF (v/v). Concentrations shown are final concentrations of metal.

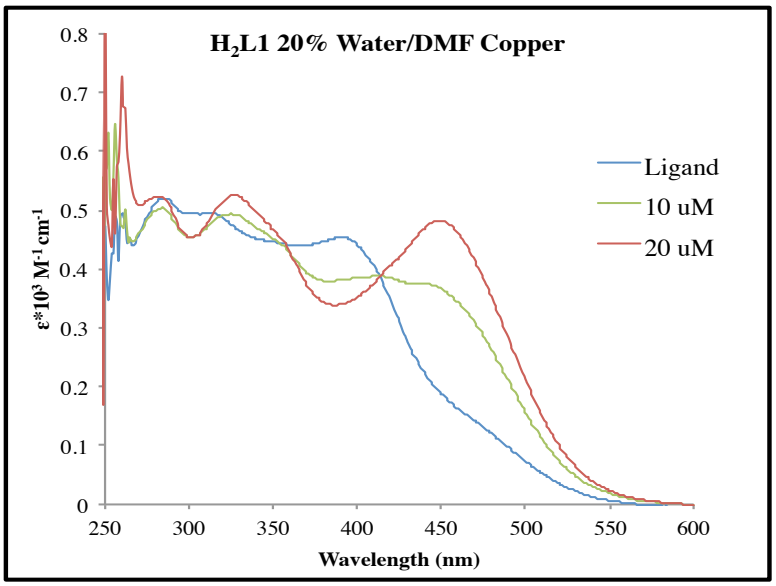

Figure A3.10: Batch copper titration for H_2L1 (20 μM) in 20% water/DMF (v/v). Concentrations shown are final concentrations of metal.

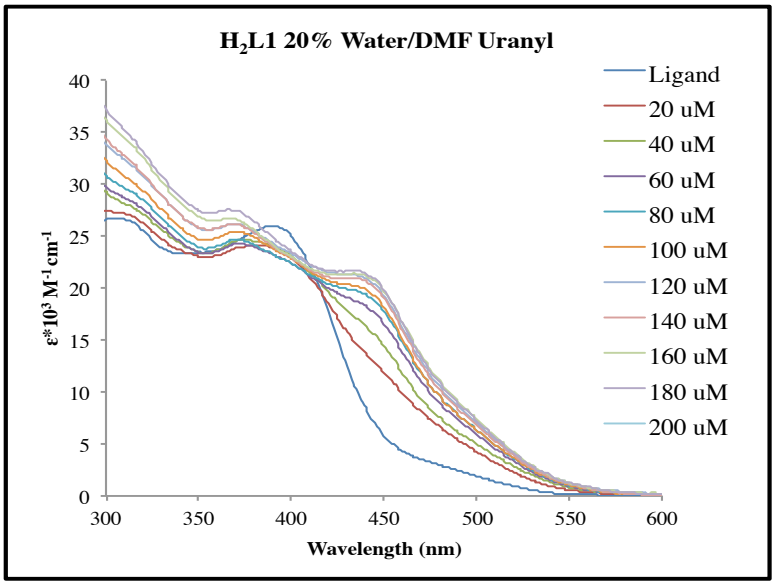

Figure A3.11: Batch uranyl titration for H_2L1 (20 μM) in 20% water/DMF (v/v). Concentrations shown are final concentrations of metal.

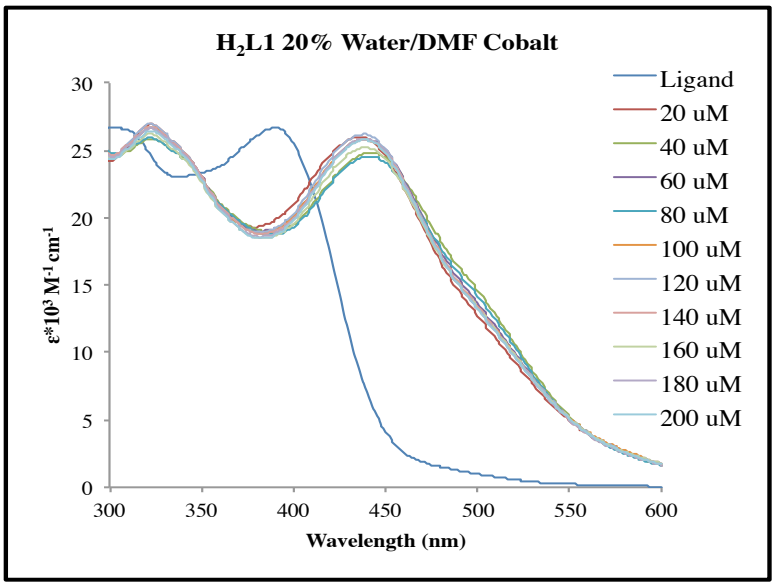

Figure A3.12: Batch cobalt titration for H_2L1 (20 μM) in 20% water/DMF (v/v). Concentrations shown are final concentrations of metal.

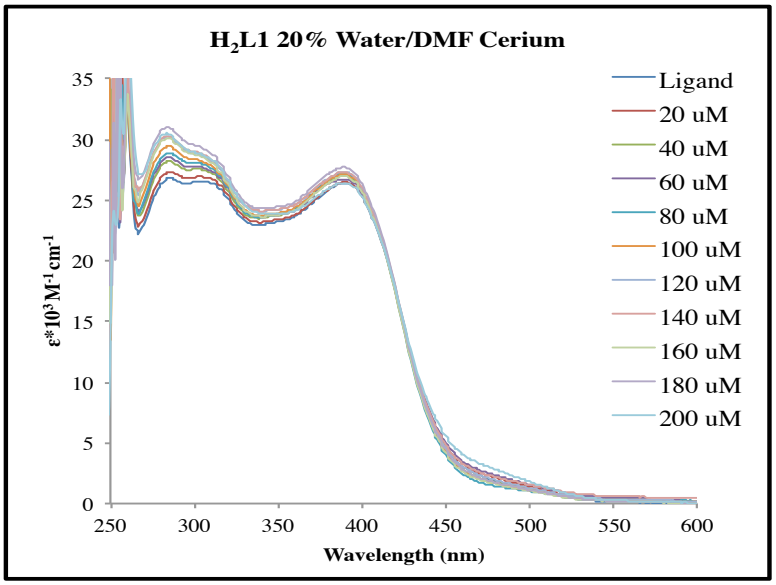

Figure A3.13: Batch cerium titration for H_2L1 (20 μM) in 20% water/DMF (v/v). Concentrations shown are final concentrations of metal.

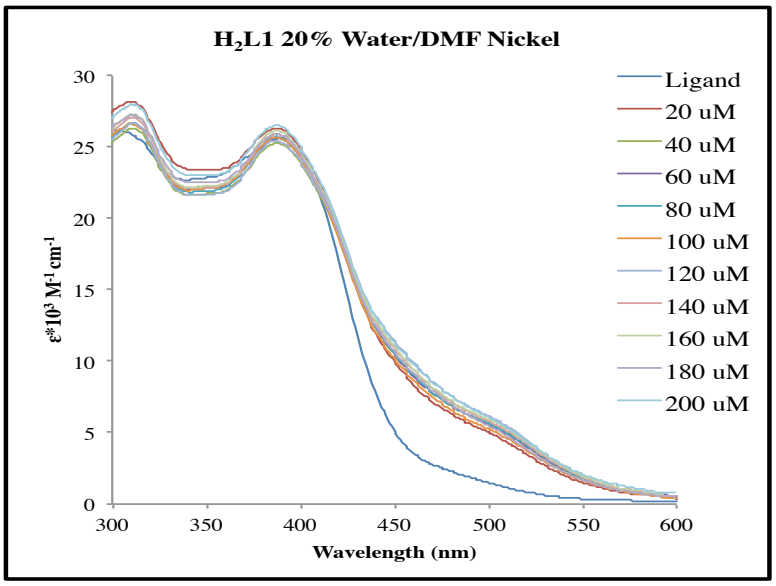

Figure A3.14: Batch nickel titration for H_2L1 (20 μM) in 20% water/DMF (v/v). Concentrations shown are final concentrations of metal.

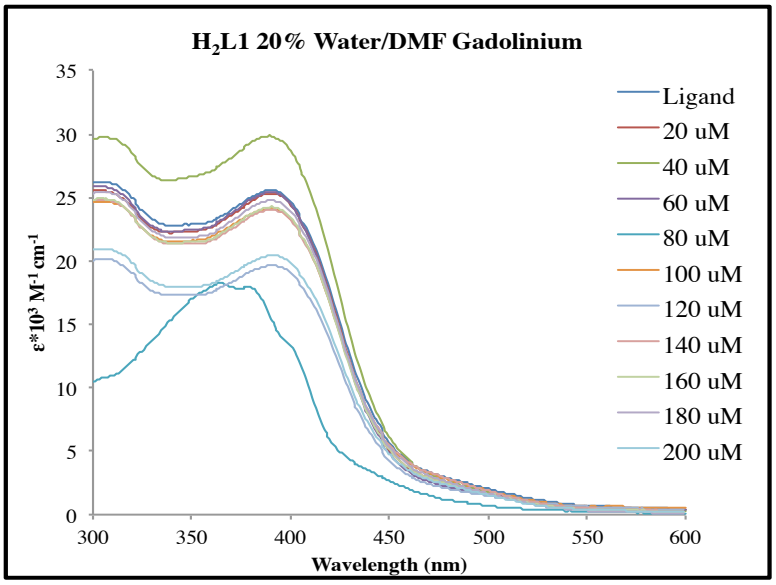

Figure A3.15: Batch gadolinium titration for H_2L1 (20 μM) in 20% water/DMF (v/v). Concentrations shown are final concentrations of metal.

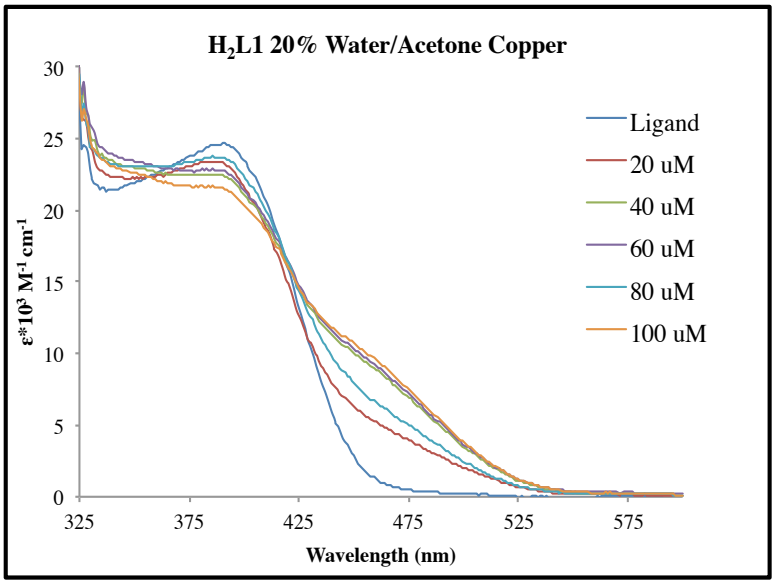

Figure A3.16: Batch copper titration for H_2L1 (20 μM) in 20% water/acetone (v/v). Concentrations shown are final concentrations of metal.

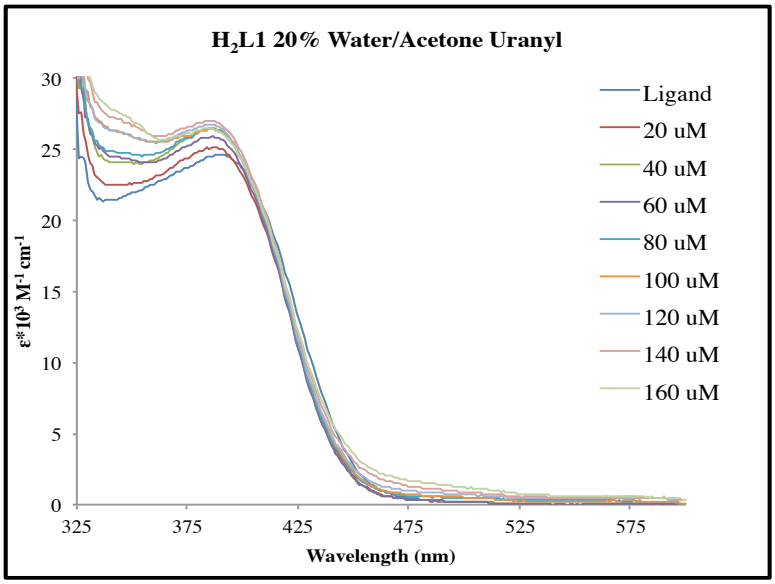

Figure A3.17: Batch uranyl titration for H_2L1 (20 μM) in 20% water/acetone (v/v). Concentrations shown are final concentrations of metal.

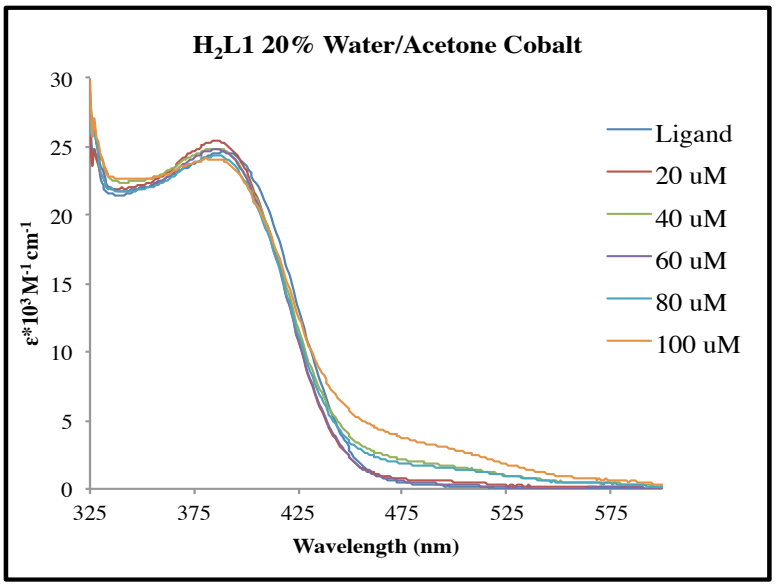

Figure A3.18: Batch cobalt titration for H_2L1 (20 μM) in 20% water/acetone (v/v). Concentrations shown are final concentrations of metal.

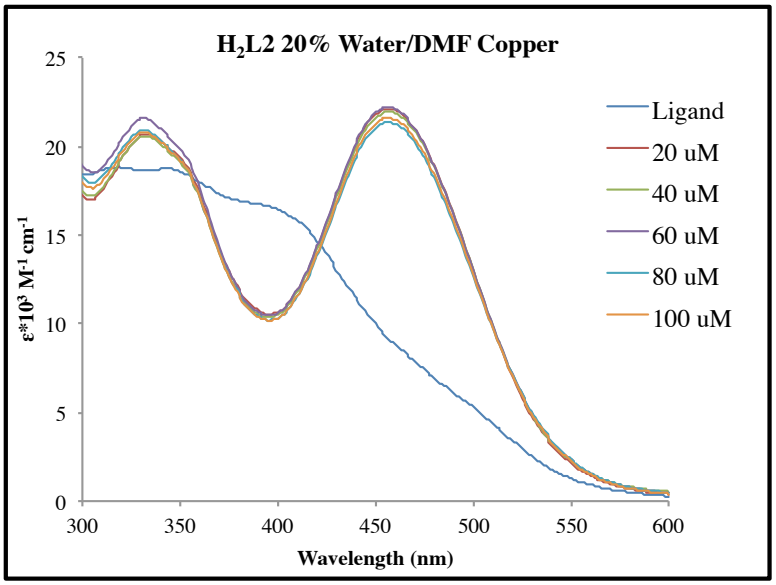

Figure A3.19: Batch copper titration for H_2L2 (20 μM) in 20% water/DMF (v/v). Concentrations shown are final concentrations of metal.

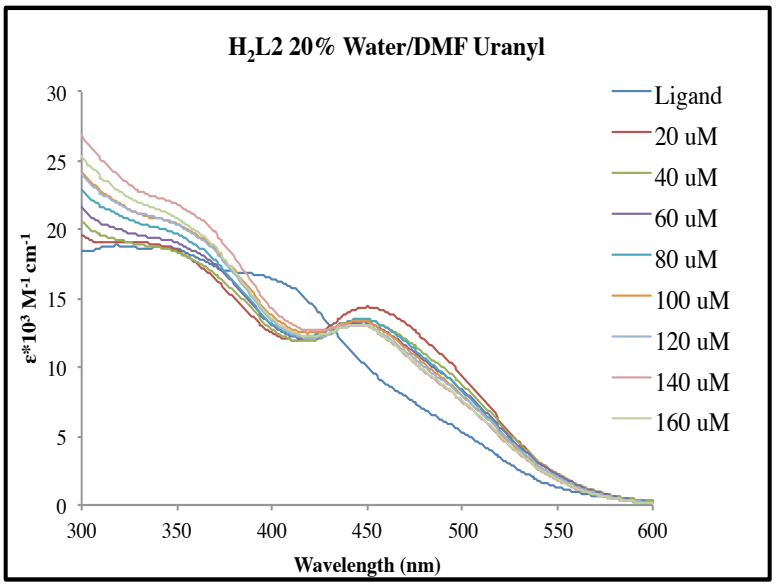

Figure A3.20: Batch uranyl titration for H_2L2 (20 μM) in 20% water/DMF (v/v). Concentrations shown are final concentrations of metal.

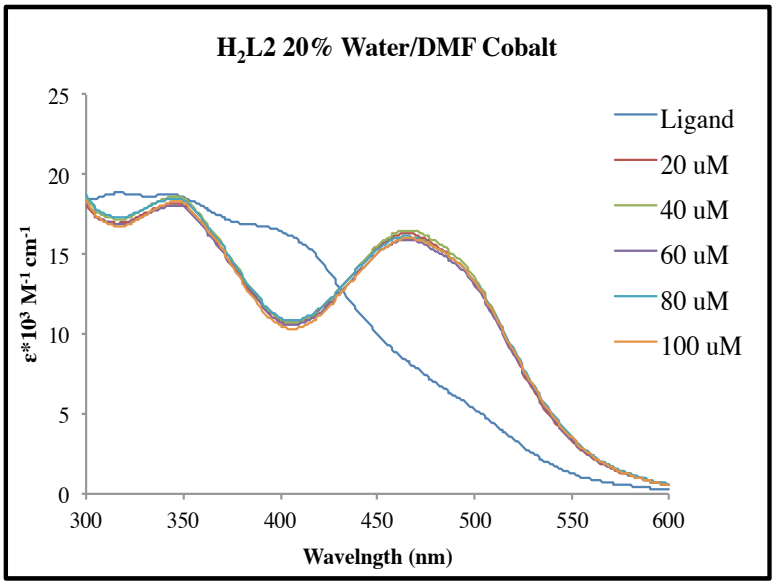

Figure A3.21: Batch cobalt titration for H_2L2 (20 μM) in 20% water/DMF (v/v). Concentrations shown are final concentrations of metal.

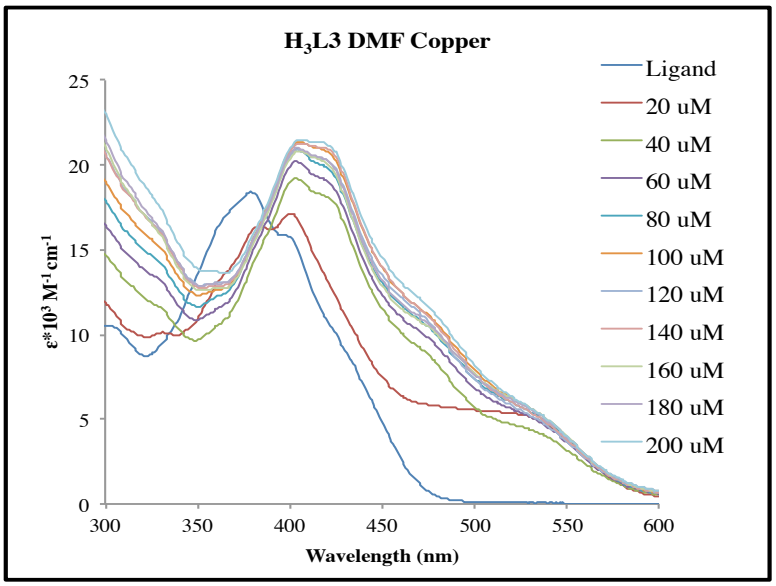

Figure A3.22: Batch copper titration for H_3L3 (20 μM) in < 1% DMF (v/v). Concentrations shown are final concentrations of metal.

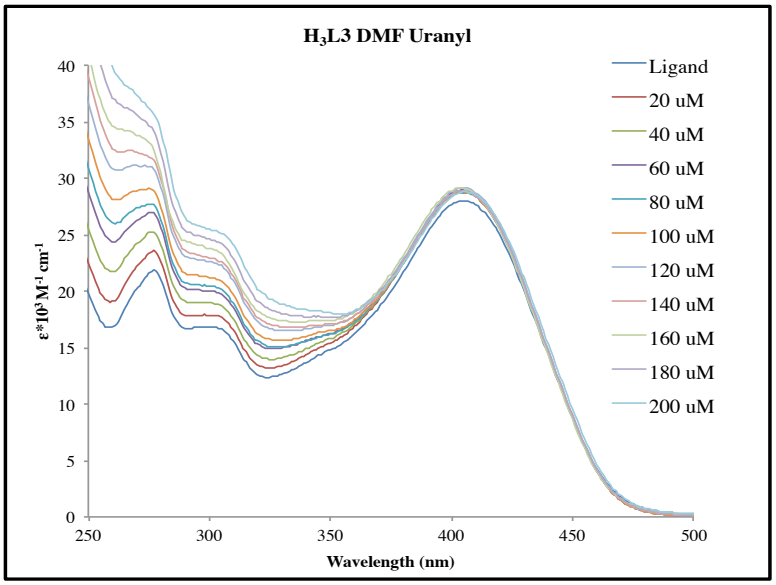

Figure A3.23: Batch uranyl titration for H_3L3 (20 μM) in < 1% DMF (v/v). Concentrations shown are final concentrations of metal.

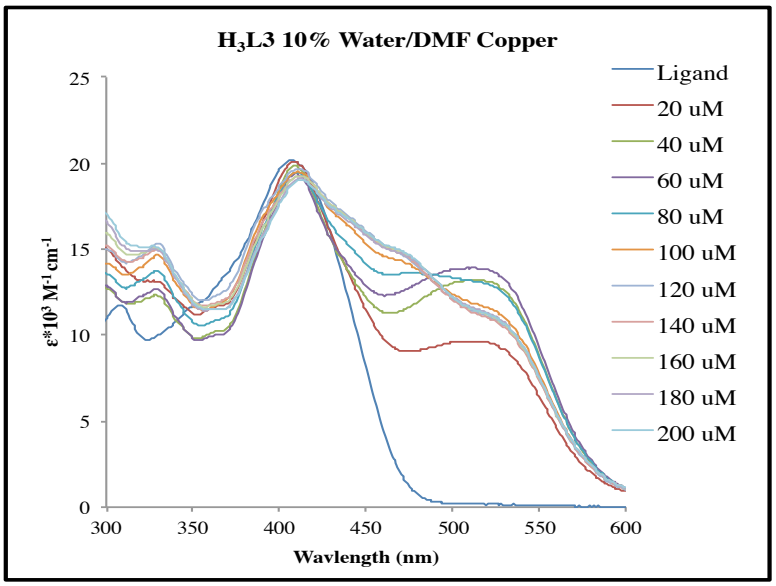

Figure A3.24: Batch copper titration for H_3L3 (20 μM) in 10% water/DMF (v/v). Concentrations shown are final concentrations of metal.

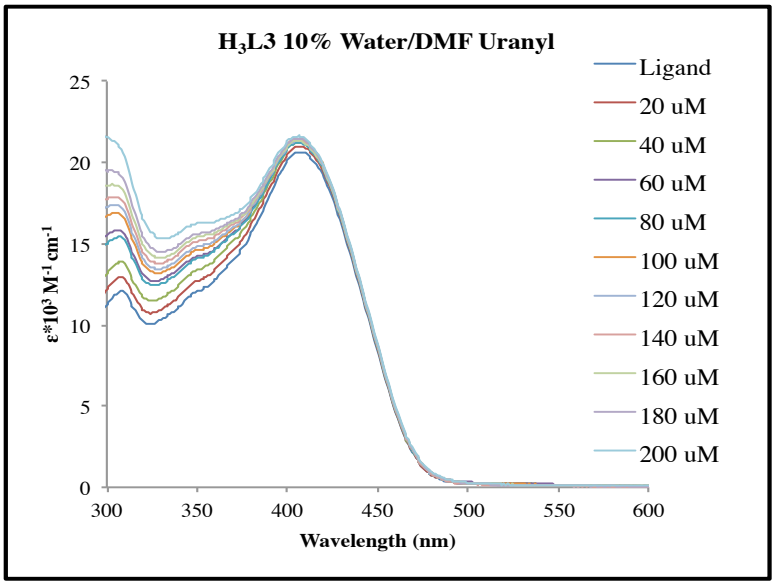

Figure A3.25: Batch uranyl titration for H_3L3 (20 μM) in 10% water/DMF (v/v). Concentrations shown are final concentrations of metal.

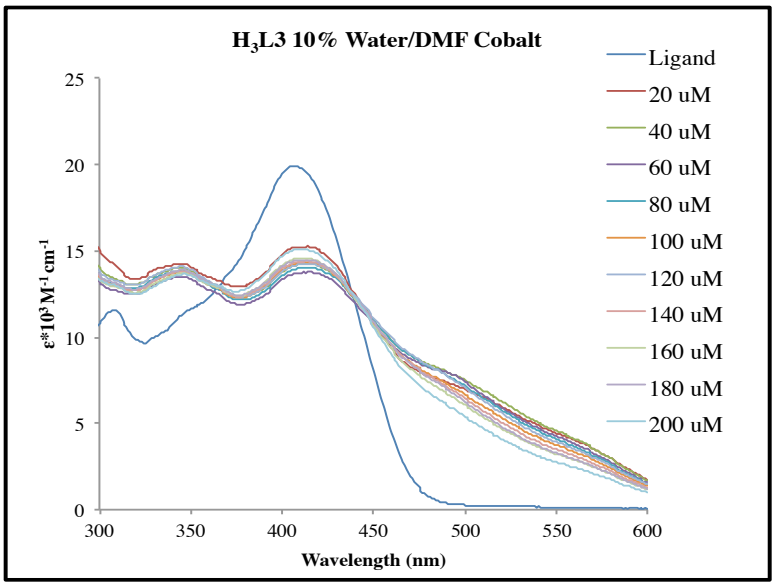

Figure A3.26: Batch cobalt titration for H_3L3 (20 μM) in 10% water/DMF (v/v). Concentrations shown are final concentrations of metal.

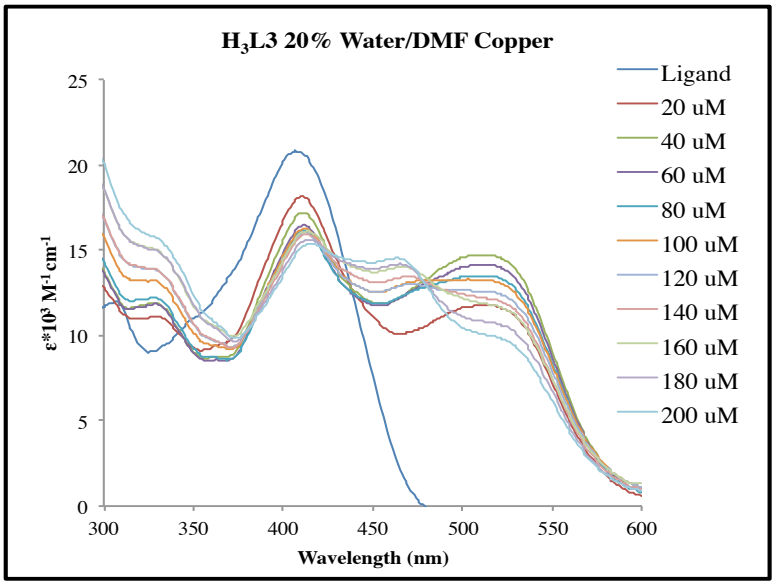

Figure A3.27: Batch copper titration for H_3L3 (20 μM) in 20% water/DMF (v/v). Concentrations shown are final concentrations of metal.

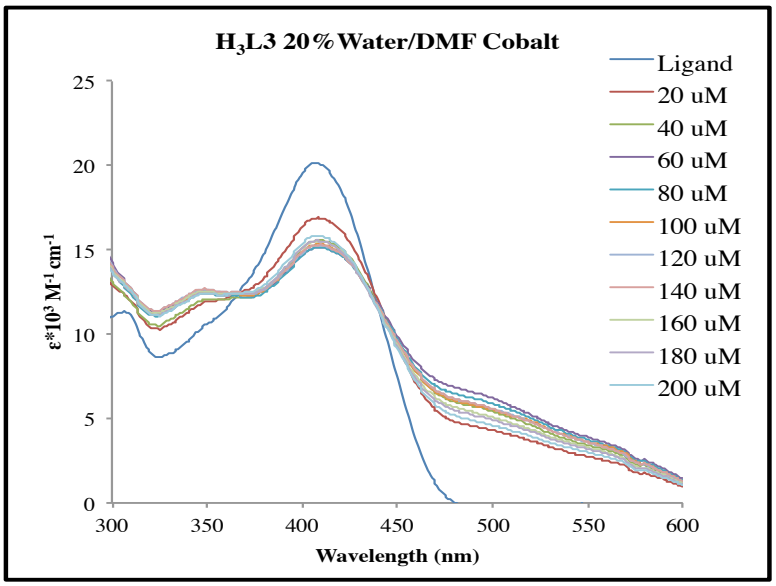

Figure A3.28: Batch cobalt titration for H_3L3 (20 μM) in 20% water/DMF (v/v). Concentrations shown are final concentrations of metal.

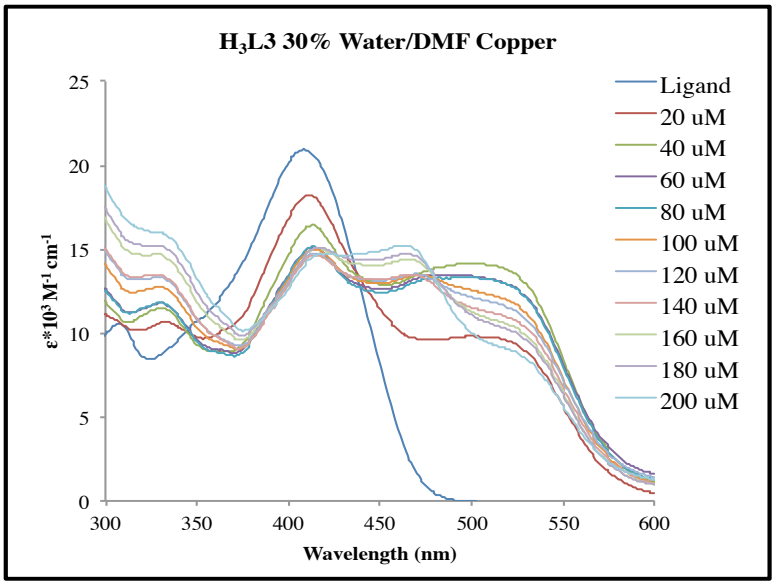

Figure A3.29: Batch copper titration for H_3L3 (20 μM) in 30% water/DMF (v/v). Concentrations shown are final concentrations of metal.

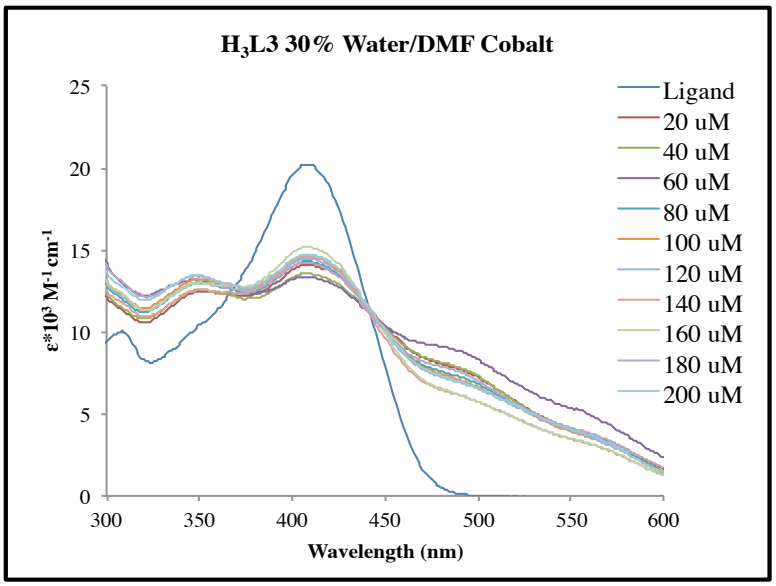

Figure A3.30: Batch cobalt titration for H_3L3 (20 μM) in 30% water/DMF (v/v). Concentrations shown are final concentrations of metal.

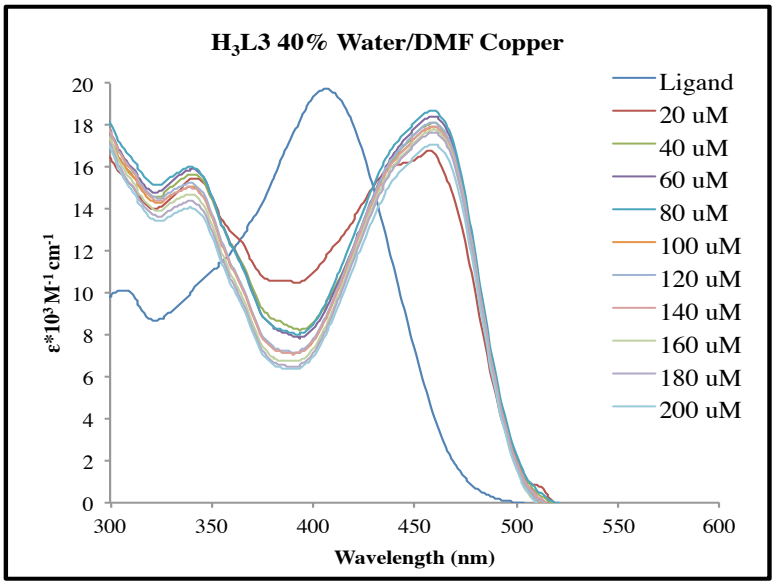

Figure A3.31: Batch copper titration for H_3L3 (20 μM) in 40% water/DMF (v/v). Concentrations shown are final concentrations of metal.

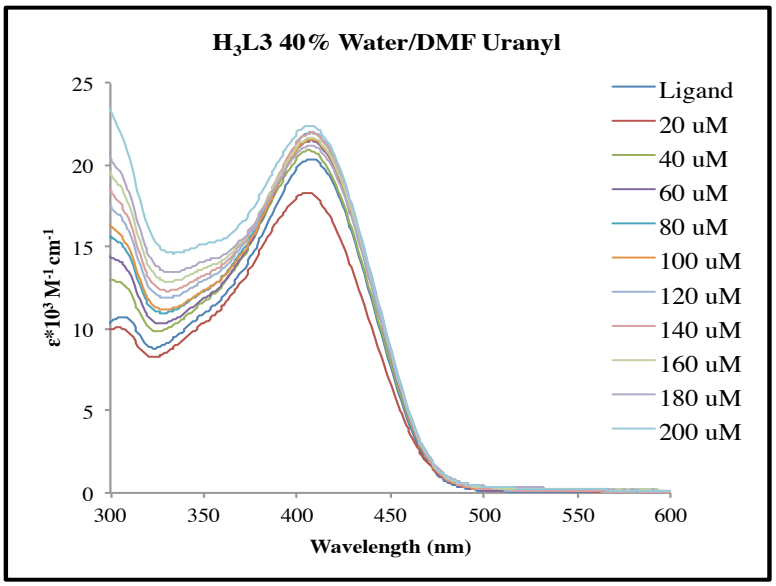

Figure A3.32: Batch uranyl titration for H_3L3 (20 μM) in 40% water/DMF (v/v). Concentrations shown are final concentrations of metal.

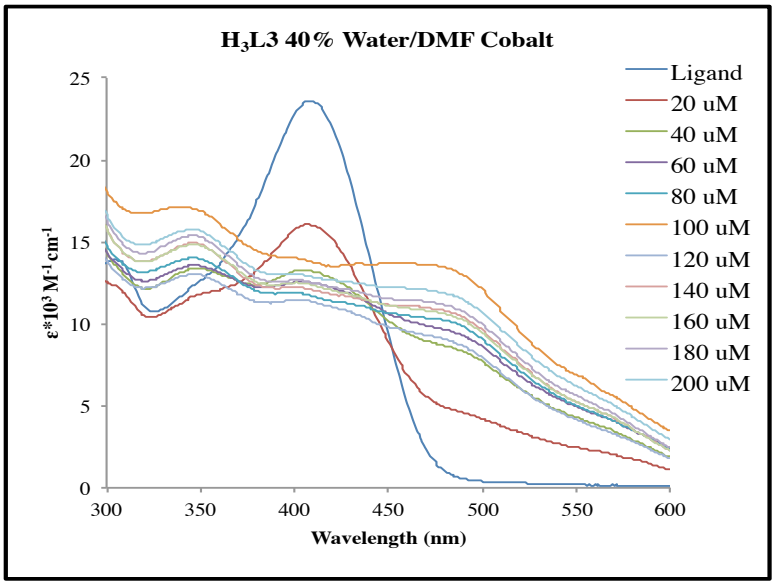

Figure A3.33: Batch cobalt titration for H_3L3 (20 μM) in 40% water/DMF (v/v). Concentrations shown are final concentrations of metal.

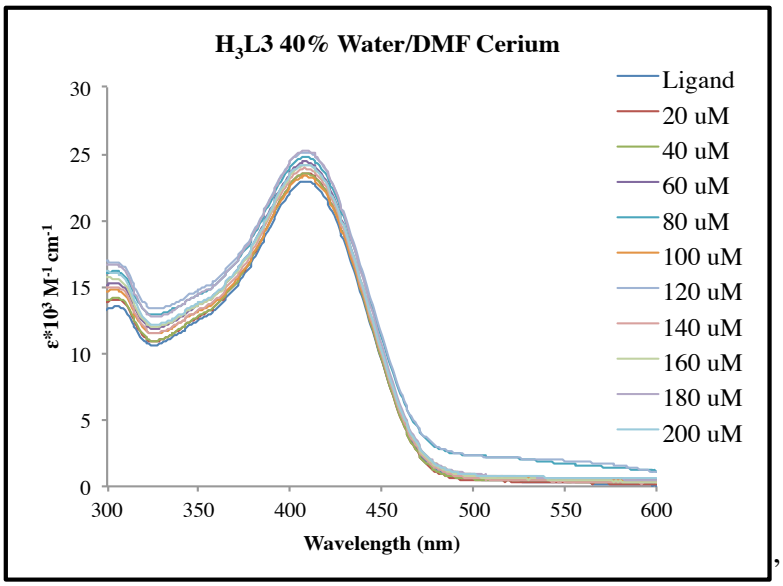

Figure A3.34: Batch cerium titration for H_3L3 (20 μM) in 40% water/DMF (v/v). Concentrations shown are final concentrations of metal.

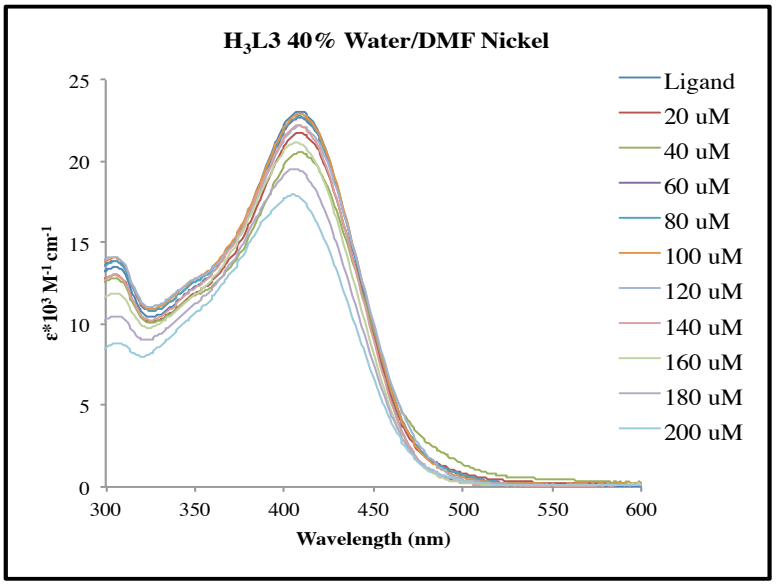

Figure A3.35: Batch nickel titration for H_3L3 (20 μM) in 40% water/DMF (v/v). Concentrations shown are final concentrations of metal.

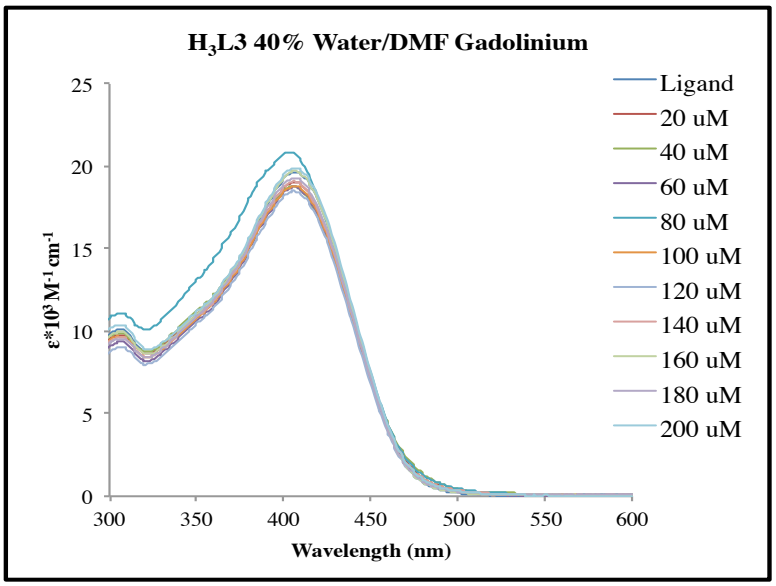

Figure A3.36: Batch gadolinium titration for H_3L3 (20 μM) in 40% water/DMF (v/v). Concentrations shown are final concentrations of metal.

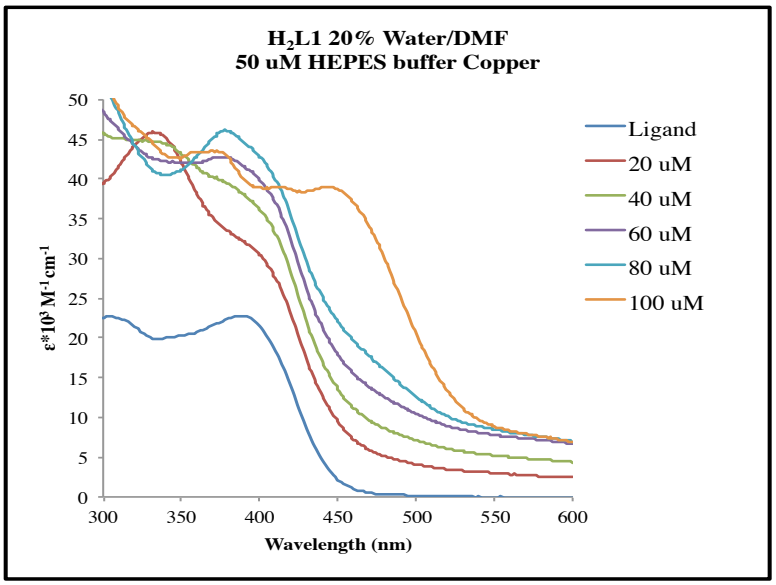

Figure A3.37: Batch copper titration for H_2L1 (20 μM) in 20% water/DMF (v/v) with 50 μM HEPES buffer. Concentrations shown are final concentrations of metal.

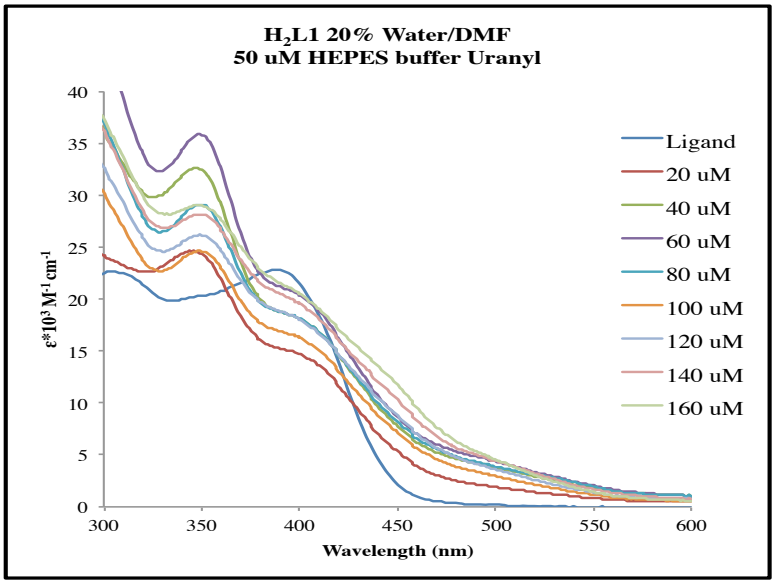

Figure A3.38: Batch uranyl titration for H_2L1 (20 μM) in 20% water/DMF (v/v) with 50 μM HEPES buffer. Concentrations shown are final concentrations of metal.

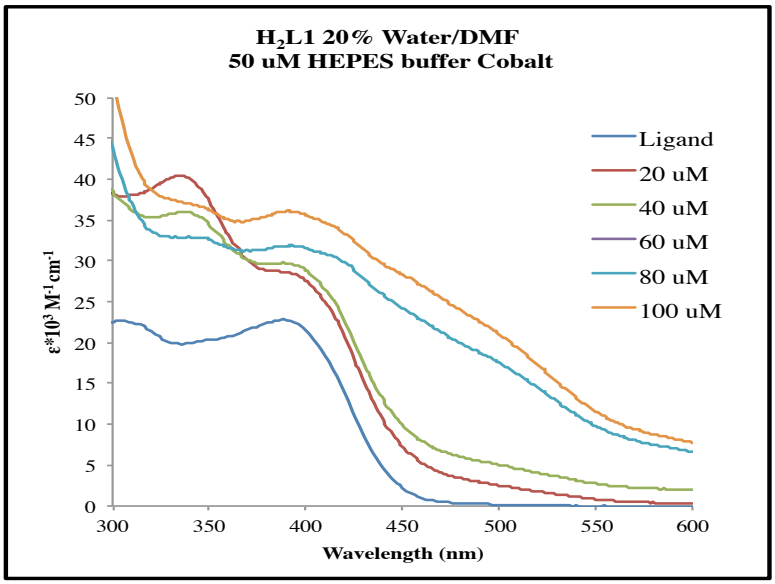

Figure A3.39: Batch cobalt titration for H_2L1 (20 μM) in 20% water/DMF (v/v) with 50 μM HEPES buffer. Concentrations shown are final concentrations of metal.

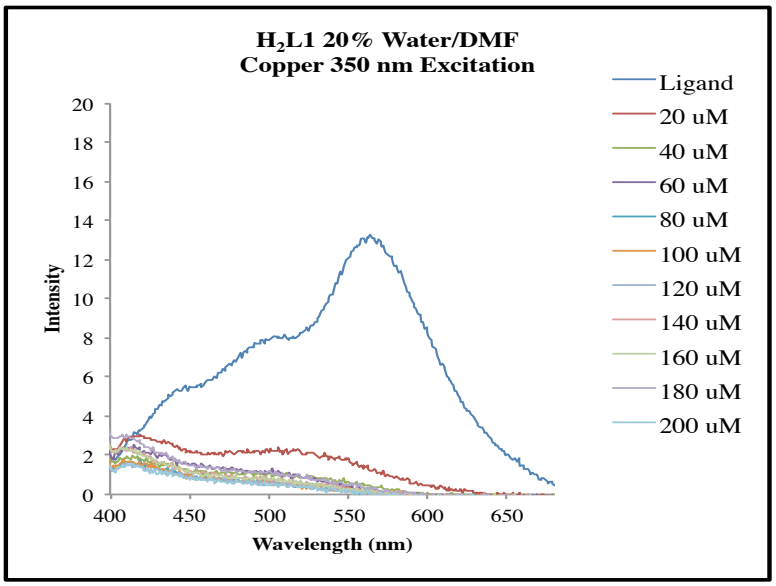

Figure A3.40: Fluorescence batch titration of H_2L1 with copper in 20% water/DMF (v/v) at 350 nm excitation. Concentrations are final metal concentrations

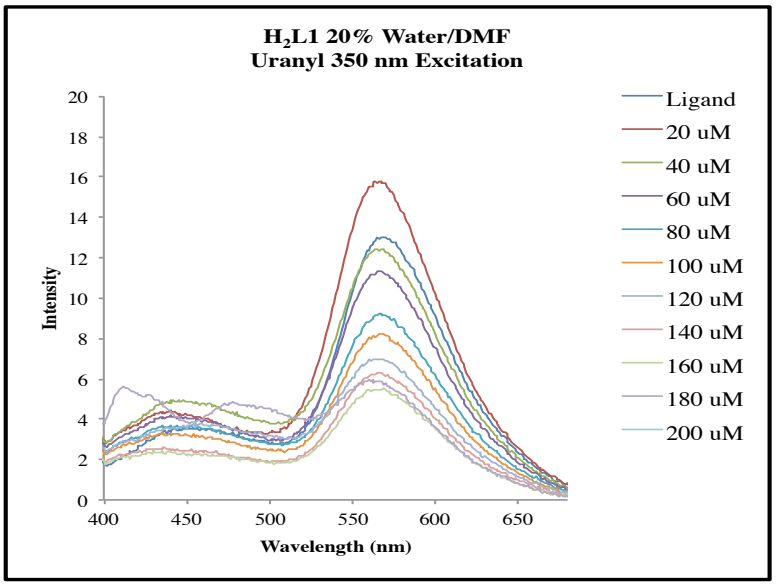

Figure A3.41: Fluorescence batch titration of H_2L1 with uranyl in 20% water/DMF (v/v) at 350 nm excitation. Concentrations are final metal concentrations

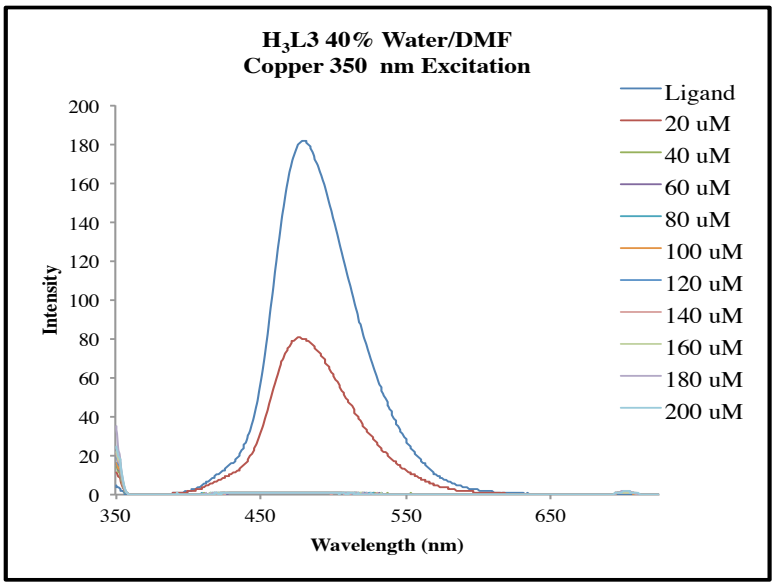

Figure A3.42: Fluorescence batch titration of H_3L3 with copper in 40% water/DMF (v/v) at 350 nm excitation. Concentrations are final metal concentrations

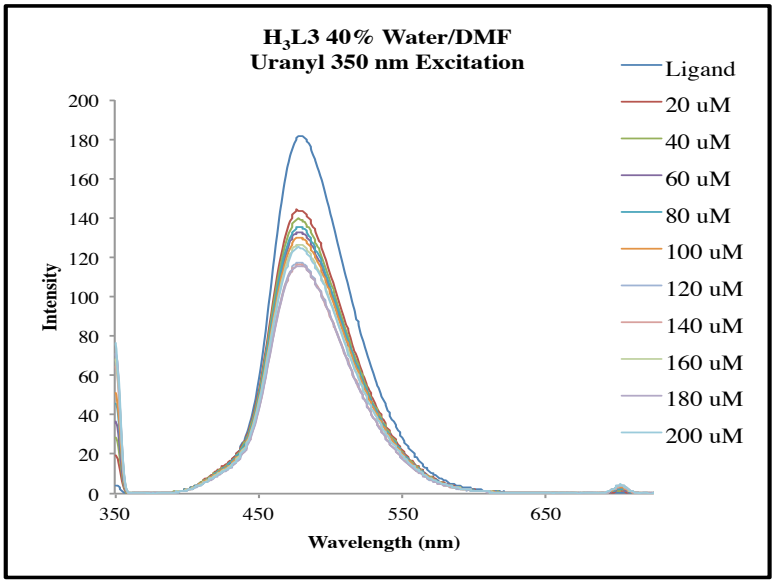

Figure A3.43: Fluorescence batch titration of H_3L3 with copper in 40% water/DMF (v/v) at 350 nm excitation. Concentrations are final metal concentrations.

Appendix 2 for Chapter 4

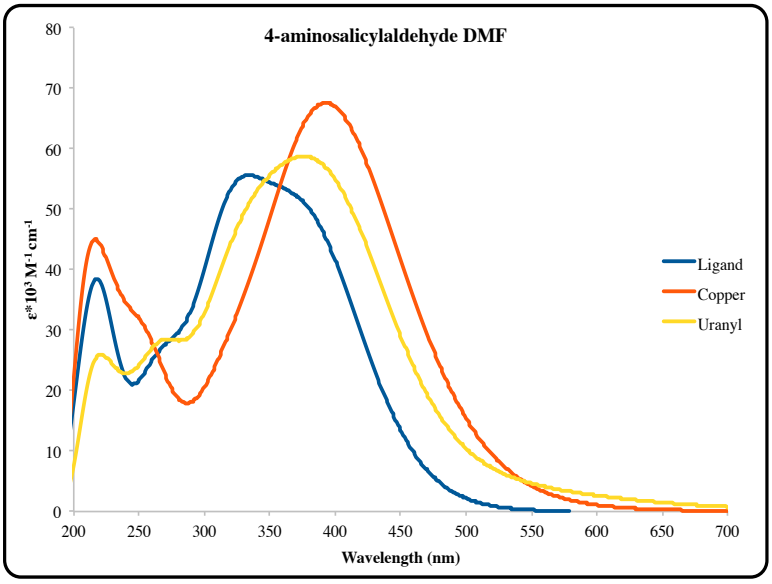

Figure A4.1: Calculated 4-aminosalicylaldehyde, copper complex, and uranyl complex UV-Vis spectrum in DMF

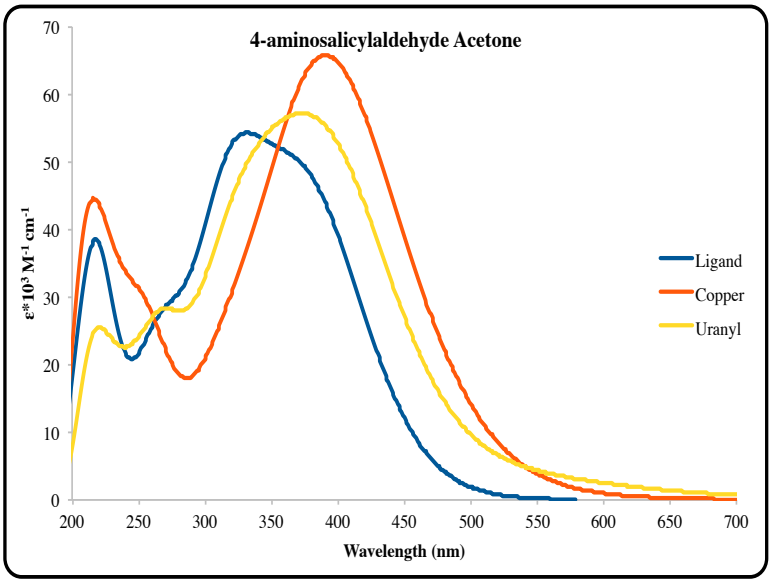

Figure A4.2: Calculated 4-aminosalicylaldehyde, copper complex, and uranyl complex UV-Vis spectrum in acetone

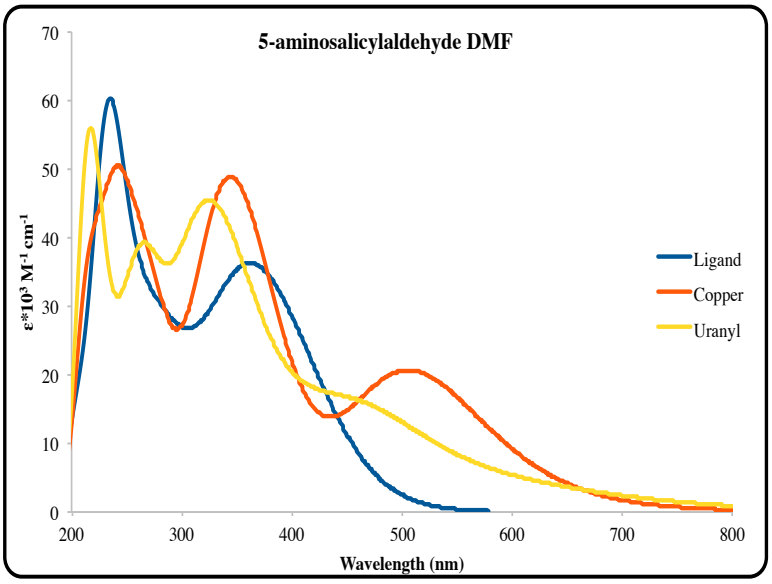

Figure A4.3: Calculated 5-aminosalicylaldehyde, copper complex, and uranyl complex UV-Vis spectrum in DMF

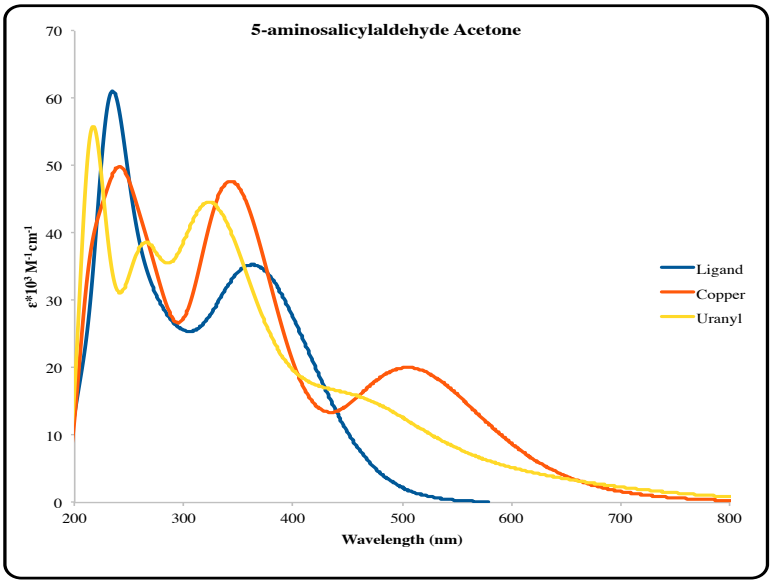

Figure A4.4: Calculated 5-aminosalicylaldehyde, copper complex, and uranyl complex UV-Vis spectrum in acetone

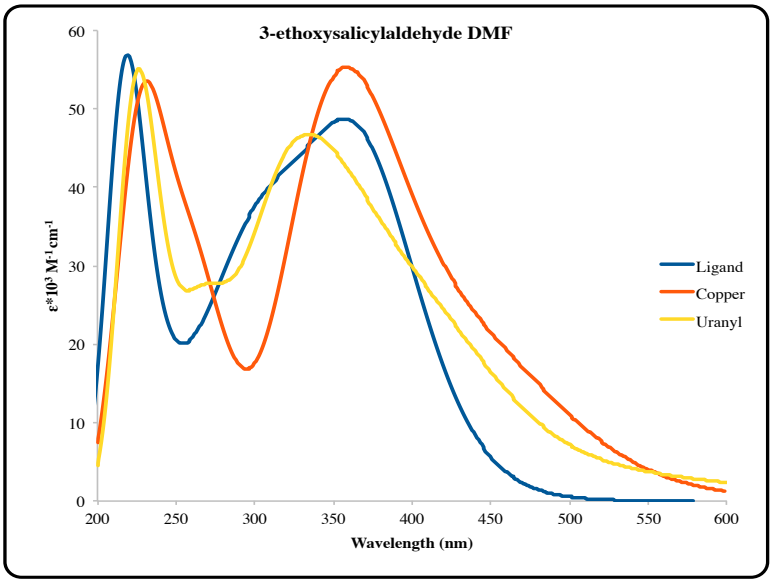

Figure A4.5: Calculated 3-ethoxysalicylaldehyde, copper complex, and uranyl complex UV-Vis spectrum in DMF

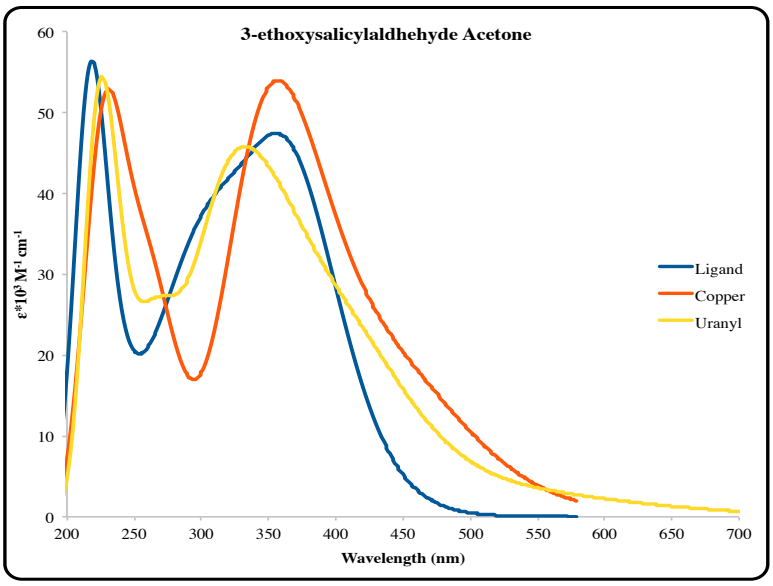

Figure A4.6: Calculated 3-ethoxysalicylaldehyde, copper complex, and uranyl complex UV-Vis spectrum in acetone

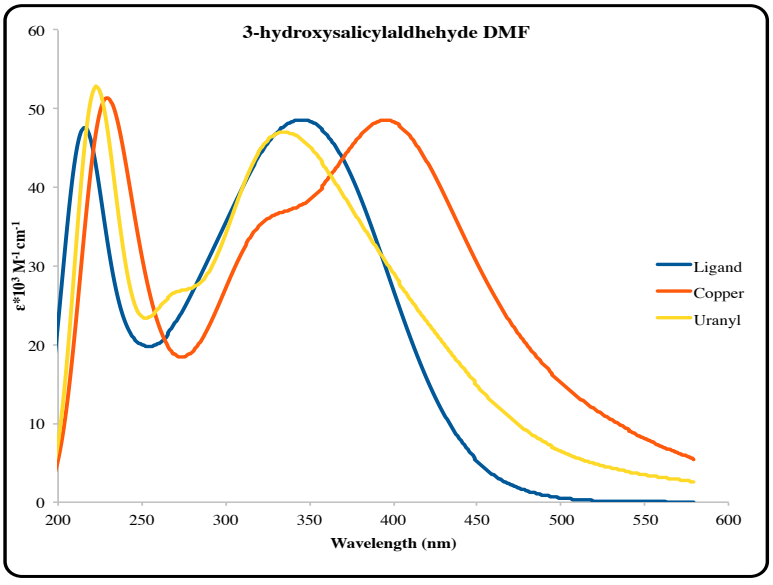

Figure A4.7: Calculated 3-hydroxysalicylaldehyde, copper complex, and uranyl complex UV-Vis spectrum in DMF

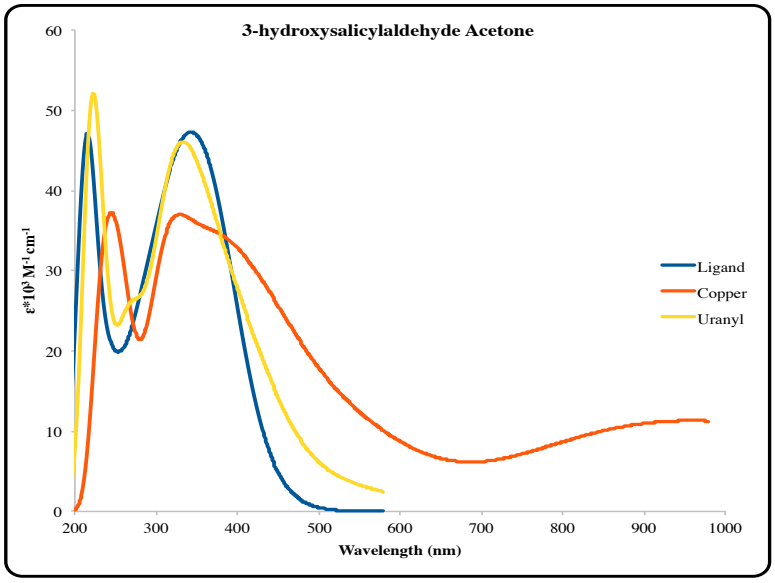

Figure A4.8: Calculated 3-hydroxysalicylaldehyde, copper complex, and uranyl complex UV-Vis spectrum in acetone

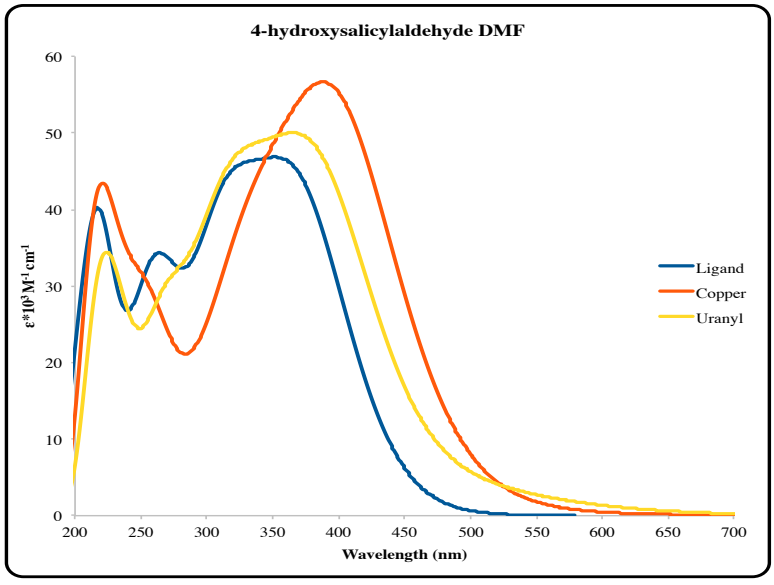

Figure A4.9: Calculated 4-hydroxysalicylaldehyde, copper complex, and uranyl complex UV-Vis spectrum in DMF

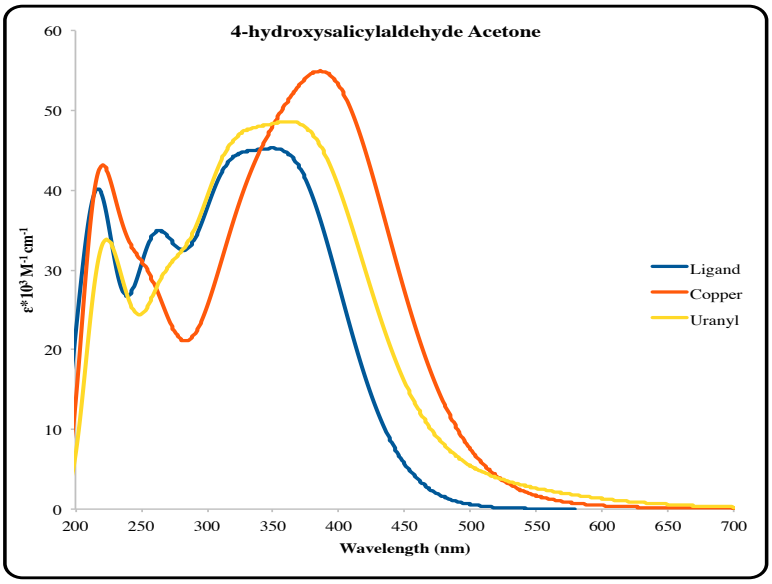

Figure A4.10: Calculated 4-hydroxysalicylaldehyde, copper complex, and uranyl complex UV-Vis spectrum in acetone

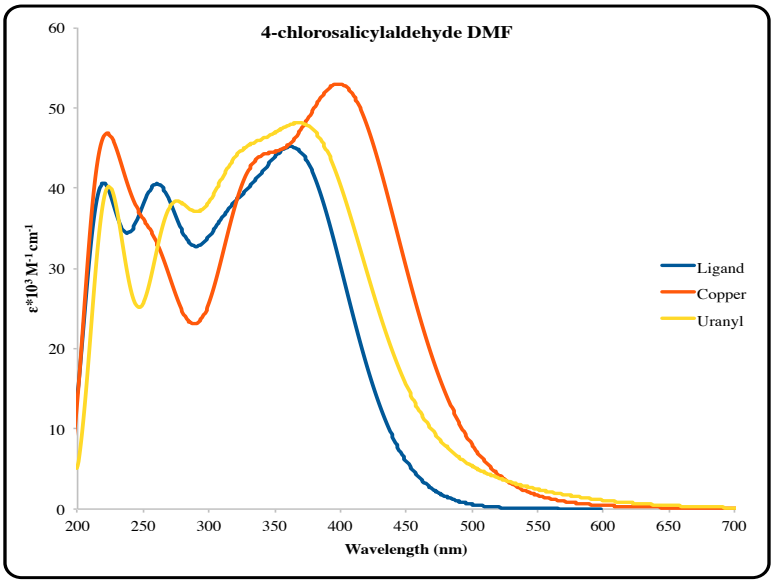

Figure A4.11: Calculated 4-chlorosalicylaldehyde, copper complex, and uranyl complex UV-Vis spectrum in DMF

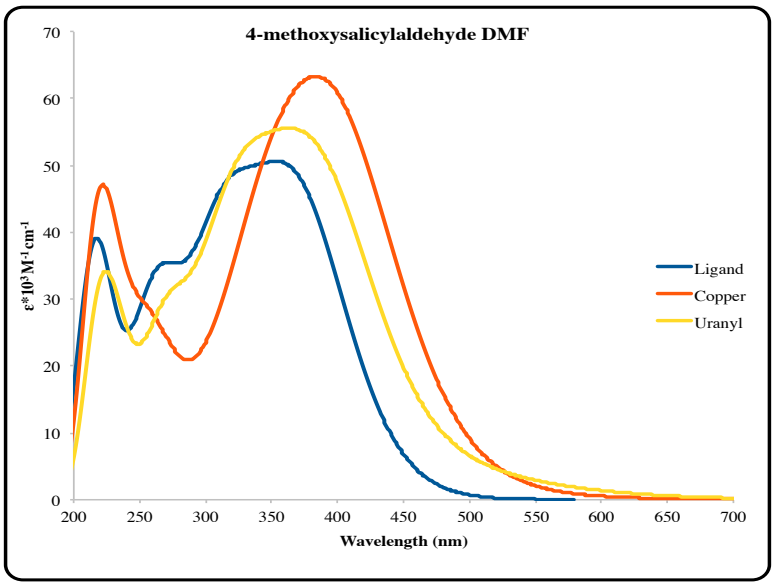

Figure A4.12: Calculated 4-methoxysalicylaldehyde, copper complex, and uranyl complex UV-Vis spectrum in DMF

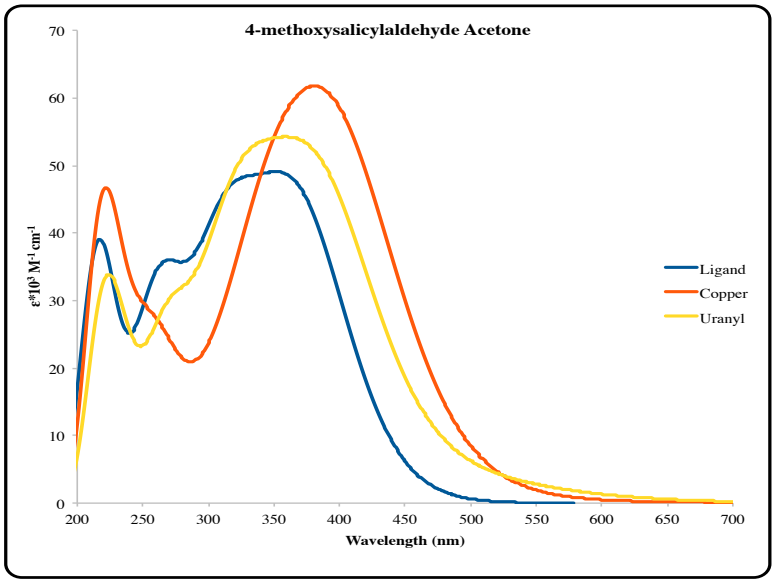

Figure A4.13: Calculated 4-methoxysalicylaldehyde, copper complex, and uranyl complex UV-Vis spectrum in acetone

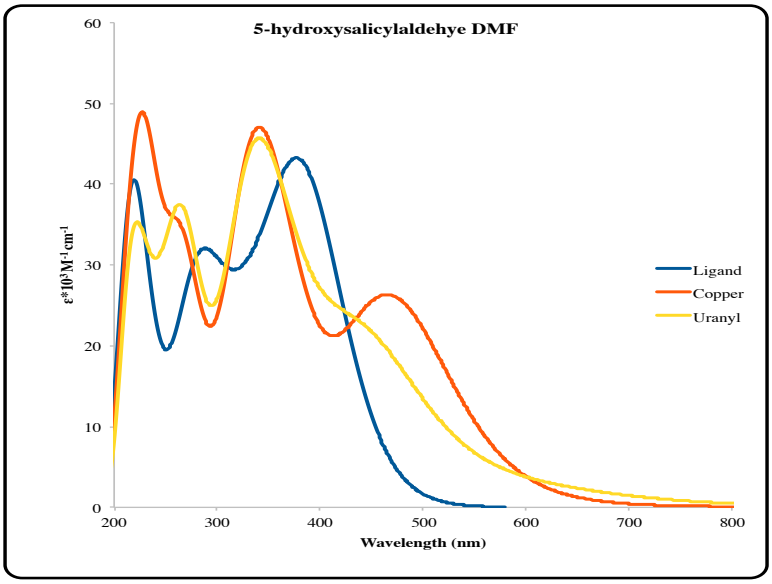

Figure A4.14: Calculated 5-hydroxysalicylaldehyde, copper complex, and uranyl complex UV-Vis spectrum in DMF

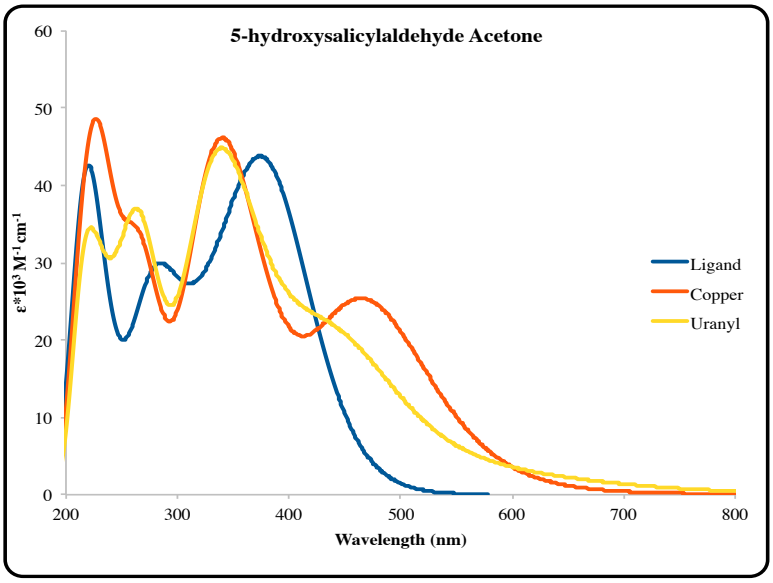

Figure A4.15: Calculated 5-hydroxysalicylaldehyde, copper complex, and uranyl complex UV-Vis spectrum in acetone

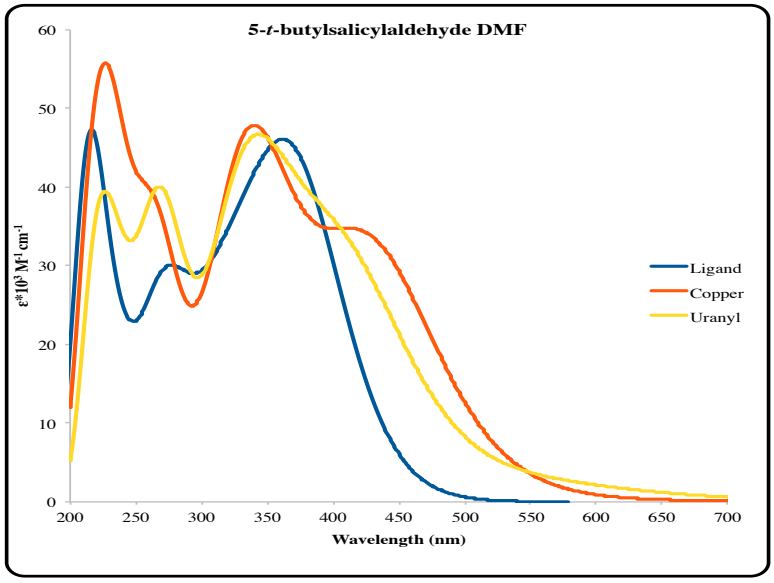

Figure A4.16: Calculated 5-*t*-butylsalicylaldehyde, copper complex, and uranyl complex UV-Vis spectrum in DMF

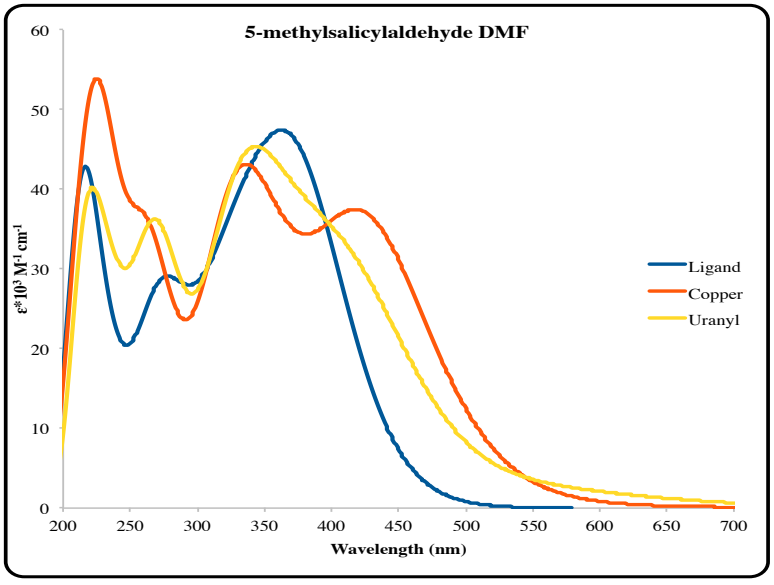

Figure A4.17: Calculated 5-methylsalicylaldehyde, copper complex, and uranyl complex UV-Vis spectrum in DMF

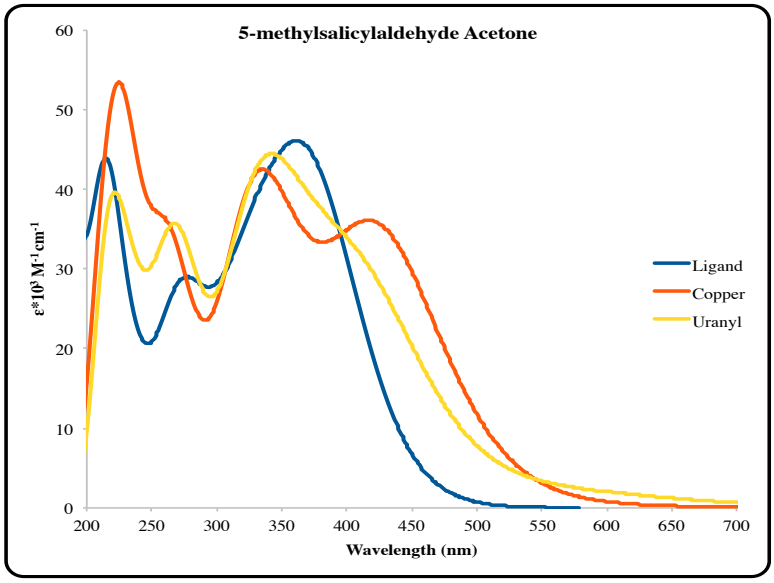

Figure A4.18: Calculated 5-methylsalicylaldehyde, copper complex, and uranyl complex UV-Vis spectrum in acetone

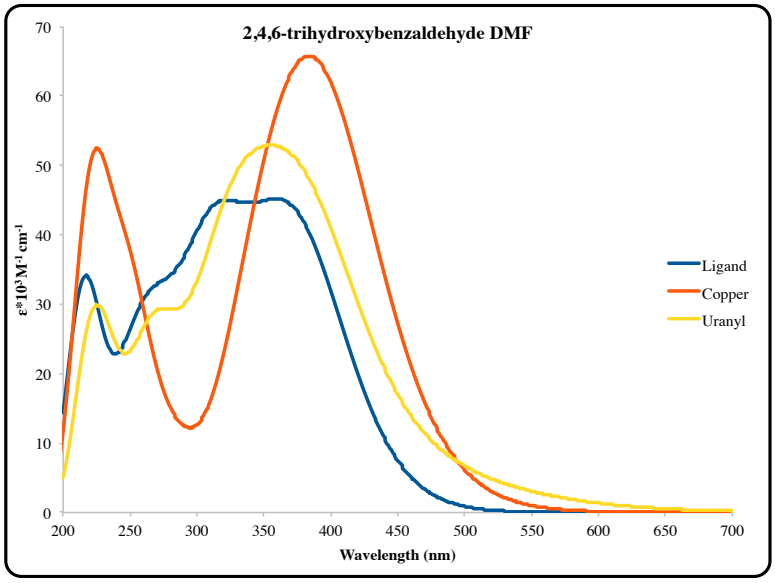

Figure A4.19: Calculated 2,4,6-trihydroxysalicylaldehyde, copper complex, and uranyl complex UV-Vis spectrum in DMF

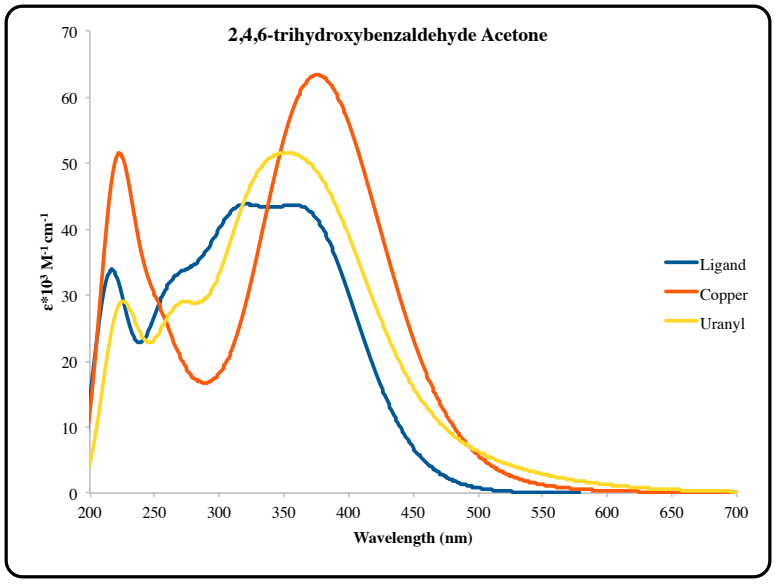

Figure A4.20: Calculated 2,4,6-trihydroxysalicylaldehyde, copper complex, and uranyl complex UV-Vis spectrum in acetone

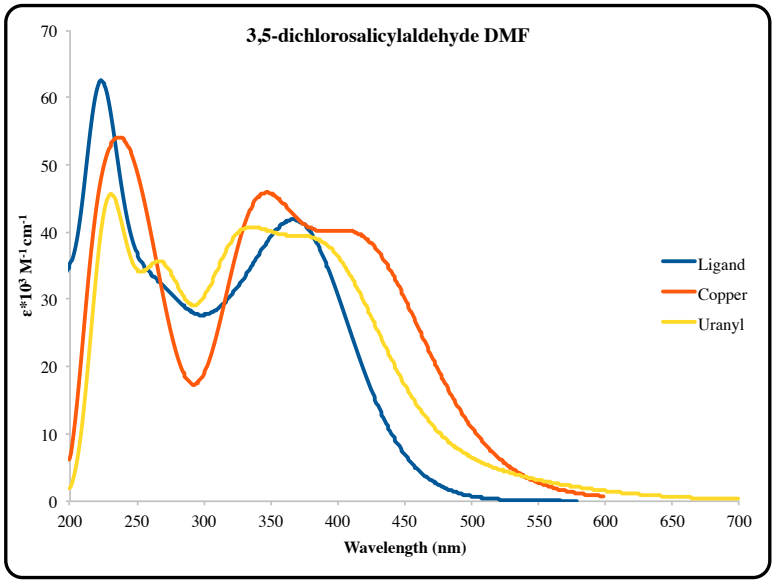

Figure A4.21: Calculated 3,5-dichlorosalicylaldehyde, copper complex, and uranyl complex UV-Vis spectrum in DMF

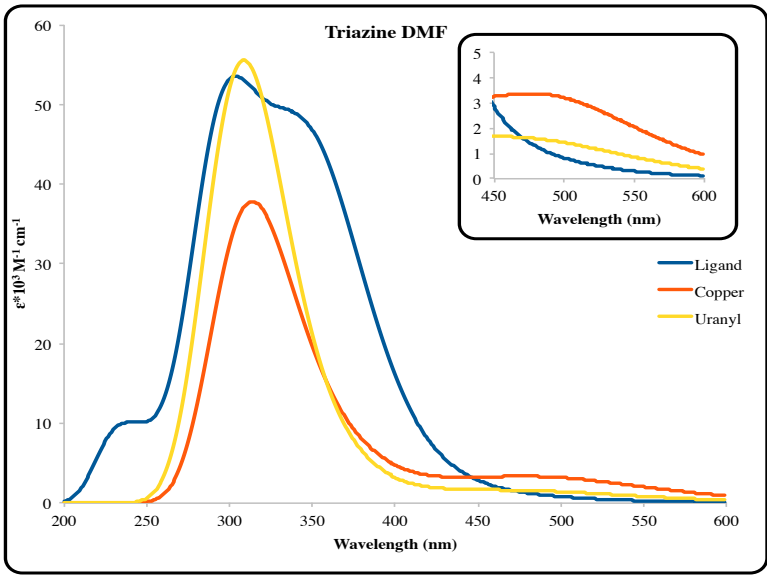

Figure A4.22: Calculated triazine, copper complex, and uranyl complex UV-Vis spectrum in DMF

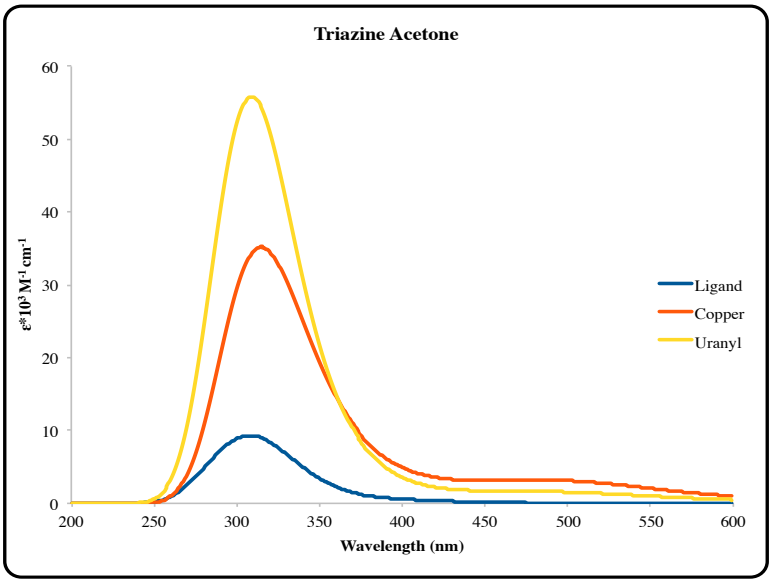

Figure A4.23: Calculated triazine, copper complex, and uranyl complex UV-Vis spectrum in acetone

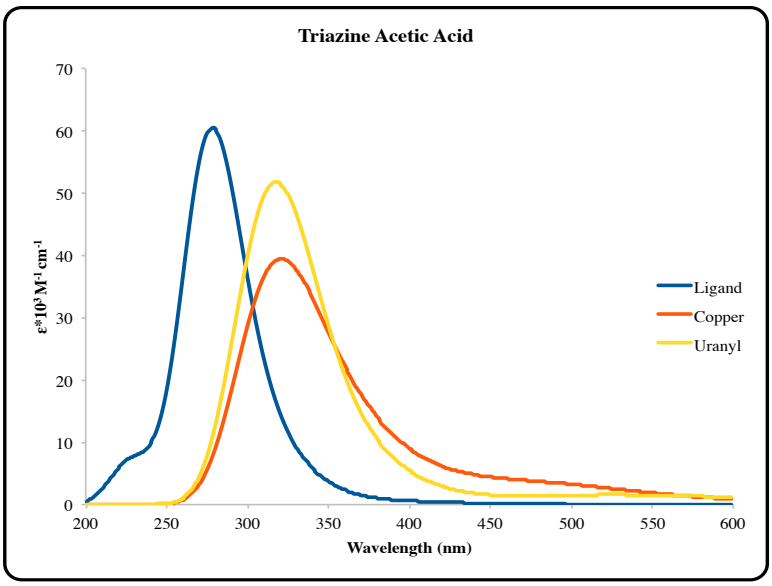

Figure A4.24: Calculated triazine, copper complex, and uranyl complex UV-Vis spectrum in acetic acid

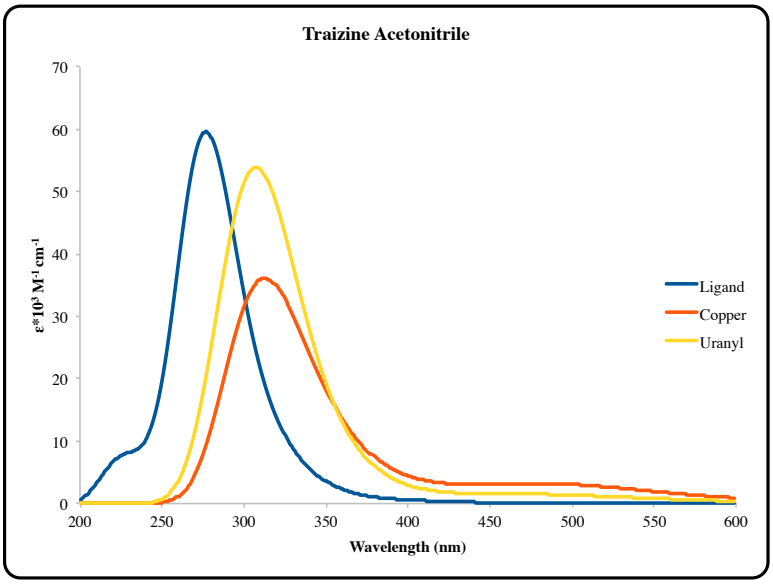

Figure A4.25: Calculated triazine, copper complex, and uranyl complex UV-Vis spectrum in acetonitrile

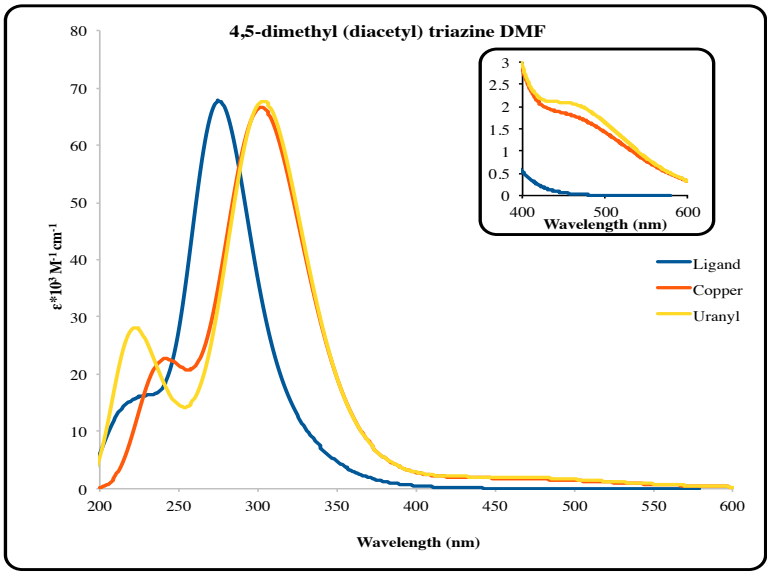

Figure A4.26: Calculated 4,5-dimethyl triazine, copper complex, and uranyl complex UV-Vis spectrum in DMF

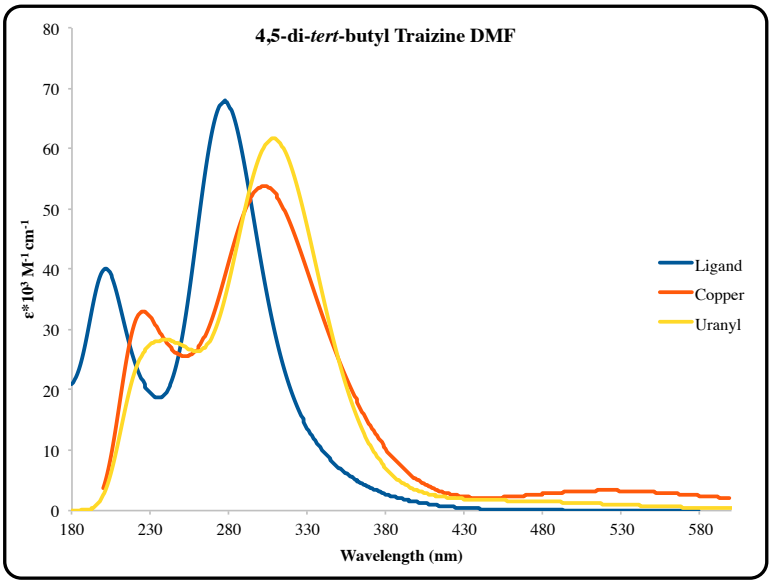

Figure A4.27: Calculated 4,5-di-*t*-butyltriazine, copper complex, and uranyl complex UV-Vis spectrum in DMF

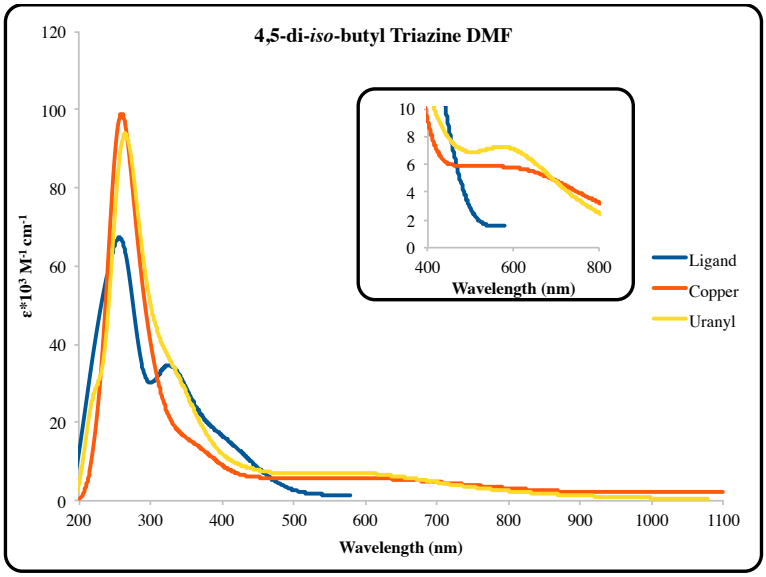

Figure A4.28: Calculated 4,5-di-*i*-butyltriazine, copper complex, and uranyl complex UV-Vis spectrum in DMF

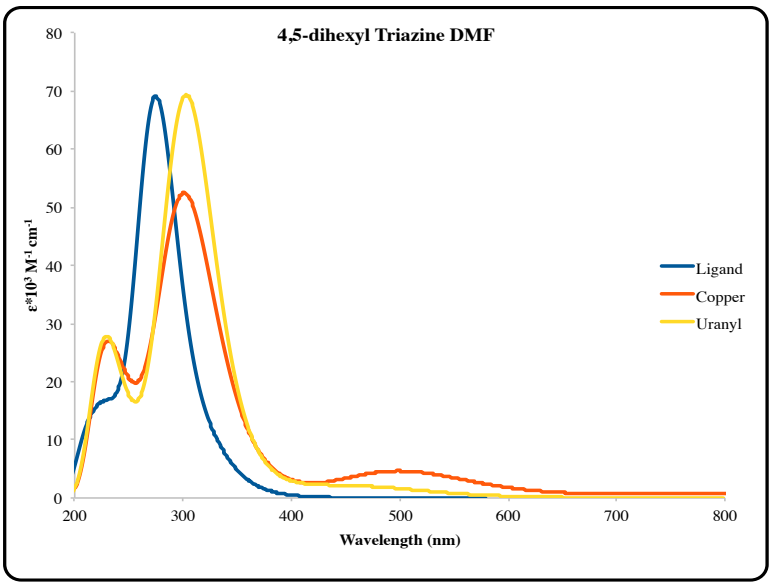

Figure A4.29: Calculated 3-ethoxysalicylaldehyde, copper complex, and uranyl complex UV-Vis spectrum in DMF

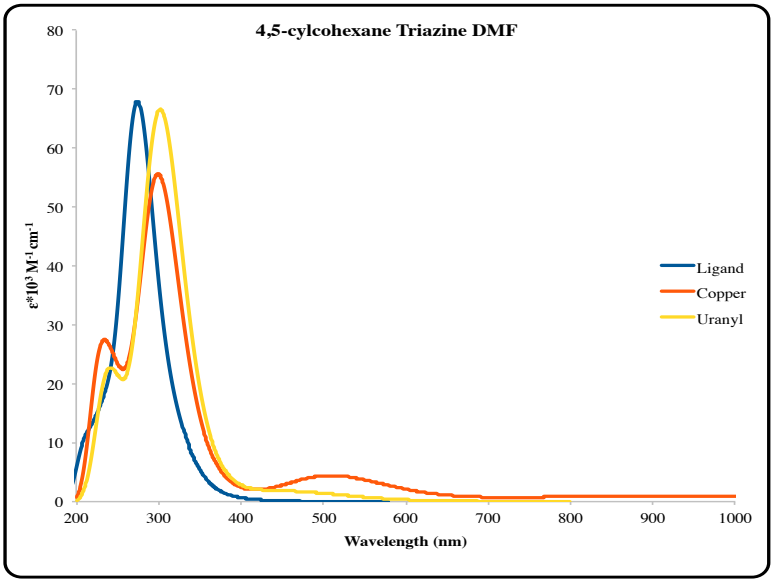

Figure A4.30: Calculated 4,5-cylcohexane, copper complex, and uranyl complex UV-Vis spectrum in DMF

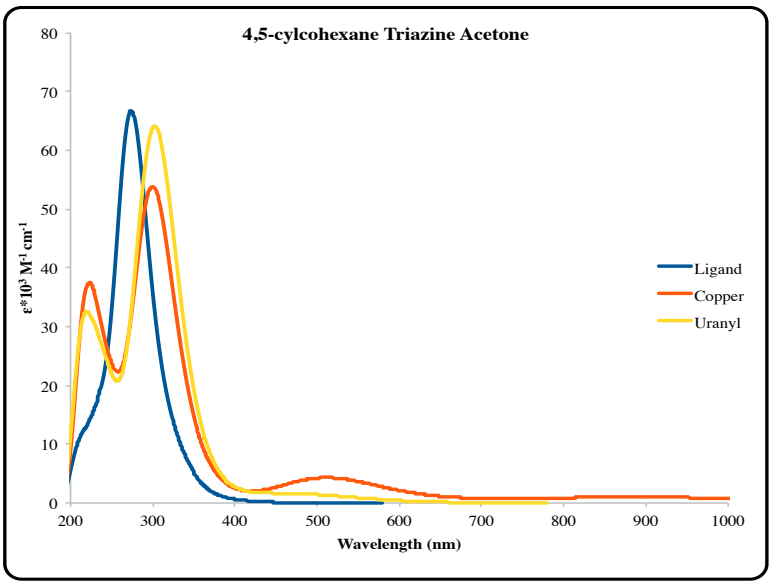

Figure A4.31: Calculated 4,5-cyclohexane, copper complex, and uranyl complex UV-Vis spectrum in acetone

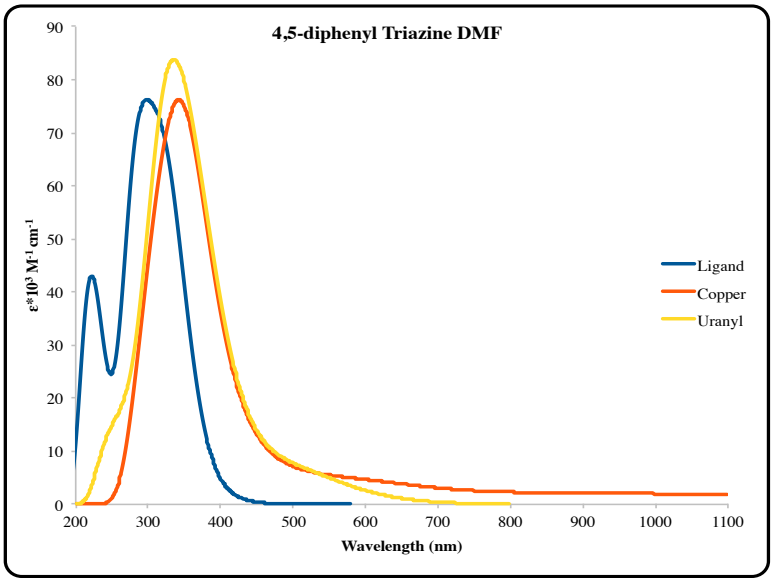

Figure A4.32: Calculated 4,5-diphenyltriazine, copper complex, and uranyl complex UV-Vis spectrum in DMF

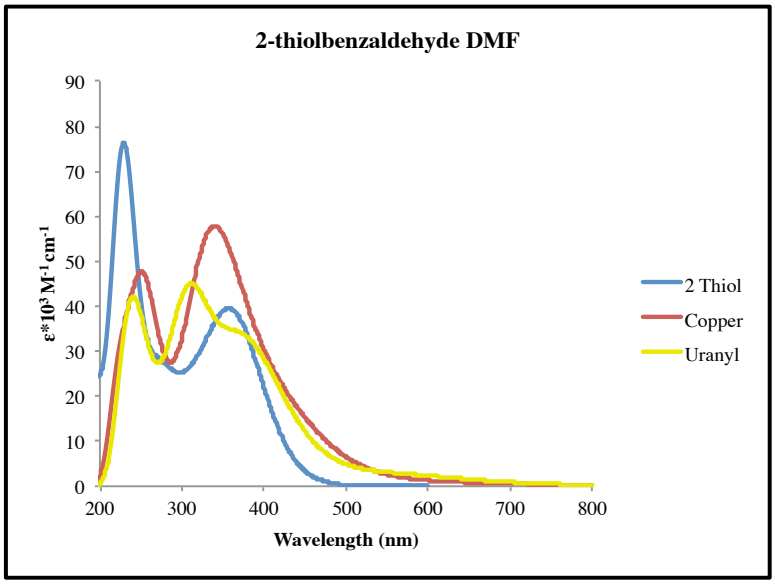

Figure A4.33: Calculated 2-thiobenzaldehyde, copper complex, and uranyl complex UV-Vis spectrum in DMF

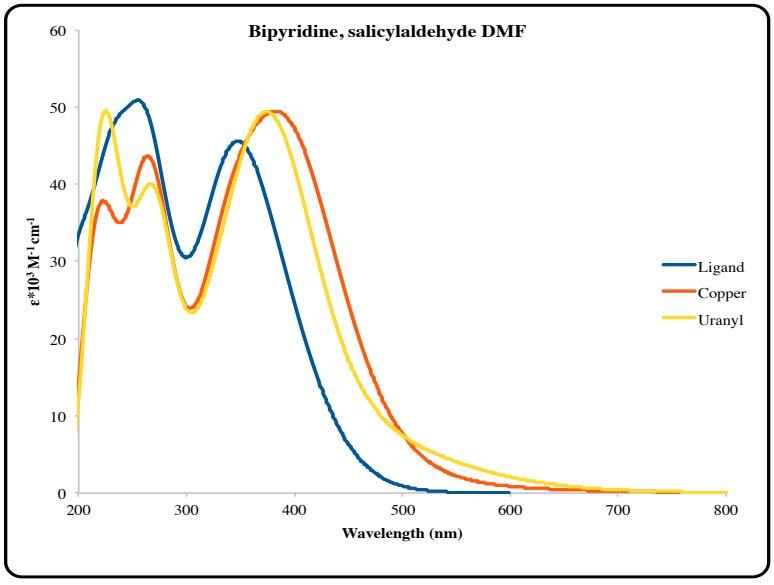

Figure A4.34: Calculated bipyridine salicylaldehyde, copper complex, and uranyl complex UV-Vis spectrum in DMF

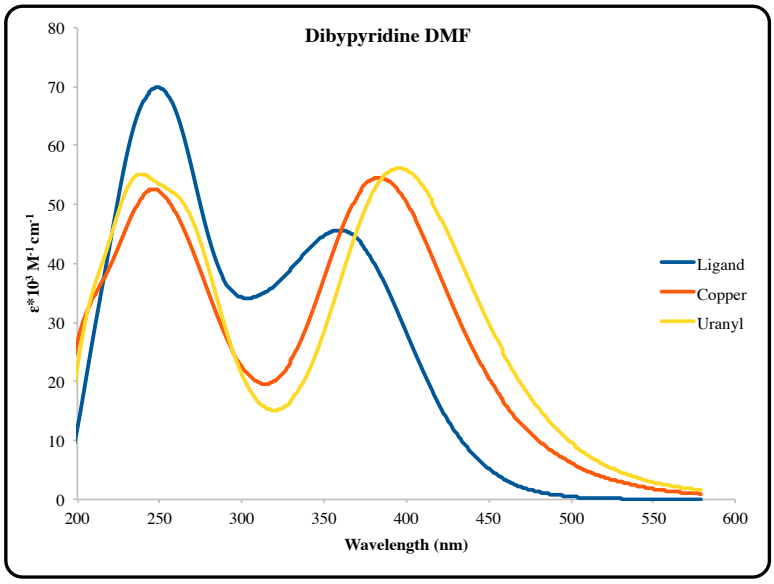

Figure A4.35: Calculated bis-bipyridine, copper complex, and uranyl complex UV-Vis spectrum in DMF

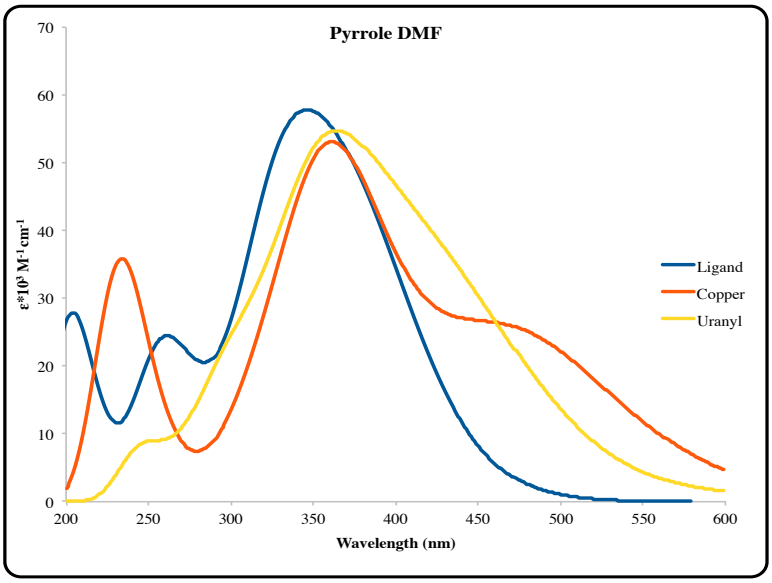

Figure A4.36: Calculated pyrrole, copper complex, and uranyl complex UV-Vis spectrum in DMF

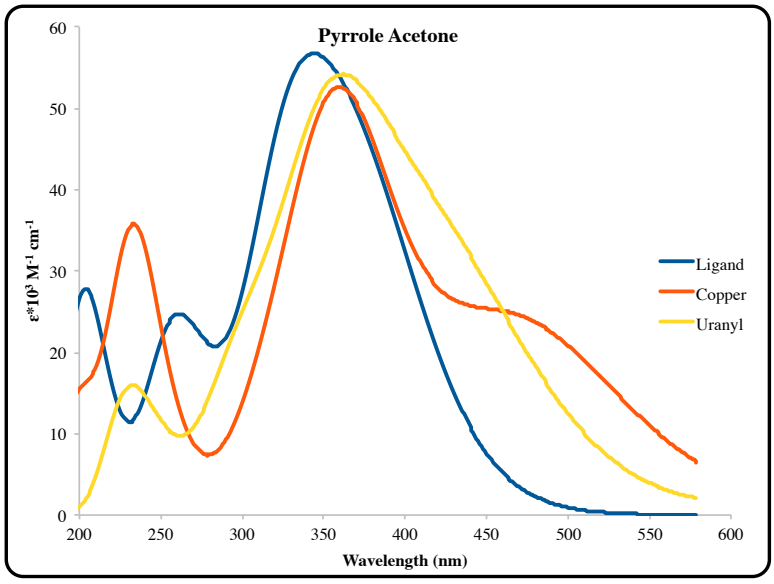

Figure A4.37: Calculated pyrrole, copper complex, and uranyl complex UV-Vis spectrum in acetone

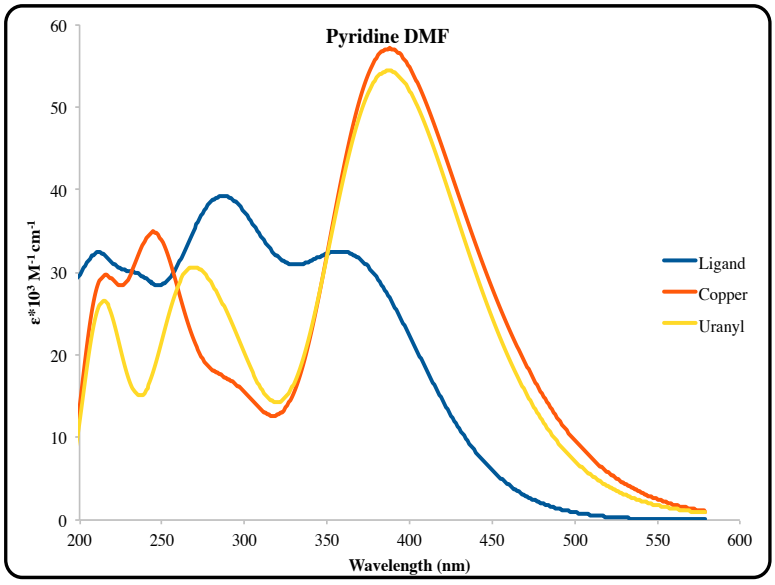

Figure A4.38: Calculated pyridine, copper complex, and uranyl complex UV-Vis spectrum in DMF

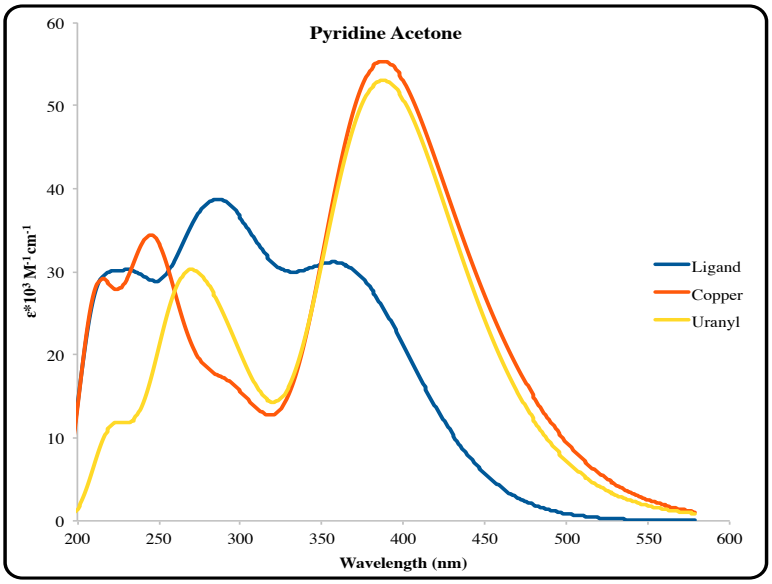

Figure A3.39: Calculated pyridine, copper complex, and uranyl complex UV-Vis spectrum in acetone

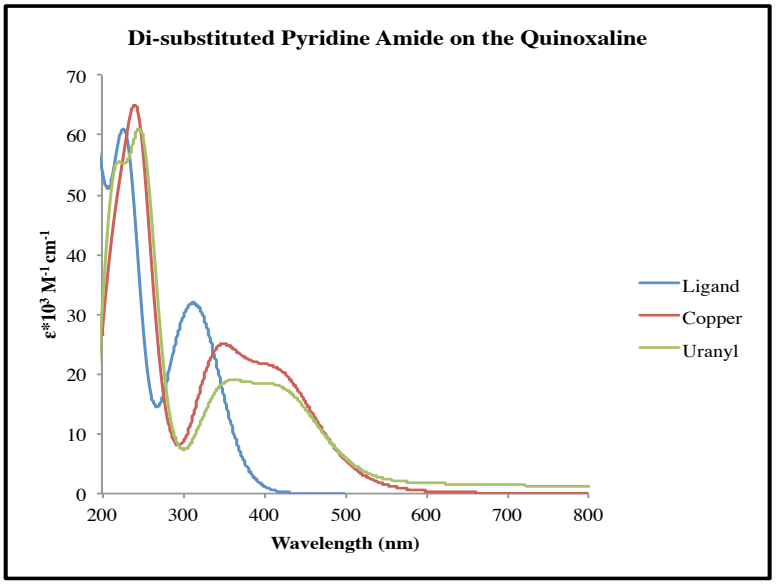

Figure A3.40: Calculated di-substituted pyridine amide on quinoxaline, copper complex, and uranyl complex UV-Vis spectrum in DMF

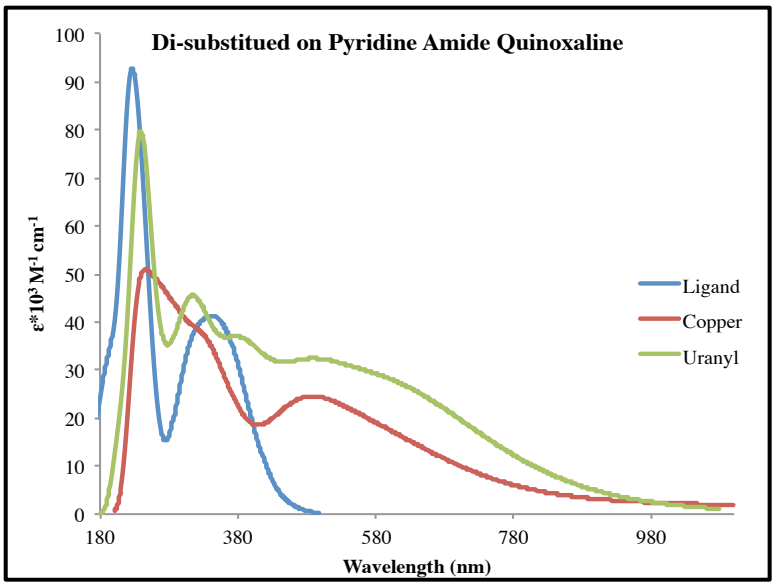

Figure A4.41: Calculated disubstituted pyridine amide on pyridine, copper complex, and uranyl complex UV-Vis spectrum in DMF